MODIS VEGETATION INDEX (MOD 13)

ALGORITHM THEORETICAL BASIS DOCUMENT

Version 3.1

Principal Investigators

A. R. Huete[1], K. Didan[1], MODIS Science Team Members
Wim Van Leeuwen[1], MODIS Associate Science Team Member

Development Team

Alfredo Huete[1]
Kamel Didan[1]
Wim Van Leeuwen[1]

[1]The University of Arizona

didan@email.arizona.edu

Contributors

Andrea Jacobson[1]
Ramon Solanos[1]
Trevor Laing[1]

MODIS Product ID: MOD13
Version 3.1 - April 1999

Vegetation Index and Phenology Lab
http://vip.arizona.edu

EXECUTIVE SUMMARY

One of the primary interests of the Earth Observing System (EOS) program is to study the role of terrestrial vegetation in large-scale global processes with the goal of understanding how the Earth functions as a system. This requires an understanding of the global distribution of vegetation types as well as their biophysical and structural properties and spatial/temporal variations. Vegetation Indices (VI) are robust, empirical measures of vegetation activity at the land surface. They are designed to enhance the vegetation signal from measured spectral responses by combining two (or more) different wavebands, often in the red (0.6-0.7 μm) and NIR wavelengths (0.7-1.1 μm).

The MODIS vegetation index (VI) products will provide consistent, spatial and temporal comparisons of global vegetation conditions which will be used to monitor the Earth's terrestrial photosynthetic vegetation activity in support of phenologic, change detection, and biophysical interpretations. Gridded vegetation index maps depicting spatial and temporal variations in vegetation activity are derived at 16-day and monthly intervals for precise seasonal and interannual monitoring of the Earth's vegetation.

The MODIS VI products are made globally robust and improves upon currently available indices with enhanced vegetation sensitivity and minimal variations associated with external influences (atmosphere, view and sun angles, clouds) and inherent, non-vegetation influences (canopy background, litter), in order to more effectively serve as a 'precise' measure of spatial and temporal vegetation 'change'.

Two vegetation index (VI) algorithms are to be produced globally for land, at launch. One is the standard normalized difference vegetation index (NDVI), which is referred to as the "continuity index" to the existing NOAA-AVHRR derived NDVI. At the time of launch, there will be nearly a 20-year NDVI global data set (1981 - 1999) from the NOAA- AVHRR series, which could be extended by MODIS data to provide a long term data record for use in operational monitoring studies. The other is an 'enhanced' vegetation index (EVI) with improved sensitivity into high biomass regions and improved vegetation monitoring through a de-coupling of the canopy background signal and a reduction in atmosphere influences. The two VIs compliment each other in global vegetation studies and improve upon the extraction of canopy biophysical parameters. A new compositing scheme that reduces angular, sun-target-sensor variations is also utilized. The gridded vegetation index maps use MODIS surface reflectances, corrected for molecular scattering, ozone absorption, and aerosols, and adjusted to nadir with use of a BRDF model, as input to the VI equations. The gridded vegetation indices will include quality assurance (QA) flags with statistical data, that indicate the quality of the VI product and input data. The products can be summarized as:

- 250 m NDVI and QA at 16 day (high resolution)
- 1 km NDVI, EVI, and QA at 16 day and monthly (standard resolution)
- 25 km NDV, EVI, and QA at 16 day and monthly (coarse resolution)

An important aspect of the VI products will be their translation to biophysical canopy parameters. The use of biophysical data forms an integral component of the vegetation index validation plan, tying the radiometric VI to measurable physical parameters on the ground. This enables the acquisition of the necessary “ground truth” information needed to assess error, uncertainties, and performance as part of validation. This document describes the theoretical basis for the development and implementation of the MODIS VI products along with validation and a thorough characterization of VI performance and uncertainties.

Table of Contents

List of Figures

List of Tables

1 Introduction

One of the primary interests of the Earth Observing System (EOS) program is to study the role of terrestrial vegetation in large-scale global processes with the goal of understanding how the Earth functions as a system. This requires an understanding of the global distribution of vegetation types as well as their biophysical and structural properties and spatial/temporal variations. Remote sensing observations offer the opportunity to monitor, quantify, and investigate large scale changes in vegetation in response to human actions and climate. Vegetation influences the energy balance, climate, hydrologic, and biogeochemical cycles and can serve as a sensitive indicator of climatic and anthropogenic influences on the environment.

The MODIS vegetation indices (VIs) will provide consistent, spatial and temporal comparisons of global vegetation conditions that will be used to monitor the Earth's terrestrial photosynthetic vegetation activity for phenologic, change detection, and biophysical derivation of radiometric and structural vegetation parameters. The MODIS vegetation index (VI) products will play a major role in several EOS studies as well as be an integral part in the production of many global and regional biospheric models and biogeochemical cycles. Currently, satellite-derived vegetation indices are being integrated in interactive biosphere models as part of global climate modelling (Sellers et al. 1994; Raich and Schlesinger, 1992; Fung et al., 1987; Tans et al., 1990) and production efficiency models (Prince et al., 1994; Prince, 1991). They are also used for a wide variety of land applications, including natural resource management, agriculture, the Global Health and Human Monitoring Program (NASA, 1988), and operational Famine Early Warning Systems (Prince and Justice, 1991; Hutchinson, 1991). This latter example is one of the few examples where derived satellite data are currently being used to drive policy decisions.

1.1 Identification of Algorithm

MODIS product #13, Gridded Vegetation Indices (Level 3)

The level 3 gridded vegetation indices are standard products designed to be fully operational at launch. The level 3, spatial and temporal gridded vegetation index products are composites of daily bidirectional reflectances. The gridded VIs are 16- and 30 day spatial and temporal, re-sampled products designed to provide cloud-free, atmospherically corrected, and nadir-adjusted vegetation maps at nominal resolutions of 250 m, 1 km, and 0.25°. The latter is also known as the climate modeling grid (CMG).

Two vegetation index (VI) algorithms are to be produced globally for land, at launch. One is the standard normalized difference vegetation index (NDVI), which is referred to as the “continuity index” to the existing NOAA-AVHRR derived NDVI. At the time of launch, there will be nearly a 20-year NDVI global data set (1981 - 1999) from the NOAA- AVHRR series, which could be extended by MODIS data to provide a long term data record for use in operational monitoring studies. The other is an ‘enhanced’ vegetation index with improved sensitivity to differences in vegetation from sparse to

dense vegetation conditions. The two VIs compliment each other in global vegetation studies and improve upon the extraction of canopy biophysical parameters.

- Normalized Difference Vegetation Index (NDVI), Parameter No. 2749a
- Enhanced Vegetation Index (EVI), Parameter No. 4334a.

The compositing algorithm utilizes the bidirectional reflectance distribution function of each pixel to normalize the reflectances to a nadir view and standard solar angular geometry. The 16 day VI composites will be archived at 250 m resolution and will include the selected, nadir-adjusted VI value, the nadir-adjusted red and NIR surface reflectances, median solar zenith, relative azimuth, and quality control parameters.

- 250 m NDVI (16 day)
- 1 km NDVI and EVI (16 day and monthly)
- 25 km NDVI and EVI (16 day and monthly)

The 250 m MODIS VI product will consist of only the NDVI, since the EVI utilizes the 500 m blue channel and only the red and NIR bands are at 250 m resolution. The composited surface reflectance data from each pixel will be used to compute both the NDVI and the EVI gridded products.

1.2 Key Science Applications of the Vegetation Index

Vegetation indices have a long history of use throughout a wide range of disciplines. Some examples are listed below:

- Inter- and intra-annual global vegetation monitoring on a periodic basis;
- Global biogeochemical, climate, and hydrologic modeling;
- Net primary production and carbon balance;
- Anthropogenic and climate change detection;
- Agricultural activities (plant stress, harvest yields, precision agriculture…);
- Famine early warning systems;
- Drought studies
- Landscape disturbances (volcanic, fire scars, etc..);
- Land cover and land cover change products;
- Biophysical estimates of vegetation parameters (%cover, fAPAR, LAI) ;
- Public health issues (rift valley fever, mosquito producing rice fields…).

2 Overview and Background Information

2.1 Experimental Objective

The overall objective is to design an empirical or semi-empirical robust vegetation measure applicable over all terrestrial biomes of the earth. Vegetation indices (VI's) are dimensionless, radiometric measures of vegetation exploiting the unique spectral signatures and behavior of canopy elements, particularly in the red and NIR portions of the spectrum. VI's not only map the presence of vegetation on a pixel basis, but provides measures of the amount or condition of vegetation within a pixel. The basic premise is to extract the vegetation signal portion from the surface. The stronger the signal, the more vegetation is present for any given land cover type. Their principal advantage is their simplicity. They require no assumptions, nor additional ancillary information other than the measurements themselves. The goal becomes, how to effectively combine these bands in order to extract and quantify the 'green' vegetation signal across a global range of vegetation conditions while minimizing canopy influences associated with intimate mixing by non-vegetation related signals.

The vegetation index compositing objective is to combine multiple images into a single, gridded, and cloud-free VI map, taking into account the variable atmosphere conditions, residual clouds, and a wide range of sensor view and sun angle conditions. The task is to design an algorithm that is able to depict spatial variations in vegetation across a range of scales as well as depict temporal variations for phenologic studies (intra-annual) and change detection studies (inter-annual).

Specific tasks and experimental objectives include:

- develop precise, empirical measures of vegetation, depicting both spatial and temporal variations in vegetation composition, condition, and photosynthetic activity.
- continuity with current, global NOAA-AVHRR series, NDVI data fields.
- improved measures of vegetation utilizing new, improved variants of the NDVI for enhanced vegetation sensitivity and more accurate quantitative analysis.
- develop near-linear measures of vegetation parameters in order to maintain sensitivity over as wide a range of vegetation conditions as possible and to facilitate scaling and extrapolations across regional and global resolutions.
- provide estimates of biophysical parameters, comparable for insertion into global biome and climate models.
- maximize global and temporal land coverage at the finest spatial and temporal resolutions possible within the constraints of the instrument characteristics and land surface properties.
- minimize the effects of residual clouds, cloud shadow, and atmospheric aerosols.

- standardize variable sensor view and sun angle (BRDF effects) of the cloud-free pixels to a nadir view angle and nominal sun angle.
- ensure the quality and consistency of the composited data.

2.2 Historical Perspective

2.2.1 Vegetation indices

Many studies have shown the relationships of red and near-infrared (NIR) reflected energy to the amount of vegetation present on the ground (Colwell, 1974). Reflected red energy decreases with plant development due to chlorophyll absorption within actively photosynthetic leaves. Reflected NIR energy, on the other hand, will increase with plant development through scattering processes (reflection and transmission) in healthy, turgid leaves. Unfortunately, because the amount of red and NIR radiation reflected from a plant canopy and reaching a satellite sensor varies with solar irradiance, atmospheric conditions, canopy background, and canopy structure/ and composition, one cannot use a simple measure of reflected energy to quantify plant biophysical parameters nor monitor vegetation on a global, operational basis. This is made difficult due to the intricate radiant transfer processes at both the leaf level (cell constituents, leaf morphology) and canopy level (leaf elements, orientation, non-photosynthetic vegetation (NPV), and background). This problem has been circumvented somewhat by combining two or more bands into an equation or 'vegetation index' (VI).

The simple ratio (SR) was the first index to be used (Jordan, 1969), formed by dividing the NIR response by the corresponding 'red' band output,

$$SR = \frac{X_{nir}}{X_{red}} \tag{1}$$

where X can be digital counts, at- satellite radiances, top of the atmosphere apparent reflectances, land leaving surface radiances, surface reflectances, or hemispherical spectral albedos. However, for densely vegetated areas, the amount of red light reflected approaches very small values and this ratio, consequently, increases without bounds. Deering (1978) normalized this ratio from -1 to +1, with the normalized difference vegetation index (NDVI), by ratioing the difference between the NIR and red bands by their sum;

$$NDVI = \frac{X_{nir} - X_{red}}{X_{nir} - X_{red}} \tag{2}$$

For terrestrial targets the lower boundary became approximately zero and the upper boundary approximately 0.80.

Global-based operational applications of the NDVI have utilized digital counts, at-sensor radiances, 'normalized' reflectances (top of the atmosphere), and more recently, partially atmospheric corrected (ozone absorption and molecular scattering) reflectances. Thus, the NDVI has evolved with improvements in measurement inputs. Currently, a partial atmospheric correction for Rayleigh scattering and ozone absorption is used operationally for the generation of the Advanced Very High Resolution Radiometer; Agbu et al., 1994, (AVHRR) Pathfinder and the IGBP Global 1km NDVI data sets (James and Kalluri 1994; Townshend et al. 1994). The NDVI is currently the only operational, global-based vegetation index utilized. This is in part, due to its 'ratioing' properties, which enable the NDVI to cancel out a large proportion of signal variations attributed to calibration, noise, and changing irradiance conditions that accompany changing sun angles, topography, clouds/shadow and atmospheric conditions.

As a vegetation monitoring tool, the NDVI is utilized to construct seasonal, temporal profiles of vegetation activity enabling interannual comparisons of these profiles. The temporal profile of the NDVI has been shown to depict seasonal and phenologic activity, length of the growing season, peak greenness, onset of greenness, and leaf turnover or 'dry-down' period. Myneni et al. (1997) presented a 10 year NDVI data record of northern Boreal forests showing a warming trend whereby the length of the growing season had increased by nearly 2 weeks. They showed the usefulness of such NDVI growing season plots for change detection and monitoring. Tucker (1985) similarly used NDVI seasonal profiles to show desert expansions and contractions in the Sahara. The time integral of the NDVI over the growing season has been correlated with net primary production (NPP) (Running and Nemani, 1988; Prince, 1991; Justice et al., 1985; Goward et al., 1991, Tucker and Sellers, 1986).

Many studies have shown the NDVI to be related to leaf area index (LAI), green biomass, percent green cover, and fraction of absorbed photosynthetically active radiation (fAPAR) (Asrar et al., 1984; Baret and Guyot, 1991; Goward and Huemmrich, 1992; Sellers, 1985; Sellers, 1986; Running and Nemani, 1988; Tucker et al., 1981; Curran, 1980). Relationships between fAPAR and NDVI have been shown to be near linear (Pinter, 1993; Begué, 1993; Wiegand et al., 1991; Daughtry et al., 1992), in contrast to the non-linearity experienced in LAI – NDVI relationships with saturation problems at LAI values over 2. Other studies have shown the NDVI to be related to carbon-fixation, canopy resistance, and potential evapotranspiration allowing its use as input to models of biogeochemical cycles (Raich and Schlesinger, 1992; Fung et al., 1987; Sellers, 1985; Asrar et al., 1984; Running et al., 1989; Running, 1990; IGBP, 1992).

2.2.2 Compositing

The construction of seasonal, temporal profiles requires a separate 'compositing' algorithm in which several VI images, over a given time interval (7-days, 10-days, etc…) are merged to create a single cloud-free image VI map with minimal atmospheric and sun-surface-sensor angular effects (Holben, 1986). Moderate and coarse resolution satellite systems, such as MODIS, the AVHRR, SPOT4-VEGETATION (*Systeme Pour*

l'Observation de la Terre 4-VEGETATION; Archard et al., 1994), SeaWiFS (Sea-Viewing Wide Field-of-View Sensor; Hooker et al., 1994), and GLI (*Global Imager;* Nakajima et al., 1998) acquire global bi-directional radiance data of the Earth's surface under a wide variety of solar illumination angles, sensor view angles, atmospheres, and cloud conditions.

The current procedure for generation of composited, AVHRR-based, NDVI products is the maximum value compositing (MVC) technique. This is accomplished by selecting, on a pixel by pixel basis, the input pixel with the highest NDVI value as output to the composited product. The procedure generally includes cloud screening and data quality checks (Goward et al., 1994; Eidenshink and Faundeer, 1994). Since residual cloud cover, not accounted for in the cloud masking procedure, and atmospheric sources of contamination both lower NDVI values, a maximum NDVI would select the least cloud- and atmospheric-contaminated pixels. Furthermore, since the influence of atmospheric contamination and residual cloud cover increases with optical path length, the maximum NDVI criterion also has a tendency to select the most near-nadir view and smallest solar zenith angle pixels (least optical path lengths), thus standardizing to a certain degree the variable sun-surface-sensor observation geometries over a compositing cycle (Holben 1986; Cihlar et al. 1994a).

The MVC works nicely over near-Lambertian surfaces where the primary source of pixel variations within a composite cycle is associated with atmosphere contamination and path length, however, its major shortcoming is that the anisotropic, bi-directional influences of the surface is not considered. The bidirectional spectral behavior of numerous, 'global' land cover types and terrestrial surface conditions have been widely documented and shown to be highly anisotropic due to canopy structure, shadowing, and background contributions (Kimes et al., 1985; Leeuwen et al., 1994; Vierling et al., 1997). Ratioing of the NIR and red spectral bands to compute vegetation indices does not remove surface anisotropy (Walter-Shea et al., 1997) due to the spectral dependence of the BRDF response (Gutman, 1991; Roujean et al., 1992). The atmosphere counteracts and dampens the surface BRDF signal, mainly through the increasing path lengths associated with off-nadir view angles and/or sun angles.

The maximum NDVI value selected is thus, related to ***both*** the bidirectional properties of the surface and the atmosphere, which renders the MVC-based selection unpredictable. The MVC favors cloud free pixels, but does not necessarily pick the pixel closest to nadir or with the least atmospheric contamination. Although the NDVI tends to increase for atmospherically corrected data, it does not mean that the highest NDVI is an indication of the best atmospheric correction. Many studies have shown the MVC approach to select off-nadir pixels with large, forward-scatter (more shaded) view angles and large solar zenith angles, which are not always cloud-free or atmosphere clear (Goward et al., 1991; Moody and Strahler, 1994; Cihlar et al., 1994b, 1997). This degrades the potential use of the VI for consistent and accurate comparisons of global vegetation types.

The MVC method works best for data uncorrected for atmosphere (Cihlar et al., 1994a), although numerous inconsistencies result (Gutman, 1991; Goward et al., 1991,

1994; Cihlar et al., 1994b, 1997). The MVC approach becomes less appropriate with atmospherically-corrected data sets, since the anisotropic behavior of surface reflectances and vegetation indices is stronger (Cihlar et al., 1994b). The influence of surface anisotropy and bidirectional reflectances on the VI composited products will become more pronounced in the EOS era as a result of improved atmospheric removal algorithms, which will accentuate differences and cause surface BRDF-related anisotropies to become more prominent (Cihlar et al.,1994a). In many cases, the nadir view direction may produce the lowest VI value, particularly in atmospherically corrected data.

There are other alternatives to simply choosing the highest NDVI value over a compositing cycle. One may integrate or average all cloud-free pixels over the period. Meyer et al. (1995) suggested that averaging the NDVI would be superior to the MVC approach. The Best Index Slope Extraction (BISE; Viovy et al., 1992) method reduces noise in NDVI time series by selecting against spurious high values through a sliding compositing cycle. Use of the thermal channel has also been shown to be helpful. Knowledge of the ecological evolution of a land cover with respect to a VI temporal response might also be of use for the improvement of compositing techniques (Viovy et al.,1992; Qi et al., 1994; Moody and Strahler, 1994). This was not considered for the MODIS compositing algorithm due to the amount of knowledge required of the dynamics of land cover growth patterns, seasonality, and response to climate change (precipitation, temperature). Such an approach might be more applicable at regional scales. Other VI compositing techniques are discussed by Cihlar et al. (1994b) and Qi and Kerr (1997).

2.2.3 VI optimization

The global operational use of a vegetation index requires that it not only be calculated in a uniform manner, but that the results be comparable over time and location. Although the NDVI has been shown useful in change detection, land surface monitoring, and in estimating many biophysical vegetation parameters, there is a history of vegetation index research identifying limitations in the NDVI, which may impact upon its utility in global studies. These limitations form the basis of VI optimization techniques and are useful to understand before utilization of the VI product. The limitations can result from various external influences including:

- Calibration and instrument characteristics
- Clouds and cloud shadows
- Atmospheric effects due to variable aerosols, water vapor, and residual clouds.
- Sun-target-sensor geometric configurations and the resulting interactions of surface and atmospheric anisotropies on the angular dependent signal.

In addition to these external influences, there are influences inherent to vegetated canopies which restrict the use and/or interpretation of vegetation indices. These include:

- Canopy background contamination in which the background reflected signal intimately mixes with the vegetation signal and influences the resulting VI value. Canopy background signals vary with soils, litter covers, snow, and surface wetness.
- Saturation problems whereby VI values remain invariant to changes in the amount, type, and condition of vegetation, normally associated with a saturated chlorophyll signal in densely vegetated canopies.

Furthermore, if one were to extend VI capabilities to the derivation of biophysical vegetation parameters, then one must take into account the following:

- Canopy structural effects associated with leaf angle distributions, clumping and non-photosynthetically-active components (woody, senesced, and dead plant materials). Thus for a given LAI, %cover, and/ or biomass, the NDVI may vary with changes in the structure and orientation of the canopy. The 'strength' of the vegetation signal is simultaneously dependent upon several 'physical' measures of vegetation amount, including leaf area index, %green cover, and wet or dry green biomass.
- Non-linearity in VI relationships with fAPAR and/ or LAI.

2.2.4 Calibration and instrument characteristics

2.2.5 Atmospheric effects

The atmosphere degrades the NDVI value by reducing the contrast between the red and NIR reflected signals. The red signal normally increases as a result of scattered, upwelling path radiance contributions from the atmosphere, while the NIR signal tends to decrease as a result of atmospheric attenuation associated with scattering and water vapor absorption. The net result is a drop in the NDVI signal and an underestimation of the amount of vegetation at the surface. The degradation in NDVI signal is dependent on the aerosol content of the atmosphere, with the turbid atmospheres resulting in the lowest NDVI signals. The impact of atmospheric effects on NDVI values is most serious with aerosol scattering (0.04 - 0.20 unit decreases), followed by water vapor (0.04 - 0.08), and Rayleigh scattering (0.02 - 0.04) (Goward et al. 1991; Teillet, 1989).

The atmosphere problem may be corrected through direct and indirect means (Kaufman and Tanre, 1996). Atmospheric effects on the MODIS VI's will become minimal as a result of the atmospheric correction algorithms being implemented (MODIS-09) prior to VI computation. However, some residual aerosol contamination will be expected in the NDVI product, due to the coarse resolution of the aerosol product (~20 km resolution) (Vermote et al., 1994) compared to the 250m NDVI product. Thus, spatial variations in smoke, gaseous and particulate pollutants, and light cirrus clouds, may be present at the finer spatial resolutions. The accuracy of atmospheric correction will also vary with the availability of 'dark-objects', which are needed for the best corrections.

Kaufman and Tanré (1992) developed the atmospherically resistant vegetation index (ARVI) as an example of an indirect approach to atmosphere correction, utilizing the difference of the blue and red bands as an indicator of atmospheric noise. The ARVI accounts for atmosphere aerosol scattering and requires atmospheric correction of molecular scattering and ozone absorption prior to its use. Myneni and Asrar (1993), in a sensitivity study with simulated data, found the ARVI to reduce atmospheric effects and to mimic ground-based NDVI data. Pinty and Verstraete (1992) have proposed an AVHRR-specific, global environment monitoring index (GEMI), which minimizes atmospheric effects specific to AVHRR data sets. We propose to use the atmosphere resistance concept (blue/ red) in the enhanced VI (EVI) to aid with highly variable aerosol conditions, such as smoke from biomass burning.

2.2.6 Angular considerations

The NDVI has been shown to be affected by variations in bidirectional reflectances resulting from differences in sun-target-sensor geometries. MODIS viewing angles will vary ±55° cross-track accompanied by solar illumination angle differences of up to 20° from edge to edge of the MODIS swath. In addition sun angles will vary with latitude and time of the year. The strong anisotropic properties from vegetation canopies seriously affect vegetation indices, an effect that will become more pronounced with MODIS data in which atmosphere correction will further enhance surface-based anisotropies, which vary with land cover type, relative amounts of characteristic vegetation and soil components, and sun-earth-sensor geometry. The resulting deviations must be considered in the derivation of the vegetation index products. This resulting variability in view and sun angles is important for the (seasonal and interannual) intercomparison of vegetative covers on a global basis. Therefore, some knowledge of the bi-directional reflectance distribution function (BRDF) is needed for successful utilization of directional reflectance data and vegetation indices, and the derivation of land cover-specific biophysical parameters (Cihlar et al., 1994a).

The influence of variable sun-target-sensor configurations on derived vegetation indices can be standardized in various manners, including: (1) standardize reflectances to nadir view angle at a solar zenith angle representative of the observations; (2) standardize reflectances to nadir view angle and a temporally and globally constant solar zenith angle; (3) adjust to a constant “off-nadir” view angle with a constant sun angle; or (4) use of spectral (bi-hemispherical) albedos. For the standard MODIS VI products, we propose to use the first method (Justice et al., 1998) and examine the other three approaches post-launch. There is considerable research and understanding of bidirectional reflectances with the development of physical, semi-empirical, and empirical BRDF models (Wanner et al., 1995). Preliminary analysis (Huete et al., 1996) also suggests that both the third and fourth approaches may enhance vegetation detection only over a limited range of land cover conditions (Kimes et al., 1984; Privette et al., 1996), and will result in overall decreased sensitivity from desert to forest, and present greater saturation problems in more densely vegetated canopies.

2.2.7 Canopy background contamination

In contrast to the previous sources of noise and uncertainty, this source of uncertainty is best handled in the formulation of the VI equation itself, since canopy background (soil, litter, snow, and water) effects on the VI are not readily corrected for prior to VI computation. Background effects are best removed within the VI equation itself because (1) they cannot be assessed independently as in atmosphere and BRDF; and (2) in validation, a 'true' VI value for a given canopy is needed, one that does not depend upon the background optical properties.

Numerous ground-, air-, and satellite-based observations have shown the NDVI to be overly sensitive to the brightness of the underlying canopy background (Elvidge and Lyon, 1985; Huete et al., 1985; Heilman and Kress, 1987; Huete and Warrick, 1990; Qi et al., 1993a). Canopy backgrounds exhibit spatial and temporal reflectance variations resulting from rain events, snowfall, litterfall, roughness, and the organic matter content and mineralogy of the soil substrate material. In all of these studies there is a systematic increase in the NDVI value as the reflectance or 'brightness' of the background decreases. This change in NDVI with background brightness is also confirmed with canopy radiative transfer models including the SAIL and two-stream approximation models (Baret and Guyot, 1991; Baret at al., 1989; Myneni and Asrar, 1993); Sellers, 1985; Choudhury, 1987). Goward and Huemmrich (1992) noted how difficult it is to observe or quantify background effects in global scale imagery, although snow background was deemed to be of particular concern, introducing errors in the estimation of fAPAR in excess of 50% relative to more typical canopy backgrounds (soil and litter), where errors were in excess of ±15%.

A common misconception is that canopy background considerations are only important in sparsely vegetated, arid and semi-arid areas, where spectral variations in background are the greatest. However, most studies and simulations show NDVI background sensitivity to be greatest at intermediate levels of vegetation, comparable to humid and sub-humid land cover types, including open forest stands. Bausch (1993) and Huete et al. (1985) showed the influence of canopy background reflectance on NDVI values to be highest at LAI = 1 (~40% green cover) where the NDVI varied by 0.30 units for background reflectances that varied from 0.06 to 0.33 in the red. Background influences start to disappear at LAI > 2, which is where 'saturation' begins. The range in background reflectances becomes greater when snow, wetlands, and irrigated rice paddy fields are included.

Several approaches have been proposed to minimize background influences on vegetation indices. Richardson and Wiegand (1977) introduced the perpendicular vegetation index (PVI) which utilized a 'soil line' concept for site specific background corrections. The soil line is a "baseline" value of zero vegetation over a wide 'brightness' range of soil backgrounds, from which vegetation can be measured in NIR-red space, relative to the baseline. Clevers (1989) found the weighted difference vegetation index (WDVI) to greatly improve upon the estimation of LAI while minimizing background effects. Elvidge and Chen (1995) showed how narrower-band channels, as input to vegetation indices, reduce background-related problems present in broad-band

vegetation indices. Similarly, Hall et al. (1990) and Demetriades-Shah et al. (1990) have discussed the value of narrow-band, derivative spectra for reducing background effects. Major et al. (1990) proposed a series of ratio-based vegetation indices, which effectively estimated the slope of the vegetation isoline derived with a simple reflectance model (Baret and Guyot, 1991).

Some studies have utilized knowledge of vegetation isoline equations, derived from simple reflectance models, to produce vegetation indices which minimize soil background effects (Huete 1988: Major et al. 1990). The soil-adjusted vegetation index (SAVI), proposed by Huete (1988), uses vegetation isoline equations derived by approximating canopy reflectances by a first-order photon interaction model between canopy and soil layers (Huete 1987). This was further improved by Baret et al. (1989) yielding the transformed soil adjusted vegetation index (TSAVI) and by Qi et al. (1993b) with the modified SAVI (MSAVI).

Canopy background influences on vegetation indices are also atmosphere-sensitive, Huete and Liu (1994) found background influences on the NDVI to decrease greatly with increases in atmospheric aerosol contents and that at a horizontal visibility of 5km (turbid atmosphere), background influences became nearly zero. This was also observed with satellite imagery (Qi et al., 1993). Consequently, we anticipate canopy background problems to become more pronounced in MODIS-NDVI imagery due to the improved atmospheric correction algorithms being implemented. A feedback problem is evident whereby the improvement of one form of noise increases other forms of noise. Liu and Huete (1995) developed a feedback-based approach to correct for the interactive canopy background and atmospheric influences, incorporating both background adjustment and atmospheric resistance concepts. This enhanced, soil and atmosphere resistant vegetation index (EVI) was simplified to:

$$EVI = 2 \cdot \frac{(\rho_{nir} - \rho_{red})}{(L + \rho_{nir} + C_1 \rho_{red} + C_2 \rho_{blue})} \quad (3)$$

where ρ is 'apparent' (top-of-the-atmosphere) or 'surface' directional reflectances, L is a canopy background adjustment term, and C_1 and C_2 weigh the use of the blue channel in aerosol correction of the red channel (Huete and Liu, 1996).

2.2.8 NDVI saturation considerations

There are several explanations for the NDVI saturation problem over densely vegetated areas in which NDVI values no longer respond to variations in green biomass. The NDVI has been reported to be an insensitive measure of LAI at values exceeding 2 or 3. This is of concern since land use change detection, vegetation monitoring, net primary production, and scaling studies cannot be carried out in an NDVI 'saturated' mode (Townshend et al., 1991). Land cover classification based on multitemporal NDVI profiles would similarly be hampered. Gitelson et al. (1996) attributed this to the high sensitivity of the NDVI to the red (chlorophyll) absorption band, which also saturates quickly. Maximum sensitivity to chlorophyll-a (Chl-a) pigment absorption is at 670nm. For Chl-a concentration beyond 3-5 $\mu g/cm^2$, the

inverse relationship of reflectance at 670nm vs. chlorophyll concentration 'saturates' and is no longer sensitive despite a global range in chlorophyll concentrations from 0.3 to 45 $\mu g/cm^2$ (Vogelmann et al. 1994; Buschmann and Nagel 1993).

Gitelson et al. (1996) reported enhanced sensitivity could be achieved by replacing the red channel with a green channel, which was found to remain sensitive to chlorophyll-a over a wider range of concentrations. They proposed a green NDVI equation which was five times more sensitive to Chl-a concentration. Yoder and Waring (1994) similarly have used a green NDVI for improved estimates of photosynthetic activity in Douglas-fir trees. The potential, however, for improved vegetation analysis with narrower-band channels is also well demonstrated (Elvidge and Chen 1995). This is of concern to the MODIS-NDVI equation because the MODIS red channel is much narrower (620 - 670nm) and chlorophyll-sensitive than that of the AVHRR (580 - 680nm) and may thus saturate more quickly.

Although bandwidth may affect saturation, one must also consider the nature of the NDVI mathematical transform involving the red and NIR bands. The NDVI is a non-linear 'stretch' of the functionally equivalent, NIR/red ratio designed to confine its values from -1 to +1 (Deering, 1978). The stretch has the effect of enhancing low ratio values while compressing higher ratio values. As ratio values increase from 5 to 10 and 15, the corresponding NDVI values shift from 0.67 to 0.82 (20% increase), and 0.87 (6% increase). A further increase in the NIR/red ratio to a value of 20 yields very little change in the NDVI (0.90). The non-linear stretch has the effect of enhancing vegetation index values under low biomass conditions while compressing the NDVI values at high biomass conditions. This results in very low sensitivity to spatial and temporal variations in densely vegetated areas.

2.2.9 Canopy structural effects (biophysical interpretations):

Sellers (1985) calculated the variation of the NDVI with canopy greenness fractions and demonstrated how the presence of dry and dead plant material severely alters the relationship between NDVI and LAI. He showed the NDVI to vary greatly with leaf angle which alters the optical thickness of the canopy. He also showed that due to the non-linear nature of the NDVI-LAI relationship, the contribution of the bare ground fraction to the NDVI is disproportionately strong when equal amounts of greenness (LAI) are distributed differently, such as in clumps. The same LAI in smaller cover fractions yielded the lowest NDVI. Clevers and Verhoef (1993) used the SAIL canopy and PROSPECT leaf models to show how the main variable that influences vegetation indices is the leaf inclination angle distribution. The more planophile a canopy the greater the vegetation index value for a given LAI.

Because of the overwhelming influence of canopy structure on spectral reflectances and vegetation indices, it is very difficult to derive biophysical plant parameters directly from the VI. Many of the VI to biophysical parameter relationships involve site specific, regression plots which are subject to variability associated with canopy background, atmosphere, instrument calibration, sun angle, and view angle. It is necessary to accomodate the effects of the different factors when interpreting VI values, especially if

we are to detect deviations in behavior indicative of directional or 'global' change (Wickland, 1989; Prince and Justice, 1991). A direct approach would be to utilize a canopy radiative transfer model to handle the radiative transfer processes within the structure of the canopy. Alternatively, an indirect approach may be utilized whereby 'land cover type' empirical parameters are used in the translation from NDVI to LAI, green cover, or fAPAR.

2.2.10 Vegetation indices, summary

The MODIS VI's are envisioned as improvements over the current NOAA-AVHRR NDVI as a result of both improved instrument design and characterization and the significant amount of VI research conducted over the last decade. Many new indices have been proposed to further improve upon the ability of the NDVI to estimate biophysical vegetation parameters (Prince et al., 1994). However, the robustness and global implementation of these indices have not been tested and one must be cautious that new problems are not created by removing the 'ratioing' properties of the NDVI. The 'ratioing' properties of the NDVI were extremely vital when the NOAA-AVHRR production of the NDVI first began, particularly with un-normalized, uncalibrated, and uncorrected for atmosphere data sets. Since the MODIS NDVI product will utilize well-calibrated and atmospherically corrected, surface reflectances, one needs to re-assess the continued importance and benefits of 'ratios'.

On one hand there is a need for continuity, while on the other hand improvements to make the NDVI more quantitative are needed. In the next section of this algorithm, "Algorithm Description", we describe the implementation of multiple indices and assess their capability in improving vegetation monitoring and change detection.

In summary, the criteria for and definition of a global vegetation index includes:

- the index should maximize sensitivity to plant biophysical parameters, preferably with a linear response in order that some degree of sensitivity be available for a wide range of vegetation conditions and to facilitate validation and calibration of the index,
- the index should normalize or model external effects such as sun angle, viewing angle, and atmosphere for consistent spatial and temporal comparisons,
- the index should normalize canopy background (brightness) variations for consistent spatial and temporal comparisons,
- the index should be applicable to the generation of a global product, allowing precise and consistent, spatial and temporal comparisons of vegetation conditions,
- the index should be coupled to key biophysical parameters such as LAI and fAPAR as part of the validation effort, performance, and quality control.

The processing flow for optimized VI computation is shown below:

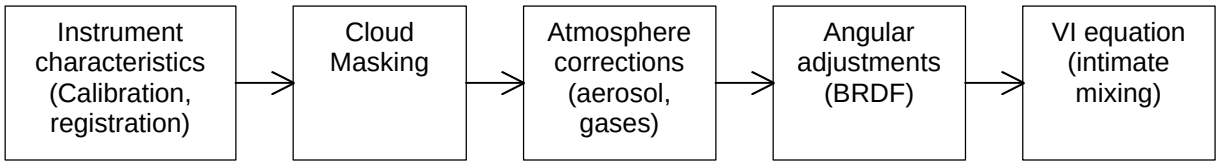

Improved vegetation sensitivity will be achieved with improved MODIS sensor characteristics and from the optimal utilization of MODIS sensor wavebands (Table 1). An "improved" index can increase sensitivity by enhancing the reflected signal from vegetation and by further normalizing internal and external "noise" influences (atmosphere, view and sun angles, canopy background). Atmospheric correction algorithms and atmospheric resistant versions of the NDVI will greatly minimize atmospheric sources of noise. Angular concerns (view and sun angles) will be handled through the use of BRDF models and improved compositing methods.

2.3 Instrument Characteristics

This section identifies those aspects of the instrument (Salomonson et al., 1989) critical to the VI parameters. The atmospherically corrected reflectances of MODIS bands 1 and 2 are directly input into the NDVI equation (Table 1). For the EVI, band 3 will also be utilized and band 4 is being tested to minimize chlorophyll saturation problems. The MODIS NDVI will not be completely the same as that derived from the NOAA-AVHRR instrument due to different sensor characteristics. An example is the narrower spectral widths of the MODIS bands, which eliminates the water absorption region in the NIR (Table 1) and also renders the red band more sensitive to chlorophyll absorption. This causes differences in the spectral response of vegetation canopies with consequent differences in vegetation index response (Teillet et al., 1997). New and improved atmospheric correction algorithms (Rayleigh scattering and aerosols) may further modify the red and NIR inputs into the NDVI equation, especially when surface reflectances derived from MODIS data are utilized.

MODIS (250 m, 500 m, and 1 km at nadir) is a whiskbroom sensor, similar to the AVHRR (1.1 km at nadir) and SeaWiFS (1.13 km at nadir) (Sea-Viewing Wide Field-of-View Sensor; Hooker et al., 1994) sensors, in which the pixel size increases with scan angle by as much as a factor of four. This is in contrast to the ADEOS-2 Global Imager (GLI, 250 m and 1 km at nadir) (*Global Imager;* Nakajima et al., 1998) and SPOT4-VEGETATION (1 km) (*Systeme Pour l'Observation de la Terre 4-VEGETATION;* Archard et al., 1994), which are pushbroom sensors with equal pixel sizes across all scan angles. The variable pixel sizes of MODIS will affect the interpretation of the vegetation index products and can be a source of error in evaluating anisotropic and biophysical properties of both heterogeneous and homogeneous land surfaces (Leeuwen et al., 1997a).

The MODIS repeat cycle is sixteen days, during which each point on the earth will be viewed with a range of view angles between ~55° in the forward and backscatter

direction. The scan angle is slightly lower than the view zenith angle due to the curvature of the earth. Complete coverage of the earth may further be attained within a scan angle of 20° in an 8-day period. Since the repeat cycle is 16 days, it is suggested to make the compositing period half of this time, thus 8 days. This number seems appropriate since it gives a consistent distribution of view angles and a possibility to cover all latitudes within small viewing angles, providing the best spatial resolution (250 m NDVI) and most accurate atmospheric correction.

Table 1: MODIS sensor characteristics in support of the vegetation index algorithm products.

#	Bandwidth (nm)	IFOV	Spectral Radiance[1]	Required SNR	Bandwidth Tolerance
1	620-670	250	21.8	128	+/- 4.0 nm
2	841-876	250	24.7	201	4.3
3	459-479	500	35.3	243	2.8
4	545-565	500	29.0	228	3.3
5	1230-1250	500	5.4	120	7.4
6	1628-1652	500	7.3	275	9.8
7	2105-2155	500	1.0	110	12.8

[1]=Watts/m2/µm/sr

Quantization:	12 bits
Scan width:	2330 km by 10 km (track) at 705 km platform altitude +/-55^0 cross track
Absolute Calibration:	+/-5%; +/-2% Reflectance
Spectral Stability:	stable to < 2nm;
Co-registration:	+/-20% along and off track at 1km with +/-10% goal.

Critical to the quality of the composited VI product will be the co-registration of the red and NIR 250m channels, spectral stability of the channels, pixel registration (Townshend et al., 1992) and calibration over time (Price, 1987). Actual day to day registration accuracy over a set composite period (16 days) will be determined post-launch. Geolocation accuracy is very important for temporal composites. The geometry of the detector (weighted triangular response) and the scan geometry determine the accuracy of the Earth location. The MODIS Land team requires the Earth location accuracy to be 0.1 pixels (for 1 km pixels) to support image registration for change detection and temporal compositing. Actual day to day registration accuracy over a 16 day period will be determined post-launch.

3 Algorithm Description

Vegetation indices are empirical measures of vegetation activity. The primary goal is to formulate a precise measure of spatial/ temporal variations in vegetation while maintaining an equation that is robust and sensitive over a global range of vegetation conditions. The conditions of robustness and sensitivity are essential in order for VIs to

be effective in intercomparisons of vegetation and extraction of biophysical parameters from arid regions to rainforest areas. The vegetation index equations presented here utilize the red and NIR reflected signals to isolate and enhance the 'green', photosynthetically-active vegetation component of a given pixel. The red and NIR responses are radiometrically calibrated, cloud-filtered, atmospherically corrected, spatially and temporally gridded, and adjusted for view angle influences to produce the level 3 vegetation index maps. The level 3 products are 16- and 30-day, cloud-free vegetation maps at 250 m, 1 km, and 0.25^{o} spatial resolutions.

In discussing VI robustness and sensitivity to vegetation "variations", it is useful to express such measures of performance in terms of various physical parameters of the vegetation such as LAI or %green cover. This also serves as a useful validation tool to ensure that spatial and temporal variations depicted through the VI maps are associated with 'real' changes in vegetation. In the following section the theory and physical principles from which the VI products are derived are presented along with an assessment of their robustness as precise measures of vegetation activity. The theoretical basis of the NDVI is first presented followed by a theoretical basis for an improved vegetation index.

3.1 Theoretical Description of Vegetation Indices

The theoretical basis for 'empirical-based' vegetation indices is derived from examination of typical spectral reflectance signatures of leaves (Figure 3.1.1). The reflected energy in the visible is very low as a result of high absorption by photosynthetically active pigments with maximum sensitivity in the blue (470 nm) and red (670 nm) wavelengths. Nearly all of the near-infrared radiation is scattered (reflected and transmitted) with very little absorption, in a manner dependent upon the structural properties of a canopy (LAI, leaf angle distribution, leaf morphology). As a result, the ***contrast*** between red and near-infrared responses is a sensitive measure of vegetation amount, with maximum red - NIR differences occurring over a full canopy and minimal contrast over targets with little or no vegetation (Figure 3.1.1). For low and medium amounts of vegetation, the contrast is a result of both red and NIR changes, while at higher amounts of vegetation, only the NIR contributes to increasing contrasts as the red band becomes saturated due to chlorophyll absorption.

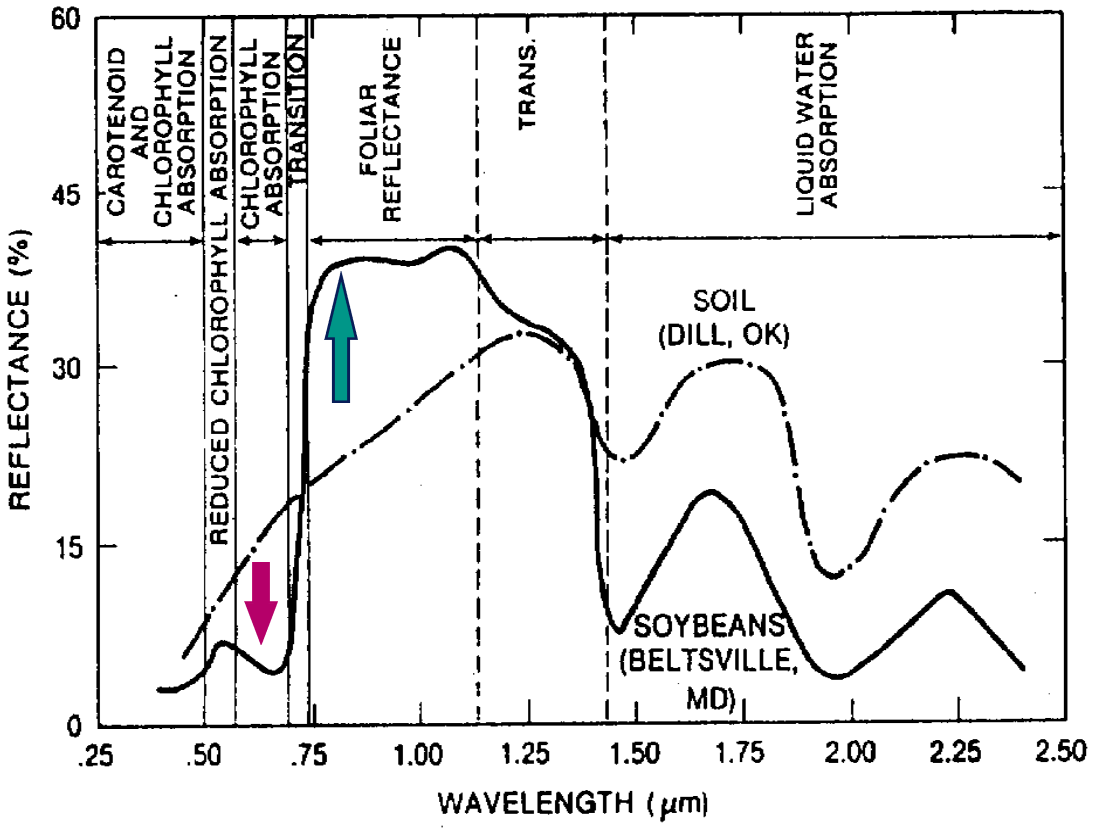

Figure 3.1.1: Spectral reflectance signature of a photosynthetically active leaf with a soil signature to show contrast (Tucker and Seller, 1986).

The red-NIR contrast can be quantified through the use of ratios (NIR/red), differences (NIR-red), weighted differences (NIR-k*red), linear band combinations (*x1* * red + *x2* * NIR), or hybrid approaches of the above. Vegetation indexes are measures of this contrast and thus are integrative functions of canopy structural (%cover, LAI, LAD) and physiological (pigments, photosynthesis) parameters.

The contrast between red and NIR canopy reflectances for a variety of canopy types and canopy backgrounds may also be depicted in graphical form, using the red and near-infrared reflectances as axes. In such a plot, a triangular, cloud of points is observed with well-defined boundaries, whether the data plotted are temporally variable reflectances of agricultural crops over the growing season (Figure 3.1.2a) or spatially variable reflectances of different land covers from desert to forests (Figure 3.1.2b).

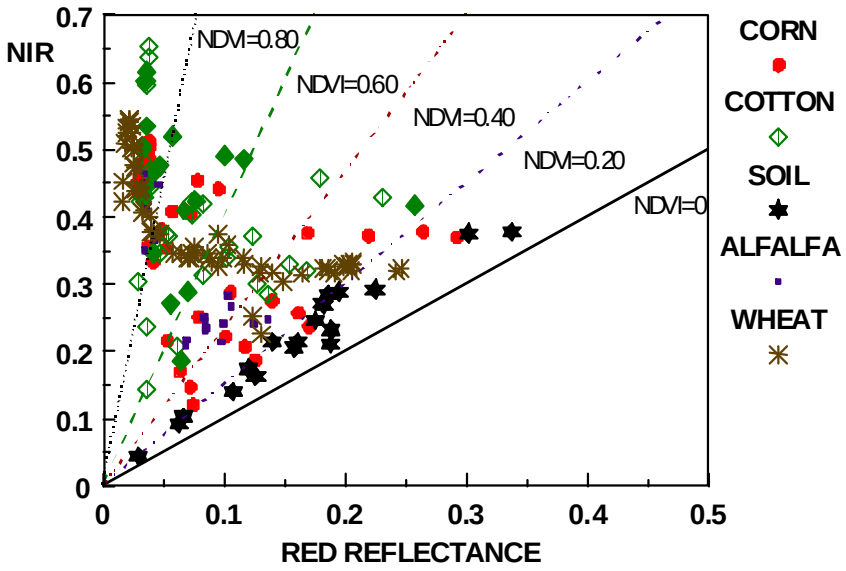

Figure 3.1.2a: Cloud of reflectance points in NIR-red waveband space for agricultural crops observed throughout the growing season.

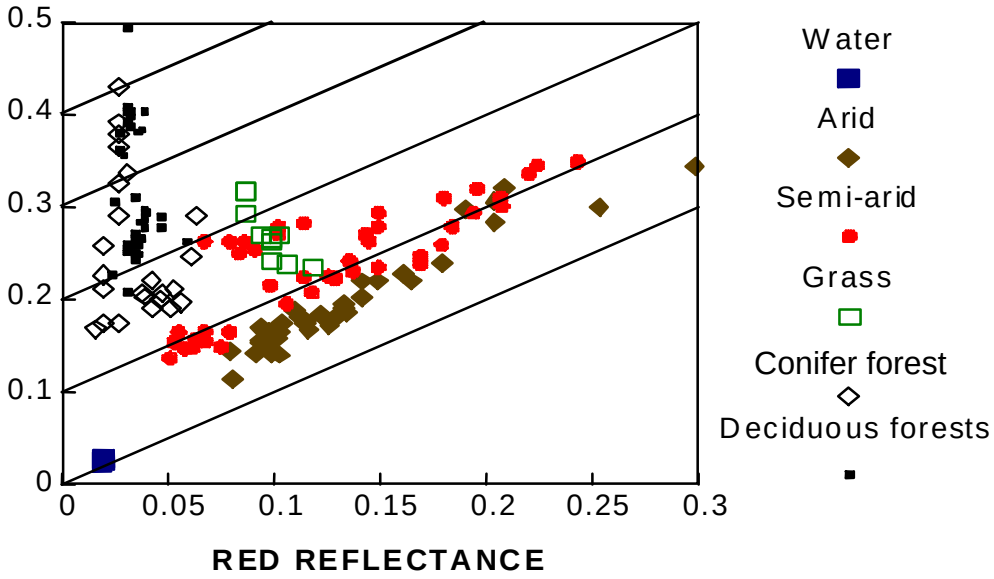

Figure 3.1.2b: Cloud of reflectance points in NIR-red reflectance space from Landsat TM for a wide range of land surface cover types.

In both cases there is a lower 'baseline' of pixels close to the 1:1 line, representing the lower boundary condition of vegetation. This baseline boundary condition can be further extended to include water targets (dark), snow backgrounds (bright), soils with variable mineralogies and litter and detrital material at variable stages of decomposition (bright to dark) or incorporation into the dark soil humus pool. The basic premise of the lower baseline is that only non-photosynthetic targets with low contrast in the red and NIR will occupy this area. The third apex represents dense vegetation which is at or

close to the lowest red values (chlorophyll-absorption) and highest NIR values. Note, the lower baseline involves non-photosynthetic canopy backgrounds and would not include a separate understory canopy, i.e., multiple canopy layers are all treated as overlying canopy and not background.

Pixels with increasing amounts of green vegetation shift away from the lower baseline toward the apex of maximum NIR and low red reflectance in a manner dependent upon the optical/ structural properties of the vegetation canopy and the optical properties of the canopy background (soil, snow, water, understory, etc.) (Figure 3.1.2). The greater the amount of 'green' vegetation present in a pixel, the greater will be the red-NIR contrast, and thus the shift away from the lower baseline. In Figure 3.1.2b, desert regions fall near the lower zero 'baseline', followed by semi-arid and grassland pixels. Closed forest canopies and open forests with green understories occupy the extreme left-hand portion, varying very little in the red ('saturation') with larger variations along the NIR axis (Figure 3.1.2), in accordance with expected optical behavior. The pixels inside the triangular cloud structure are generally 'mixed' pixels, with multiple responses from the vegetation and background components. Over 70% of the Earth's terrestrial surface is classified as "open canopies" with mixed background and vegetation signals (Graetz, 1990). The role of vegetation indices is to model the behavior and boundary conditions of the cloud of terrestrial-based pixels in NIR-red space and their associated variations in time and space.

Within the cloud of spectra we can identify pairs of red and NIR reflectances which represent equal amounts of a particular vegetation parameter. This may be described by the term "vegetation isoline" and may be derived via canopy radiative transfer models and/or observational data sets. Vegetation Index isolines, on the other hand, represent all combinations of red and NIR reflectance responses resulting in the same VI value. These are the model parameters which dissect the pixel data structure into various levels of vegetation amounts. They create the "gray levels" of the vegetation index from low to high. The concept of isolines essentially connect radiative transfer theory with vegetation indices and provide a basis for decoupling atmosphere and background signals from the vegetation signal.

3.1.1 Theoretical basis of the NDVI

The NDVI is a 'normalized' transform of the NIR to red reflectance ratio, ρ_{nir}/ρ_{red} , designed to standardize VI values to between –1 and +1;

$$NDVI = \frac{\left[\left(\rho_{nir} / \rho_{red}\right) - 1\right]}{\left[\left(\rho_{nir} / \rho_{red}\right) + 1\right]} \tag{4}$$

It is functionally equivalent to the NIR to red ratio and is more commonly expressed as:

$$NDVI = \frac{\left[X_{nir} - X_{red}\right]}{\left[X_{nir} + X_{red}\right]} \tag{5}$$

As a ratio, the NDVI has the advantage of minimizing certain types of band-correlated noise (positively-correlated) and influences attributed to variations in direct/diffuse irradiance, clouds and cloud shadows, sun and view angles, topography, and atmospheric attenuation. Ratioing can also reduce, to a certain extent, calibration and instrument-related errors. The NDVI, as a ratio, can be computed from raw digital counts, top-of-the-atmosphere radiances, apparent reflectances (normalized radiances), and partially or total atmospheric corrections. Although the units cancel out, the NDVI values themselves change so one must be consistent in how the NDVI is derived (Jackson and Huete, 1991). The extent to which ratioing can reduce noise is dependent upon the correlation of noise between red and NIR responses and the degree to which the surface exhibits Lambertian behavior.

Ratios create simple, red-NIR space, vegetation index isolines (Figure 3.1.3) of increasing slopes diverging out from the origin, i.e., slopes increase with vegetation amount and intercepts are independent of vegetation amount with a constant value of zero.

The NDVI efficiently shows increasing values from the baseline region to the 'green' apex. Furthermore, the large range in background brightness values, with little or no vegetation present, fall close to the 1:1 line showing that the NDVI is able to ratio out a significant portion of these spectral variations with NDVI values constrained to values slightly above 'zero'. The robustness of the NDVI is well established. As long as non-vegetation sources of spectral variation cause pixels to shift toward or away the origin, it is following an NDVI isoline or equal NDVI value. The NDVI is the only VI currently adapted to global processing and it is used extensively in global, regional, and local monitoring studies. It has also been used on a wide array of sensors and platforms from Landsat MSS and TM, to the NOAA-AVHRR series, SPOT, SeaWiFS, AVIRIS, and ground-based radiometers.

In the following sections, we analyze in detail the limitations of the NDVI both for the purpose of assessing product performance as well as to explore potential methods for improvement while maintaining a robust and operational algorithm. Up to now the burden of noise removal in satellite data is placed on the NDVI equation itself and thus the NDVI has the task of minimizing noise and simultaneously enhancing vegetation signals. The remotely-sensed spectral signatures, however, vary with both external and internal factors such as sensor calibration, atmosphere, sun- and view angles, and canopy background. Because of these influences, VIs also show variations which result in inaccuracies in estimating vegetation biophysical parameters. As advancements are made in minimizing many of the external influences, such as sensor calibration, noise removal, atmosphere correction, and BRDF modeling, other non-ratioing approaches, including canopy models, may be used to better depict vegetation spatial and temporal variations. For example, in contrast to the heritage AVHRR-NDVI product, the MODIS NDVI algorithm will utilize complete, atmospherically corrected, surface reflectance inputs. The instrument itself will be well calibrated and bandpasses are narrower, avoiding atmosphere contaminants such as water vapor.

The main disadvantage of ratio-based indices tend to be their non-linearities exhibiting asymptotic behaviors which lead to insensitivities to vegetation variations over certain land cover conditions. Ratios also fail to account for the spectral dependencies of additive atmospheric (path radiance) effects, canopy-background interactions, and canopy bidirectional reflectance anisotropies, particularly those associated with canopy shadowing.

3.1.2 Canopy background correction and de-coupling

Canopy background noise is inherent to the canopy, being intimately coupled to the vegetation signal. Red and NIR transmittance (extinction) through a photosynthetically-active canopy differs significantly due to the highly absorptive properties of leaf pigments in the red and the highly scattered (transmitted and reflected) signal in the NIR. Such band-disparate behavior, which includes canopy shadows, is not amenable to ratioing and the canopy transmitted and background reflected signal will vary with the 'brightness' of the background. The NDVI thus becomes very sensitive to background brightness variations, i.e., the NDVI isolines do not match nor approximate the 'true' vegetation isolines representing constant vegetation amounts over a range of background conditions. (Figure 3.1.3).

Unlike atmosphere correction algorithms and BRDF models, there are no independent methods to assess canopy background optical properties making it necessary to develop or modify a vegetation index equation to be as insensitive to background spectral variations as possible. In this way, the vegetation signal becomes de-coupled from the background and knowledge of the background brightness becomes unneccesary. This is also known as 'optimizing' the vegetation index so that they agree with basic physical, radiative transfer theory. This involves the design of VI's such that their isolines depict the parameter of interest while minimizing or canceling out undesirable variations, i.e., formulating a VI equation so that the VI isolines line up with the 'true' vegetation isolines. Non-photosynthetic background variations generally account for the principal source (axis) of spectral variations in global data sets.

3.1.3 Vegetation isolines and VI isolines

The vegetation isoline consists of the canopy reflectance points (i.e. a pair of NIR and red reflectance) obtained by changing the optical properties of the background with a fixed LAI and leaf angle distribution (LAD) for constant external conditions (sun- and view angle, atmosphere and so on). The slope and NIR- (or Y-) intercept of these isolines are functions of LAI when the LAI is the only variable other than canopy background brightness. In this case, the vegetation isoline indicates the relationship between NIR and red reflectance against the variation of the background brightness for a fixed LAI. Additionally, vegetation indices have their own isoline, or 'index isoline,' which is obtained through plots of reflectance points with the same index values.

The index isoline can be obtained algebraically and without knowledge of background brightness and LAI. The vegetation isoline represents the true behavior of a constant vegetation condition against a wide range of canopy background conditions.

These two types of isolines are typically different and usually do not coincide with each other (Baret and Guyot, 1991; Huete, 1988; Major et al., 1990; Qi et al., 1994) (e.g., NDVI in Figure 3.1.3), causing the NDVI value to vary with variations in the background brightness. In order to have a VI invariant to background brightness variation, the index isolines must be coincident with the 'true' vegetation isolines. The knowledge of the vegetation isoline is indispensable for this reason. It can be derived analytically using a simple representation of the canopy reflectance with some approximations. The summary of the analytical representation of the isoline is provided in the next section, and the derivation is explained in Appendix A.

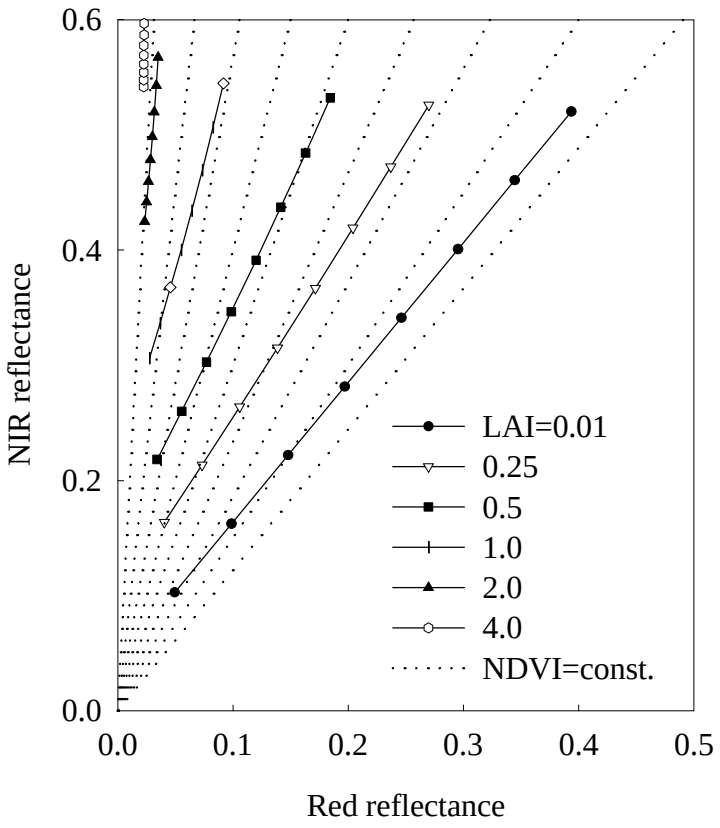

Figure 3.1.3: Plot of the vegetation points with the SAIL model (marks) for various LAI and soil reflectance and the NDVI isolines (dotted lines).

Vegetation isoline equation in red-NIR reflectance space

Yoshioka et al. (1999) presented a technique to derive vegetation isoline equations in red-NIR reflectance space for homogeneous canopies. They utilized a canopy radiative transfer model, known as the Cooper-Smith-Pitts model (or the adding method applied to the canopy reflectance modeling), which takes into account multiple interactions of photons between the canopy and its background surface. The higher order interaction terms between the two layers are truncated to derive a linear relationship of the red and NIR band reflectance. The technique consists of two model simulations, one with a perfect absorber as canopy background and the other with an arbitrary background to estimate the canopy optical properties necessary for the determination of the isoline parameters. These cases were independent of the canopy background optical properties for any specific site, hence, the results can be used for any type or series of background conditions to construct the vegetation isoline equation. The isoline equation and derivation were found to be useful for further study of two-band VIs and their variation with canopy background (Yoshioka, 1999).

We first define the red and NIR band reflectances from the coupled canopy-soil system of layers as ρ_R and ρ_N respectively. We also define the pure canopy transmittance and reflectance of the two bands. For the radiation coming into the canopy layer from the upper surface, the downward transmittance and upward reflectance are represented as $T_{\downarrow v\lambda}$ and $\rho_{v\lambda}$ where λ represents the band indices *N* and *R*. For the radiation coming into the same canopy layer from the bottom surface, the upward transmittance and downward reflectance are represented as $T_{\uparrow v\lambda}$ and $R_{v\lambda}$ respectively. Note that these four variables can be obtained by simulating the canopy reflectance with the perfect absorber as its background. The illustration of these variables is provided in Figure 3.1.4. We further define a logarithmic average of the downward and upward transmittance (square root of the canopy two-way transmittance) as simply $T_{v\lambda}$. We assume that the background reflectances of the red and NIR band follow a linear relationship known as the general soil line equation: the slope and the NIR-intercept of the soil line are represented by *a* and *b* respectively. We explain more detail of these variables in Appendix-A.

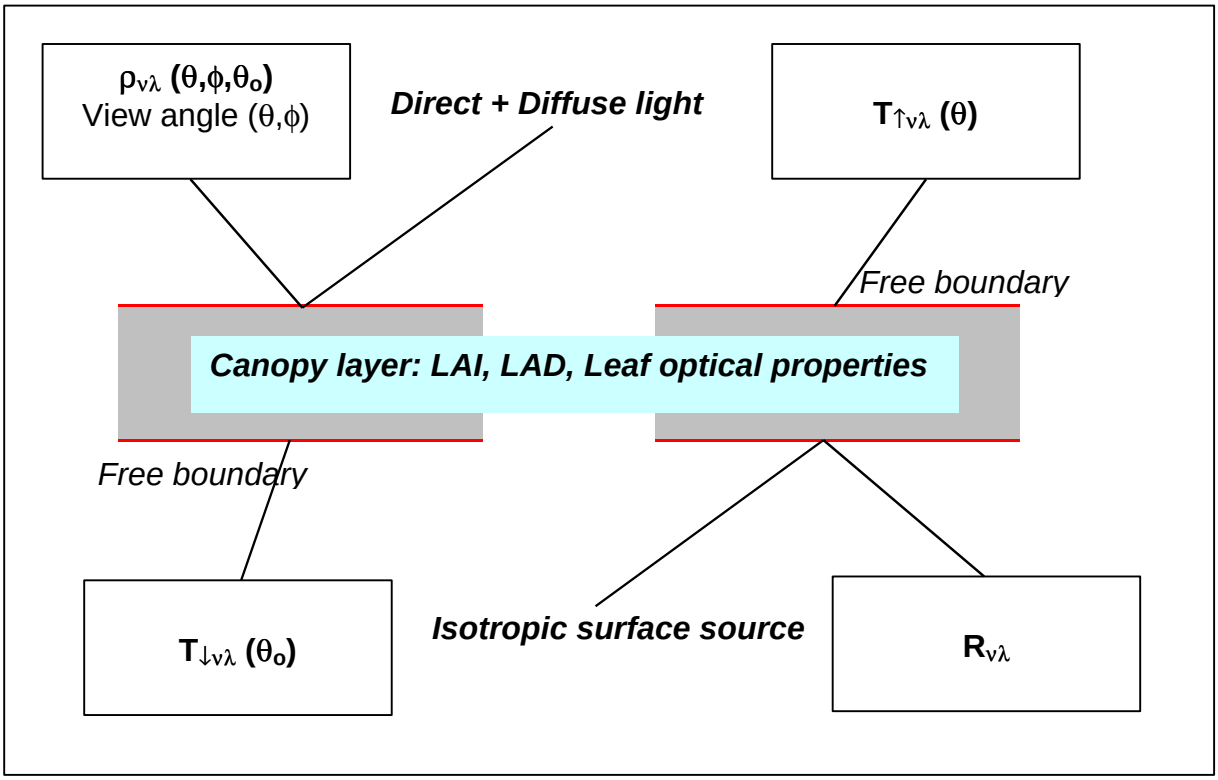

Figure 3.1.4: Illustration of canopy optical properties r_{vl}, R_{vl}, T^{-}_{vl},(q_0) and T_{-vl} (q)

Using these variables, the vegetation isoline equation can be written by the following form with some definitions,

$$\rho_N = a\gamma\rho_R + D + O^2, \tag{6}$$

$$\gamma = \frac{T_{vN}^2}{T_{vR}^2}, \tag{7a}$$

$$D = D_N - a\gamma D_R, \tag{7b}$$

$$D_N = \rho_{vN} + bT_{vN}^2, \tag{7c}$$

$$D_R = \rho_{vR}, \tag{7d}$$

$$O^2 = O_N^2 - a\gamma O_R^2, \tag{7e}$$

$$O_l^2 = \frac{T_{vl}^2 R_{vl} R_{sl}^2}{1 - R_{vl} R_{sl}} \tag{7f}$$

The meanings of the newly defined variables are as follows. γ is the ratio of the two way transmittance of the NIR band (square of the averaged transmittance) to that of the red band. γ depends only on the optical properties of the vegetation canopy as found in previous studies (Huete, 1988; Major et al., 1990). Note that the slope of the vegetation isoline is not only a function of vegetation optical properties but also the

slope of the soil line, *a*. D denotes the NIR- or Y-intercept of the vegetation isoline which is totally independent of the soil brightness. In other words, for fixed optical properties of the vegetation canopy, D does not vary with the soil brightness. D consists of D_N and D_R which are functions of only the NIR and red bands, respectively. Finally, O^2 represents the contribution of the higher order interaction terms in the red and NIR bands. If this contribution is small relative to $(a\gamma\rho_{vR} + D)$, then neglecting this term may not affect accuracy. Since many studies have shown the vegetation isoline to behave as a straight line (Baret and Guyot, 1991; Huete, 1988; Major et al., 1990; Qi et al., 1994), we suspect the contribution of the higher order interaction to be relatively small. This issue is discussed in (Yoshioka et al., 1999).

Comparison of vegetation isoline and simulation data

In order to demonstrate the derived vegetation isolines, we use the SAIL model. We employ a similar set of SAIL simulation inputs used by Baret and Guyot (1991) which involved three types of leaf angle distribution; planophile with 27 degree average leaf angle (ALA), extremophile with 45 degree ALA, and erectophile with 63 degree ALA (Goel, 1988). Ten discrete values of LAI were used (LAI= 0.01, 0.25, 0.5, 1.0, 1.5, 2.0, 2.5, 3.0, 4.0, 6.0). Leaf optical properties (Jaquemound and Baret, 1990) were as follows: for the red band, leaf reflectance and transmittance are 0.05 and 0.02 respectively, and for the NIR band, 0.465 and 0.490 are assumed. The soil reflectance values follow a soil line equation with parameters, *a* = 1.2 and *b* = 0.04, for seven soil red reflectance values of 0.05, 0.1, 0.15, 0.2, 0.25, 0.3, 0.35. A sun angle of 45 degrees (0.8 fraction of direct sun light) and nadir view angles were assumed for all the cases.

Figure 3.1.5 shows a comparison of the derived vegetation isoline with the SAIL reflectance values for the ten LAI values with seven different soil brightness for three types of leaf angle distribution (LAD). For simplicity only seven of the ten LAI values are plotted. As can be seen, the agreement of the estimated isoline and the simulated data are quite good, particularly for the darker soil (smaller soil reflectance). From Figure 3.1.5 we note two properties of a vegetation isoline: (1) the slope increases exponentially with LAI as found by Huete (1988) and Major et al. (1990) and, (2) the intercept increases with LAI, but reaches a maximum at LAI of about 2.0 (LAD dependent).

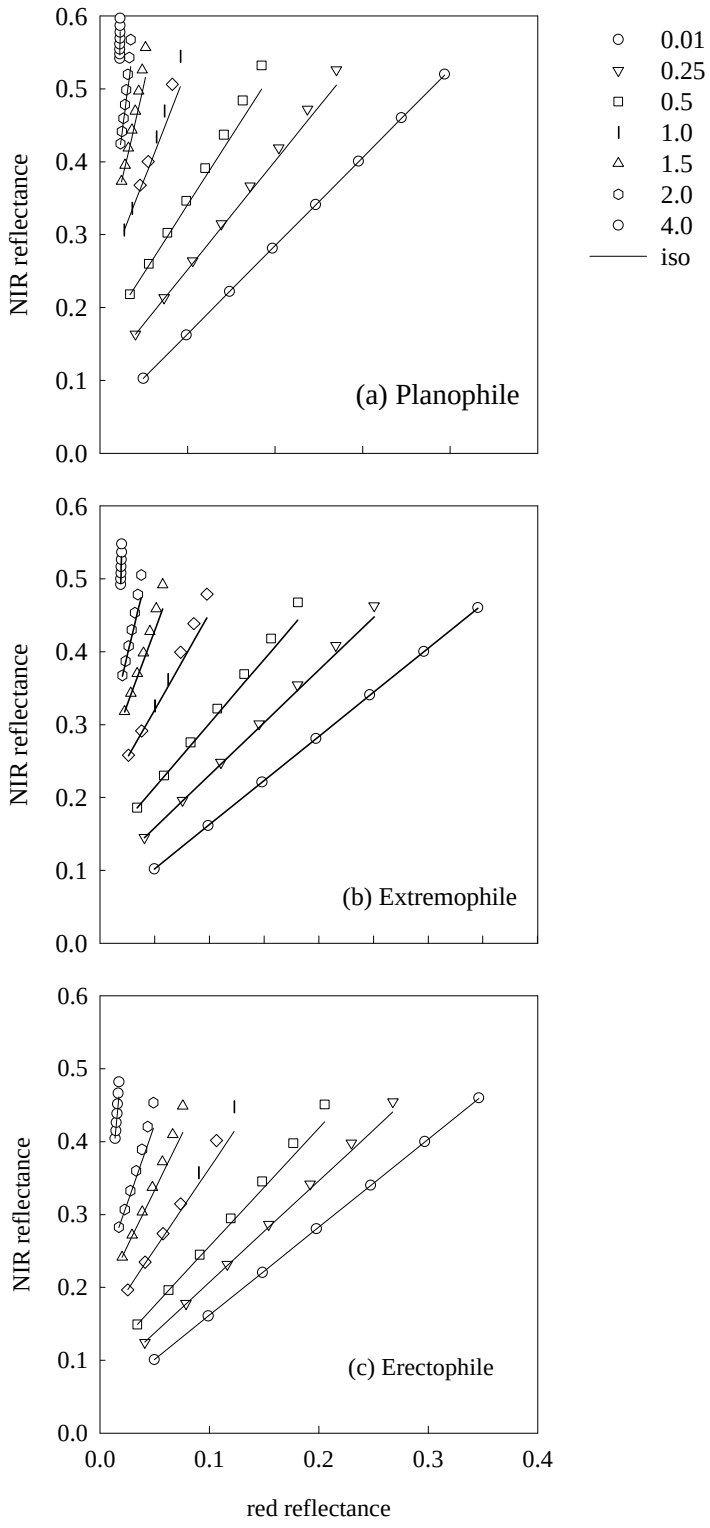

Figure 3.1.5: Derived vegetation isolines and the SAIL simulation data. The numbers in the legend denote the LAI. 'iso' means the vegetation isoline.

Comparison of vegetation indices by vegetation isoline and simulation data

The purpose of this section is to examine the accuracy of vegetation indices obtained by using the derived vegetation isoline equation. If the isoline equation yields reasonably accurate vegetation index values, then we can utilize the derived analytical representation, instead of using the simulated or experimental data points, to see the variability of vegetation indices against canopy background. The use of the vegetation isoline equation allows us to analyze the inherent behavior of these indices even analytically. One example would be the analytical expression of the NDVI only by the red reflectance for a fixed LAI. Using Eq. (6) after dropping the higher order interaction term to represent the NDVI yields,

$$NDVI = \frac{r_N - r_R}{r_N + r_R} \tag{8a}$$

$$\approx \frac{(ag - 1) r_R + D}{(ag + 1) r_R + D}. \tag{8b}$$

Since γ and D are both constant for a fixed LAI, the variation of NDVI depends on the value of the red reflectance unless D is equal to zero (where the NDVI isolines becomes identical to the vegetation isolnes). It also indicates that the variability of NDVI with background is inherent to this index unless D is equal to zero.

In this study we also investigated the estimation of SAVI by the isoline equation. SAVI is represented by

$$SAVI = \frac{\rho_N - \rho_R}{\rho_N + \rho_R + L}(1 + L) \tag{9a}$$

$$\approx \frac{(a\gamma - 1)\rho_R + D}{(a\gamma + 1)\rho_R + D + L}(1 + L), \tag{9b}$$

where *L* is a soil-adjustment factor which is assumed to be 0.1 in this study. This factor depends on the RT model.

Figures 3.1.6 and 3.1.7 show the plots of these two indices obtained from Eqs. (8b) and (9b), which truncates the higher order interaction term, and also the results of the SAIL model (including the higher order interaction model). The agreement of these two are good for all the cases (especially for the cases of lower background brightness).

The resulting equation effectively represents the known properties of the vegetation isoline, namely that the slope increases exponentially as LAI increases and that the Y-intercept increases to a maximum, rather than increasing monotonically. A technique to numerically obtain such an isoline for any fixed LAI/LAD is proposed and demonstrated with the SAIL canopy RT model (Appendix A). The technique consists of two simulations, one with the perfect absorber as a background and the other with an arbitrary, medium to dark, background to obtain the pure vegetation canopy reflectance

and the average canopy transmittance. Since the above two cases are independent of the actual soil brightness, one does not need to know the optical properties of the actual soil. The technique involved an approximation of the hemispherical canopy reflectance (from the bottom of the canopy layer, downward) by the pure canopy (perfect absorber background) reflectance.

This work has been shown to be useful as a way to investigate the inherent variation of vegetation indices (Yoshioka, 1999). Since the characteristics of the vegetation isoline are functions of the canopy optical properties and soil line parameters, this is an important starting point for the de-coupling of the canopy background from the vegetation layer to reduce the total number of simulations needed to obtain vegetation isolines numerically.

This approach is also significant to both the development and use of vegetation indices and to the use of canopy radiative transfer models for biophysical parameter extraction. For example, LAI retrieval by using the vegetation isolines is equivalent to find a particular vegetation isoline that goes through the target reflectance point in the red-NIR reflectance space. The big advantage of the use of vegetation isolines is to be able to minimize the background brightness effects, since the vegetation isoline equations do not include the soil reflectances. The ultimate goal of designing VI is to build the one whose index isolines overlap the vegetation isolines. The derivation of the vegetation isoline equations is an indispensable step toward this goal.

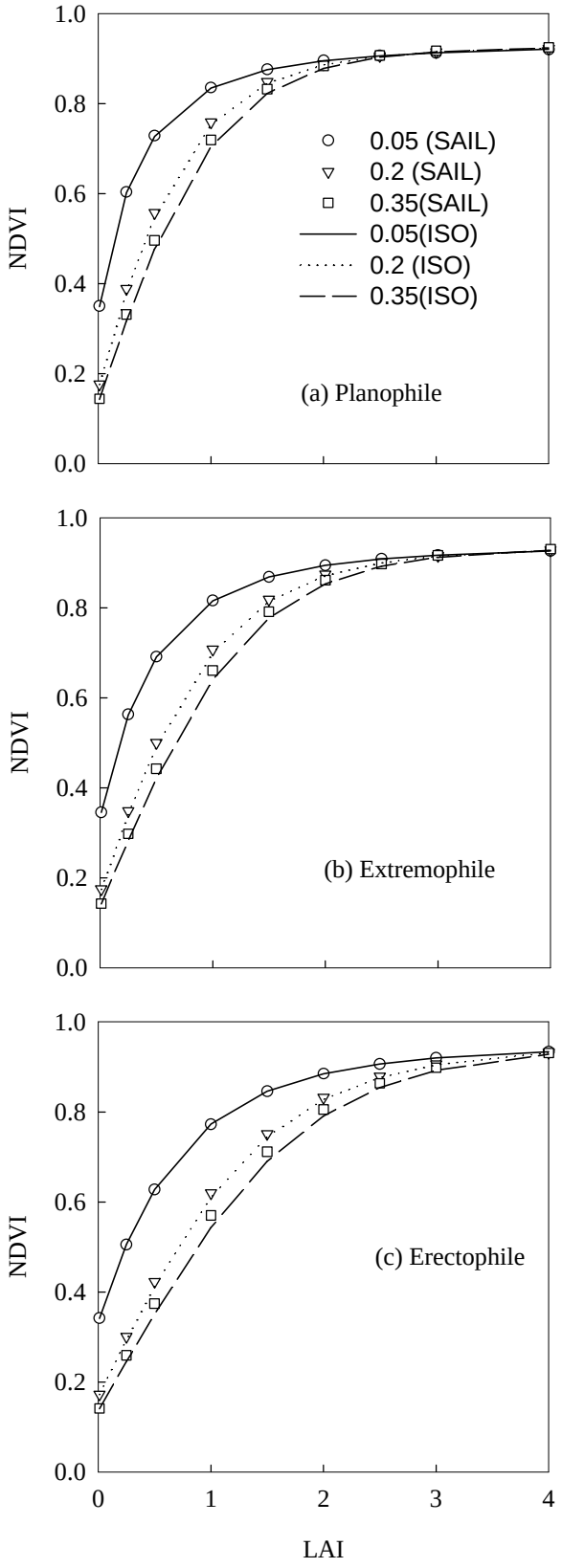

Figure 3.1.6: NDVI vs. LAI for the soil reflectance (red) of 0.05, 0.2, and 0.35. The marks are the SAIL model and the lines are the vegetation isolines.

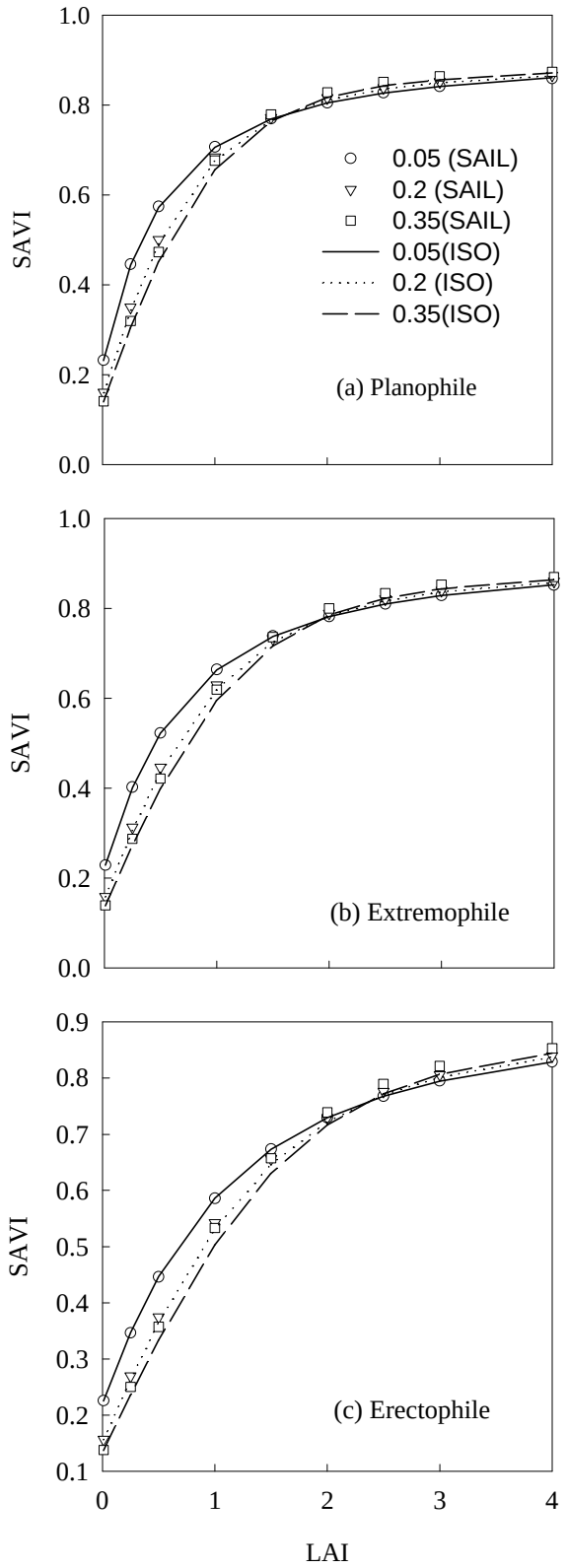

Figure 3.1.7: SAVI vs. LAI for the soil reflectance (red) of 0.05, 0.2, and 0.35. The marks are the SAIL model and the lines are the vegetation isolines.

3.1.4 Atmospheric aerosol effects on VIs

Aerosol scatters solar radiation before it reaches the surface and absorbs it again after it is reflected by the surface and before it reaches the satellite sensor (Kaufman and Tanré, 1996). Atmospheric aerosols (smoke, dust, and air pollution particles) have a significant effect on all of the vegetation indices, reducing the contrast between red and NIR reflectances, thus lowering vegetation index values, whether they are based on the NIR-red difference or the NIR/red ratio. The atmospheric aerosol influences on VI in two ways (Kaufman and Tanré, 1992): influence as path-radiance (additive effect), and influence through transmittance (multiplicative effect). The additive effect is determined regardless of the land surface (canopy-soil layers) brightness, thus has potential to be removed fairly well as demonstrated by several researchers (Kaufman and Tanré, 1992; Myneni and Asrar, 1994). On the other hand, the multipricative effect depends on the surface brightness, hence its minimization becomes more complicated.

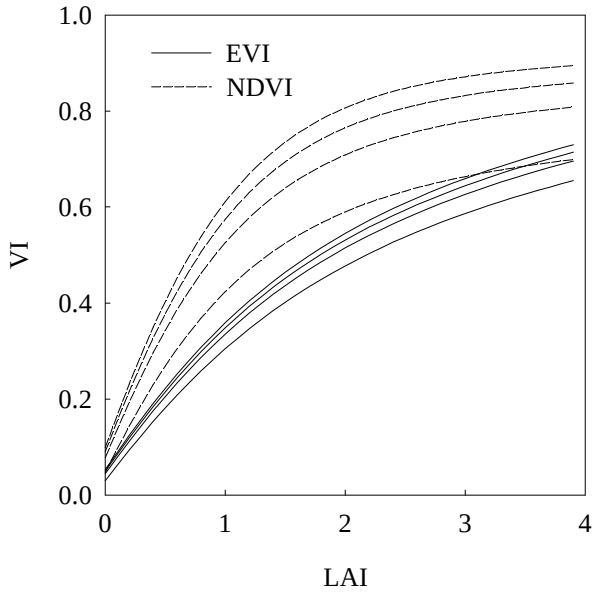

Figure 3.1.8: VI vs. LAI for different visibility with a constant soil brightness

Figure 3.1.8 shows the vegetation index - LAI relationships for a set of simulated atmospheres of four visibility levels (100km, 20km, 10km, 5km) under the same aerosol type (continental aerosol model of 6S). The figure clearly shows differences in the VI-LAI relationships for the different visibility levels.

There are basically two ways to minimize the atmospheric effects on VIs. The first way is somewhat obvious: the use of atmospherically corrected reflectances. There exists both direct and indirect correction methods, involving ground-based

measurements, radiative transfer models, climatology, and dark object subtraction approaches. However, to date, correction for aerosols over land has never been achieved on an operational basis (Kaufman and Tanré, 1996) and it may not be possible to implement a globally consistent, atmospheric correction scheme utilizing climatology and dark object subtraction methods. The second way is to use VIs stable to the atmospheric condition variations. There has been several vegetation index equations developed which mimimize aerosol influences indirectly on a pixel by pixel basis. This would be useful in smoke-filled areas, where the spatial variability of aerosols will exceed the resolution grid size of the aerosol products.

3.1.5 Atmospheric aerosol resistance in VIs

A major finding on atmospheric effect minimization is the use of the difference in blue and red reflectances as an estimator of the atmosphere influence level (Kaufman-Tanré, 1992). This concept is based on the wavelength dependency of aerosol scattering cross sections. In general the scattering cross section in the blue band is larger than that in the red band. When the aerosol concentration is higher, the difference in the two bands becomes larger. This information is used to stabilize the index value against variations in aerosol concentration levels. There are mainly two VIs using the approach: ARVI and EVI.

Kaufman and Tanré (1992) developed the atmospherically resistant vegetation index (ARVI) to minimize atmospheric-induced variations in the VI on a pixel by pixel basis. The ARVI utilizes the difference in radiance between the blue and the red channel, via a ρ^*_{rb} function, to correct the radiance in the red channel and stabilize the index to temporal and spatial variations in atmospheric aerosol content:

$$ARVI = \frac{\rho^*_N - \rho^*_{rb}}{\rho^*_N + \rho^*_{rb}}, \tag{10}$$

where

$$\rho^*_{rb} = \rho^*_R - \gamma(\rho^*_B - \rho^*_R), \tag{11}$$

and ρ^* are reflectances with prior correction for molecular scattering and ozone absorption. The performance of ARVI depends on γ, which is determined to minimize the path-radiance effect (Kaufman and Tanré, 1992) on ρ^*_{rb}.

The atmospheric resistance concept may also be incorporated into the SAVI to form a soil and atmospherically resistant vegetation index or SARVI (Kaufman and Tanré, 1992). Liu and Huete (1994), however, found soil and atmospheric influences to be interactive such that the removal of one source of noise increased the presence of the other. Consequently, a feedback term was utilized for simultaneous correction, resulting in an EVI formula written as:

$$EVI = \frac{\rho^*_N - \rho^*_R}{\rho^*_N + C_1\rho^*_R - C_2\rho^*_B + L}(1+L)\,. \qquad (12)$$

EVI is a modified NDVI with a soil adjustment factor, L, and two coefficients, C_1 and C_2, which describe the use of the blue band in correction of the red band for atmospheric aerosol scattering. An example of the smoke correcting capabilities of the EVI formula is shown in Figure 3.1.9. The coefficients, C_1, C_2 and L, are empirically determined as 6.0, 7.5 and 1.0 respectively.

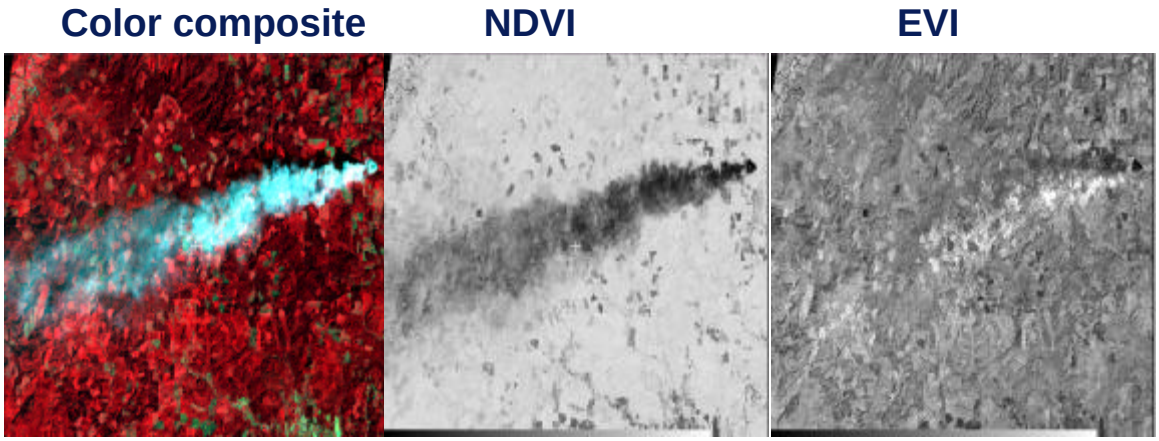

Figure 3.1.9: Landsat color composite and NDVI and EVI over a vegetated area with a smoke plume.

3.2 Vegetation Index Compositing Overview

The soon to be launched MODIS-EOS (*MODerate resolution Imaging Spectroradiometer - Earth Observing System;* Salomonson et al., 1989, Justice et al., 1998), will acquire global bi-directional radiance data of the Earth's surface under different solar illumination angles and atmospheric conditions, e.g. clouds. In this chapter, an improved vegetation index compositing scheme will be described, which minimizes cloud effects and angular variations due to the sun-target-sensor positions, and maximizes the global coverage. Vegetation index compositing is the process of combining multiple days of satellite reflectance, VI, angular and quality assurance data in an optimal manner to produce a VI image for a set temporal interval. The MODIS compositing scheme is designed to produce a spatially continuous VI image that represents the composite period, while filtering out clouds and data with bad integrity. Because the daily ascending MODIS orbits do not completely overlap, especially at the equator, two days are needed to get complete global coverage. However, the main reason why the daily orbits need to be composited over time to produce a spatially continuous and consistent VI image, is the extensive cloud cover over many parts of the Earth's surface. Also, the data from some orbits will be missing due to for example satellite calibration maneuvers, satellite data transmission interrupts or possibly data ingest problems at receiving stations. The described MODIS compositing algorithm will provide insight in the functioning of the algorithm and data processing aspects that were

taken into account to produce the VI's. Figure 3.2.1 displays a false color image of the green, red and NIR SeaWiFS reflectance bands for a days worth of orbits. Notice the incomplete coverage and the white cloud cover patches. The second image is a composition of 16 consecutive days of SeaWiFS data, obtained by a MODIS like composite algorithm. Figure 3.2.2 shows the angular variations for several SeaWiFS orbits of one day.

The data from satellite systems, such as the AVHRR (*Advanced Very High Resolution Radiometer*; Agbu et al., 1994) and SeaWiFS (Sea-Viewing Wide Field-of-View Sensor; Hooker et al., 1994 were used to test and prototype the MODIS VI compositing algorithms despite their differences in spatial and spectral resolution and orbital characteristics. The MODIS VI products will be produced at 250m, 1km and 28km resolution at set temporal intervals of 16 days and 1 calendar month. The input data for MODIS optical bands are 250m for the red and near-infrared reflectance bands and 500m for the blue and middle infrared bands. In the following sections the at-launch MODIS algorithms are presented with due consideration to the combined MODIS orbital, spectral, spatial, radiometric, calibration, temporal and upstream processing algorithm framework.

Beside mosaicking or compositing a set number of daily discontinuous data sets into one representative data set or product, the effect of sun-target-sensor geometry will influence the results significantly and gives a need to standardize the composited product as much as possible. The influence of variable sun-target-sensor configurations on derived vegetation indices can be standardized in various manners, including: (1) standardization of reflectances to nadir view angle at a solar zenith angle representative of the observations; (2) standardization of reflectances to nadir view angle and a temporally and globally constant solar zenith angle; (3) adjustment to a constant “off-nadir” view angle with a constant sun angle; or (4) the use of spectral (bi-hemispherical) albedos. Preliminary analysis (Huete et al., 1996) suggests that both the third and fourth approaches may enhance vegetation detection only over a limited range of land cover conditions (Kimes et al., 1984; Privette et al., 1996), and will result in overall decreased sensitivity from desert to forest, and present greater saturation problems in more densely vegetated canopies.

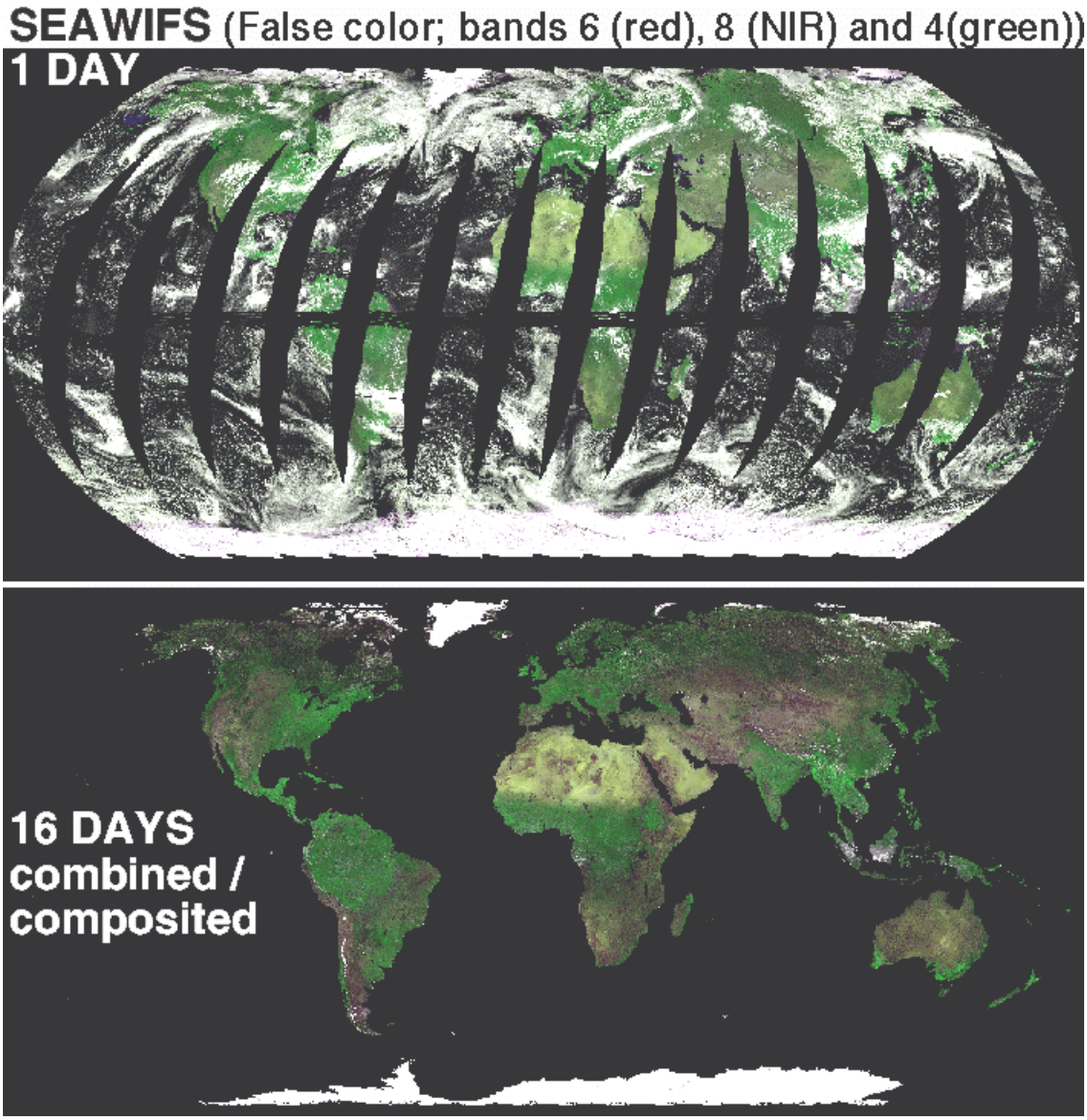

Figure 3.2.1: False color image (top) of the red, NIR and green SeaWiFS reflectance bands for one day worth of orbits. The incomplete coverage is due to the tilt-maneuvers above the equator and the swath width. White colors are clouds and snow/ice patches. The second image (bottom) is a composition of 16 consecutive days of SeaWiFS data, obtained by a MODIS like composite algorithm.

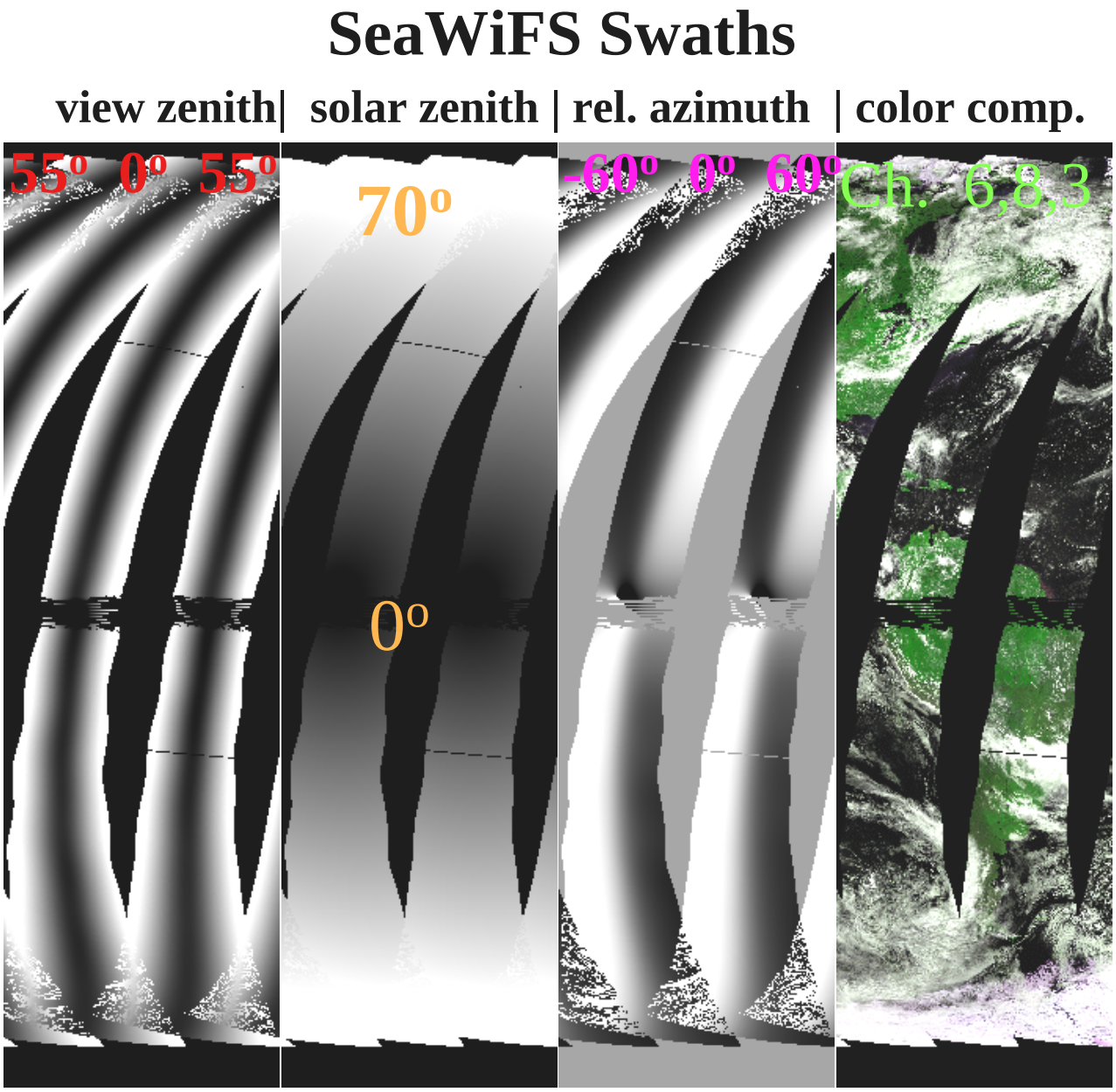

Figure 3.2.2: View and solar angular variations for several SeaWiFS orbits of one day. The right image is the color composite of red, NIR and green reflectance bands.

For the standard MODIS VI products, we propose to use the first method (Justice et al., 1998; van Leeuwen et al., 1999), and examine the other three approaches post-launch. Thus VI's will be computed after the standardization of reflectances to nadir view angle at a solar zenith angle representative of the observations. This method will involve the use of a BRDF model. The selection of the maximum NDVI value during a

composite period, constraint by view angle conditions, will be used as a back-up method in case the BRDF method can not be executed due to the lack of sufficient good quality observations.

3.2.1 MODIS VI compositing attributes

MODIS (250 m and 500 m at nadir) is a whiskbroom sensor (as well as AVHRR and SeaWiFS) causing the pixel size to increase with scan angle by as much as a factor of four. The satellite specific features associated with the spatial resolution of each pixel need to be considered when vegetation indices (VIs) are composited over time. The 16-day repeat cycle of MODIS results in variable pixel sizes in addition to a wide range of view and sun angles. Figure 3.2.3 shows a schematic diagram of the position of the sun and MODIS sensor and variations in view angle and pixel size. MODIS will image the earth's surface over a swath width of 2330 km over sensor viewing angles of ±55° cross-track with the effective view angle on the ground being slightly larger owing to the earth's curvature. Solar zenith angles across MODIS imagery may vary up to 20° from edge to edge of the 2330 km swath and also vary spatially with latitude and seasonally over the growing season. The backscatter direction of the MODIS swath has larger solar zenith angles than the forward scatter (Figure 3.2.3). The pixel size is increasing with view angle. The pixel size becomes an important variable in evaluating anisotropic and biophysical properties of both heterogeneous and homogeneous land surfaces. This introduces a source of error in that the BRDF characteristics of large pixels are not necessarily the same as those of small pixels (Leeuwen et al., 1997a).

After applying atmospheric corrections and processing the radiance data into surface reflectance data, these satellite systems capture the strong anisotropic reflectance properties that vary with land cover type, relative amounts of characteristic vegetation and soil components within each pixel, and sun-earth-sensor geometry. Therefore, some knowledge of the bi-directional reflectance distribution function (BRDF) is a requirement for successful utilization of directional reflectance data and vegetation indices, and the derivation of land cover-specific biophysical parameters (Cihlar et al., 1994a). However, due to frequent cloud cover and sensor-sun-earth geometric characteristics, the reflectance data needs to be composited in time and space to allow for temporal and spatial continuous monitoring of vegetation dynamics.

The atmospheric correction and cloud-screening approach to be used for MODIS are both significantly improved over the AVHRR approach. The experience of working with AVHRR data aided notably in the development of the MODIS product algorithms. In the following sections we demonstrate why the Maximum VI Value Composite (MVC) approach is less desirable for compositing MODIS data.

Fundamentally, the MVC is not appropriate for the atmospherically corrected surface reflectance data and vegetation indices to be generated by MODIS algorithms for several reasons. In the EOS era, surface anisotropy and bidirectional reflectances will become more pronounced as a result of improved atmospheric removal algorithms (Vermote et al., 1997a, 1997b), which will accentuate differences in surface bidirectional reflectances resulting from canopy structural influences (Cihlar et al.,

1994a). VIs computed from atmospherically-corrected surface reflectance data will therefore be strongly biased toward off-nadir viewing and larger solar zenith angles, where more vegetation is viewed or illuminated by the sensor.

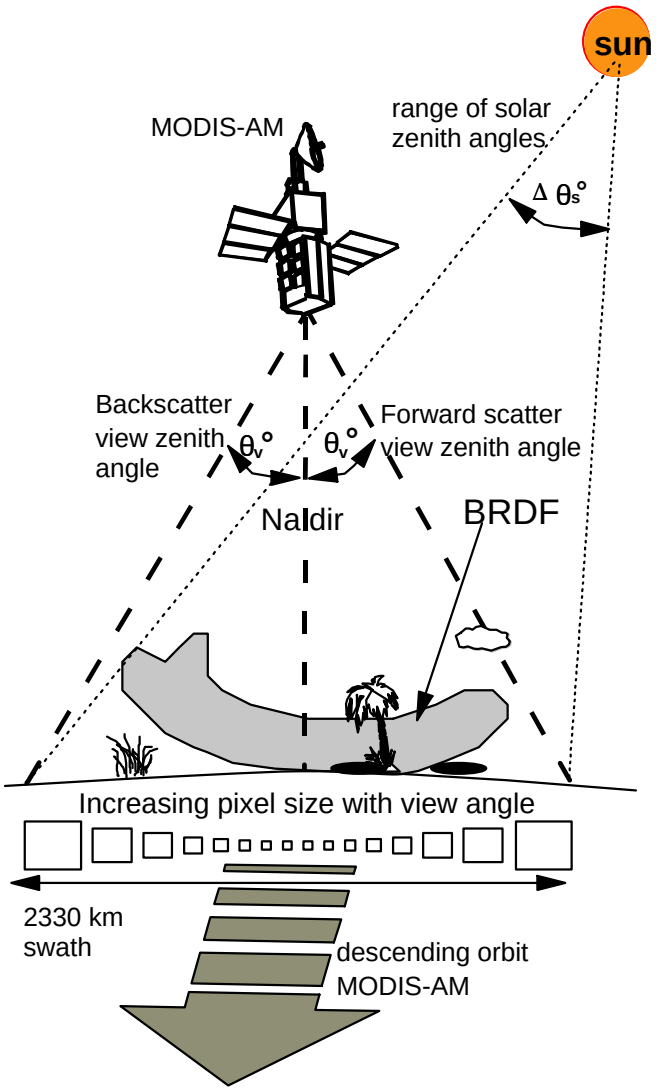

Figure 3.2.3: Illustration of MODIS data acquisition on the EOS-AM platform (not to scale). The bidirectional reflectance distribution function (BRDF) changes with view and sun geometry. Notice the shadow caused by clouds and canopy. MODIS pixel dimensions, cross-track and along-track, change with scan angles: 0° - 250 x 250 m; 15° - 270 x 260 m; 30° - 350 x 285 m; 45° - 610 x 380 m (computed for the fine resolution red and NIR detectors; 250 m at nadir on the ground).

In addition, the atmospheric correction is less accurate at off-nadir view angles if the coupling between the BRDF and the downward radiance at the surface level is not taken into account (Vermote et al., 1997a). Pixels with off-nadir viewing angles also have more distortions and are coarser in size, i.e., less detail. Furthermore, the MVC method will overestimate NDVI values, which will result in an overestimation of vegetation biophysical parameters and will contribute to the saturation of the NDVI.

The MVC criterion applied to MODIS data will thus result in the selection of off-nadir, distorted and less radiometrically accurate pixels, and deviate from the primary goal of working with the finest (nominal) resolution 250m NDVI data sets. BRDF corrections of AVHRR reflectances to a standard nadir view angle have been shown to improve the accuracy of the composited NDVI (Roujean et al., 1992; Cihlar et al., 1994a; Wu et al., 1995). Therefore, the MODIS compositing criteria will be weighted more toward angular considerations. This is done by incorporating a BRDF compositing approach, which has the goal to standardize the VI to nadir view and representative or constant solar angles. The MVC algorithm will be used as a 'backup' composite scenario in case a BRDF correction cannot be applied and if the MODIS atmospheric correction and the MODIS cloud mask are found or reported to be inaccurate. Patchiness in the VI imagery due two the dual composite scenario is not expected to be more than in the current MVC compositing schemes where angles and days selected may shift in large blocks.

3.2.2 MODIS vegetation index compositing goals and considerations

The MODIS vegetation index composite scenario was developed within the EOS (Earth Observing System) framework of providing more accurate products to monitor changes in the Earth system.

The main MODIS VI compositing goals are to:

- provide accurate and cloud-free vegetation index (VI) imagery over set temporal intervals,
- maximize global and temporal land coverage at the finest spatial and temporal resolutions possible,
- standardize variable sensor view and sun angles,
- ensure the quality and consistency of the composited data,
- depict and reconstruct phenological variations,
- accurately discriminate inter-annual variations in vegetation.

With the fore-mentioned compositing goals in mind, the following considerations are also of importance in the design of the MODIS vegetation index compositing algorithm:

- The pixels with the smallest view zenith angle will have the finest spatial resolution. This is 250 m for the red and NIR detectors. Realistically, the 250 m pixel size will increase to over 1 km across track at the edges of the scan (55°) and up to 500 m along track (Figure 3).

- Spatial degradation and blurring increase greatly with off-nadir view angles (Moody and Strahler, 1994), and off-nadir pixels will thus be more difficult to register than nadir pixels.
- Established biophysical parameter relationships with vegetation indices are based upon nadir-viewing angles.
- Vegetation index "saturation" problems become greater with off-nadir view and larger solar zenith angles.

3.2.3 BRDF

Vegetation indices are affected by variations in bidirectional reflectance factors, which vary greatly as a function of sun-target-sensor geometries (Walter-Shea et al., 1997. Since the VI tends to increase with both larger view and larger solar zenith angles, the resulting variability in both view and solar zenith angles are important for inter-comparison of vegetation covers at different latitudes and in different seasons, and should be considered in the VI compositing algorithm if we are to maintain "global" VI robustness. BRDF model parameters can be used to normalize and interpolate the surface reflectance to nadir view angles. However, the sun angle variability will be minimally incorporated in the BRDF correction, since the data necessary to standardize to a certain sun angle for each composite time interval (16 days in the case of MODIS) is very limited, and thus would be less accurate outside of the observed sun angle range. More research is needed to determine the most accurate method to extrapolate satellite observations to a standard sun angle throughout the year. Therefore, the solar zenith and azimuth angles will be included with the composited data (reflectance and vegetation index data) to be used for post-process standardization of the vegetation indices.

Numerous canopy bidirectional reflectance distribution function (BRDF) models have been developed to account for the anisotropy in land reflectances as a function of view and solar zenith angles. However, a BRDF model must be robust and operational on a global scale. Our approach is to use the simple Walthall model (Walthall et al., 1985) to standardize the reflectance data to nadir and compute nadir-based VIs. This has been shown to be superior to a maximum NDVI (MVC) approach (Leeuwen et al., 1996). Cihlar et al. (1994a) successfully used the Walthall model with AVHRR data for a range of vegetation types at a regional scale. The BRDF approach estimated nadir-equivalent VIs better than the MVC, which overestimated the nadir-equivalent NDVI.

The results from the BRDF approach are also thought to best represent the state of the land surface by involving several cloud-free observations. However, the 16-day repeat cycle of MODIS can result in variable BRDF characteristics (Leeuwen et al., 1997a) because the multi-angle reflectance values are acquired from pixels that vary in size during these sixteen days (Figure 3.2.3). In this case, the uncertainty in the VI will depend on spatial resolution and the angle-distribution at which the data was obtained, the heterogeneity of the surface area, and the choice of BRDF model (Leeuwen et al., 1997a). Increasing degradation of the spatial resolution with off-nadir view angles will minimally affect the nadir-interpolated reflectance values and resulting VI values if the

multi-angular observations are equally distributed in view angle space (Leeuwen et al., 1997a). Nadir-equivalent reflectance retrievals for Fallow and Aspen vegetation, using the Walthall model and simulated MODIS pixel size degradation for the 250 m at nadir detectors, introduced an uncertainty in the NDVI of 0.011 and 0.008 respectively (Leeuwen et al., 1997a). Off-nadir spatial degradation will impact the MODIS 1 km and coarser VI products less since the input to these products are based on finer resolution (250 m and 500 m) data sets that are aggregated to 1 km.

Privette et al. (1997) compared many linear models as described by Wanner et al. (1995), and found that nadir interpolation was best achieved with the Ross-thick/Li-sparse BRDF model over many vegetation types (data sets collected with the PARABOLA; Portable Apparatus for Rapid Acquisition of Bidirectional Observations of Land and Atmosphere; Deering and Leone, 1986). Leeuwen et al. (1996) found the Walthall model to perform best for nadir-equivalent vegetation indices for most vegetation types (Advanced Solid State Array Spectroradiometer (ASAS) data sets). The Walthall model was found to work equally well as Roujean's BRDF model. The Ross-thick/Li sparse BRDF model caused a few outliers when used in the forward modeling mode to derive nadir reflectance values. Experience with ASAS and AVHRR data showed the Walthall model to be more robust than most of the other linear models. The Walthall model also requires the least number of floating operations per pixel, which is an important consideration in the production of a global VI product at 250 m resolution and 16-day temporal intervals.

3.2.4 Compositing period

Variable composite periods have been used to obtain cloud free NDVI data on a global scale. The minimum compositing period is limited by cloud cover frequency and may vary from every 5 days at higher latitudes to as long as 30 days or more in some humid tropical areas. NDVI composite periods have varied among 7, 9, 10, 11 and 14 days and monthly intervals with variable (1 km to 1°) spatial resolutions (Townshend, 1994). The composite period depends on its application and the availability of cloud free data on a global scale. Shorter compositing periods will pick up more dynamic land cover changes and allows one to combine compositing periods to monthly or bi-weekly periods. However, the shorter the compositing period, the greater the likelihood of cloud-affected or missing pixels in the composited image. The 16-day MODIS compositing cycle was designed according to the EOS-AM1 16-day repeat cycle and consequent attainment of the full array of viewing angles. This seems appropriate since it provides the opportunity to avoid clouds as well as to cover all latitudes within a range of small viewing angles. The monthly compositing cycle is based on demand and heritage of the user community.

It is unclear if the nadir AVHRR repeat cycle of approximately 9 days versus the 16 days of MODIS will affect the derivation of nadir-equivalent reflectance values from BRDF models for either sensor. Based on the repeat cycle, more nadir AVHRR then nadir MODIS observations are possible within a 16-day period. The 2700km swath width of AVHRR will result in a larger view angle range compared to the 2330km swath width of MODIS. Furthermore, the AM overpass of MODIS results in less cloud cover in

comparison to the cloudier afternoon overpass of the AVHRR. Since data from both sensors will have random dropouts of observations due to clouds, the distribution and range of view angles will be different, but not likely to affect the final nadir-equivalent VI product significantly. The expected retrieval accuracy of bidirectional reflectance values over land for MODIS angular sampling are reported by Lucht (1998) and Wanner et al. (1997).

3.2.5 MODIS data stream

MODIS input products that are relevant to the vegetation index are shown in Figure 3.2.4. The MODIS data streams (top of the atmosphere (TOA) calibrated radiance, cloud mask, atmospheric correction and surface reflectance, vegetation indices) is set up to flow into the product algorithms in a predetermined order. For a tractable and best solution to the compositing algorithm it was logical to input the atmospherically corrected surface reflectance data in combination with the cloud mask and use as many “good” observations as possible during a composite period. This runs counter to the MVC scenario based on non-atmospherically corrected reflectance data as suggested by Cihlar et al. (1994a) for the AVHRR data. If changes in the vegetation index compositing algorithm call for a different processing scenario, significant changes in the EOS production system can be required, including hardware, software and networking redesign and implementation.

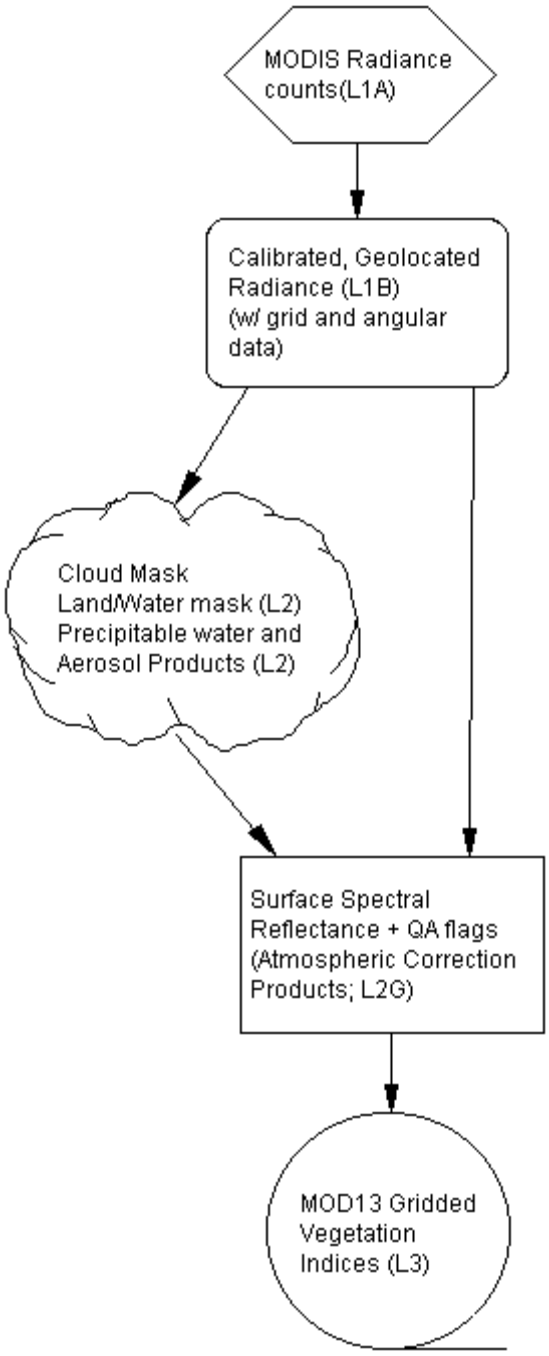

Figure 3.2.4: Flow diagram showing the relationship of relevant MODIS Land and Atmosphere Products (Level 1-L1; Level 2 - L2; Gridded L2-L2G; Level 3 - L3) that are required to generate the gridded, composited vegetation indices.

3.2.6 MODIS VI composite algorithm

The logic of the compositing algorithm is based on the MODIS specific input data and theoretical knowledge of radiative transfer and surface reflectance anisotropy. The compositing algorithm will optimize the choice of the best VI representative for each

composite period, spatial resolution and global land extent. The compositing algorithms will rely on information from the cloud mask (Ackerman et al., 1996), atmospheric correction (Vermote, 1997a), view zenith angle, solar zenith angle, relative azimuth angle, geo-registration (Wolfe et al., 1998), and surface BRDF normalization. The algorithms utilize the information in the reflectance-quality assurance (QA) flags, partially derived from the MODIS cloud mask product, to pre-process the atmospherically corrected reflectance data of MODIS bands 1, 2, and 3 and 7 (red, NIR, blue, MIR) over land only. Land pixels with clouds, shadow, and bad data integrity will be excluded from the VI composite.

The MODIS algorithm selects all the reflectance data for a 16-day period, based on data integrity and cloud flags, and fits the Walthall BRDF model to the individual band data. The empirical BRDF model developed by Walthall et al. (1985), is used to derive nadir reflectance data for each pixel and 16-day intervals:

$$\rho_\lambda(\theta_v, \phi_s, \phi_v) = a_\lambda \theta_v^2 + b_\lambda \theta_v \cos(\phi_v - \phi_s) + c_\lambda \quad (13)$$

where the atmospherically corrected reflectance (ρ_λ) values for the appropriate wavelengths (λ; i.e. red, NIR, blue) are modeled as a function of the view zenith angle (θ_v), and sun (ϕ_s) and view (ϕ_v) azimuth angles. The model parameters a_λ, b_λ and c_λ are obtained using a least squares curve fitting procedure. "c_λ" is equal to the reflectance at nadir view angle. The prevalent sun angle and VIs will be computed from the composited and normalized surface reflectance observations. Based on our experience with AVHRR and ASAS data, a minimum of 5 surface reflectance observations are currently required for a stable BRDF model (Walthall's) inversion. Nadir interpolated values will be rejected when the resulting reflectance values are negative or when the NDVI is higher or much lower than the MVC based NDVI ($0.3\text{-}NDVI_{MVC} <= NDVI_{BRDF} <= NDVI_{MVC}+0.05$). These thresholds are set to avoid the inclusion of residual cloud effects resulting in the BRDF results to be off. If observations during a 16-day interval are unequally distributed in view angle space (e.g. backscatter observations only) or unequally affected by undesirable atmospheric conditions (e.g. smoke, clouds), negative nadir reflectance values can be derived from the BRDF model. Negative reflectance values can also be generated if inaccurate atmospheric parameters (e.g. aerosol optical thickness) are used to realize atmospheric corrections.

Since not all pixels will have 5 or more cloud-free data points during a 16-day period, a back-up algorithm is used which selects the highest NDVI based on two cloud-free pixels with their view angles closest to nadir. The absolute view zenith angle is taken for all cloud-free pixels after which their view angles are sorted in ascending order. The NDVI is computed for the observations with the two smallest view zenith angles, after which the MVC rule is applied and the most optimal observation selected. This will be referred to as the constraint view angle maximum value composite (CV-MVC) approach. If only one cloud-free observation is available over the composite period, this observation will automatically be selected to represent the composite period. If all data during a 16-day period were affected by clouds, based on the cloud flags, the view angle constraint for the MVC method will be released and the VI will be calculated for all days and the best pixel chosen based on the maximum value of the

NDVI among all observations. The 16-day 250 m and 1 km VI products (MOD13A1 and MOD13A2; MODIS VI product numbers 13A1 and 13A2; Appendix B) will each be produced with similar algorithms as described in previous sections. Figure 3.2.5 gives a schematic overview of the 16 day MODIS VI compositing scenarios for the 250m and 1 km products.

The monthly 1 km and CMG (climate modeling grid resolution) VI products are created by a time-weighted average of the reflectance fields in the 16-day-1 km and CMG-16-day composited products that fall within a particular month and the ones that overlap in the beginning and end of each calendar month. The CMG resolution will be the mean of all “good” 1km composited reflectance data, after which the VIs will be computed. It must be noted that the 16-day products do not run in sink with the beginning of each calendar month. Only on the 1st of January of each calendar year will all the products be initialized. Figure 3.2.6 gives a schematic overview of the monthly MODIS VI compositing scenarios for the 1km and CMG products.

Monthly and spatially aggregated (climate modeling grid resolution- CMG- 25 km) VI products (MOD13A3, MOD13C1 and MOD13C2; Appendix B) will be based on the 16-day/1 km VI product. The aggregated CMG (0.25°) NDVI and EVI composites are calculated from cloud-free and atmospherically corrected, gridded surface reflectances which were used to produce the VIs at 1 km resolution. The number of cloudy and/or bad pixels are counted for each CMG pixel to compute the percentage cloud cover. Per pixel statistics also include: mean NDVI standard deviation of the NDVI, mean EVI, standard deviation of the EVI, cloud cover, percent with vegetation. The standard MODLAND QA will be used for all products. Figure 3.2.7 gives a schematic overview of all the input and output files needed to produce the MOD13 VI products and their associated science data sets.

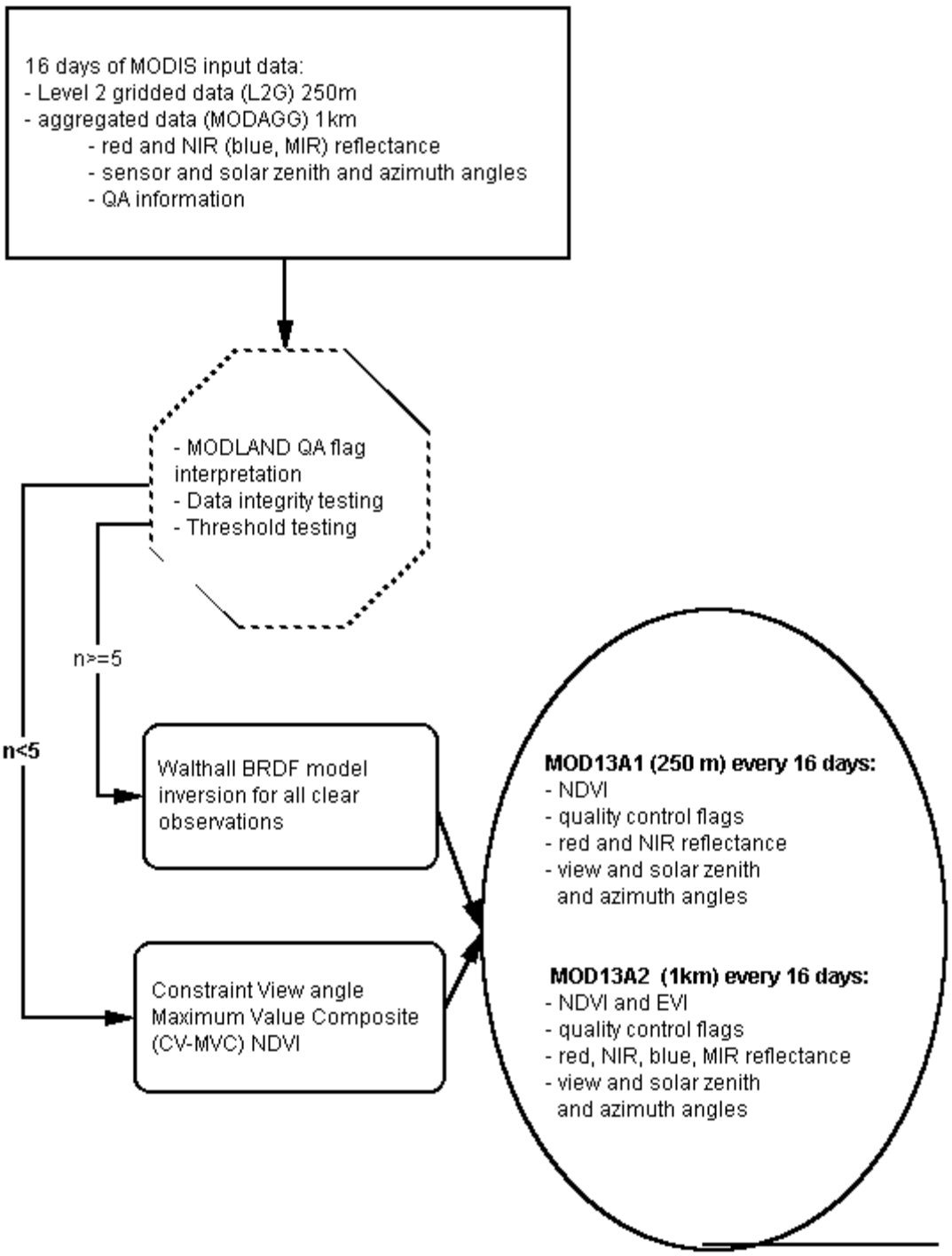

Figure 3.2.5: Diagram showing the sequence of MODIS processing steps for compositing of MODIS VI products at 250m and 1km spatial and 16 days temporal resolution.

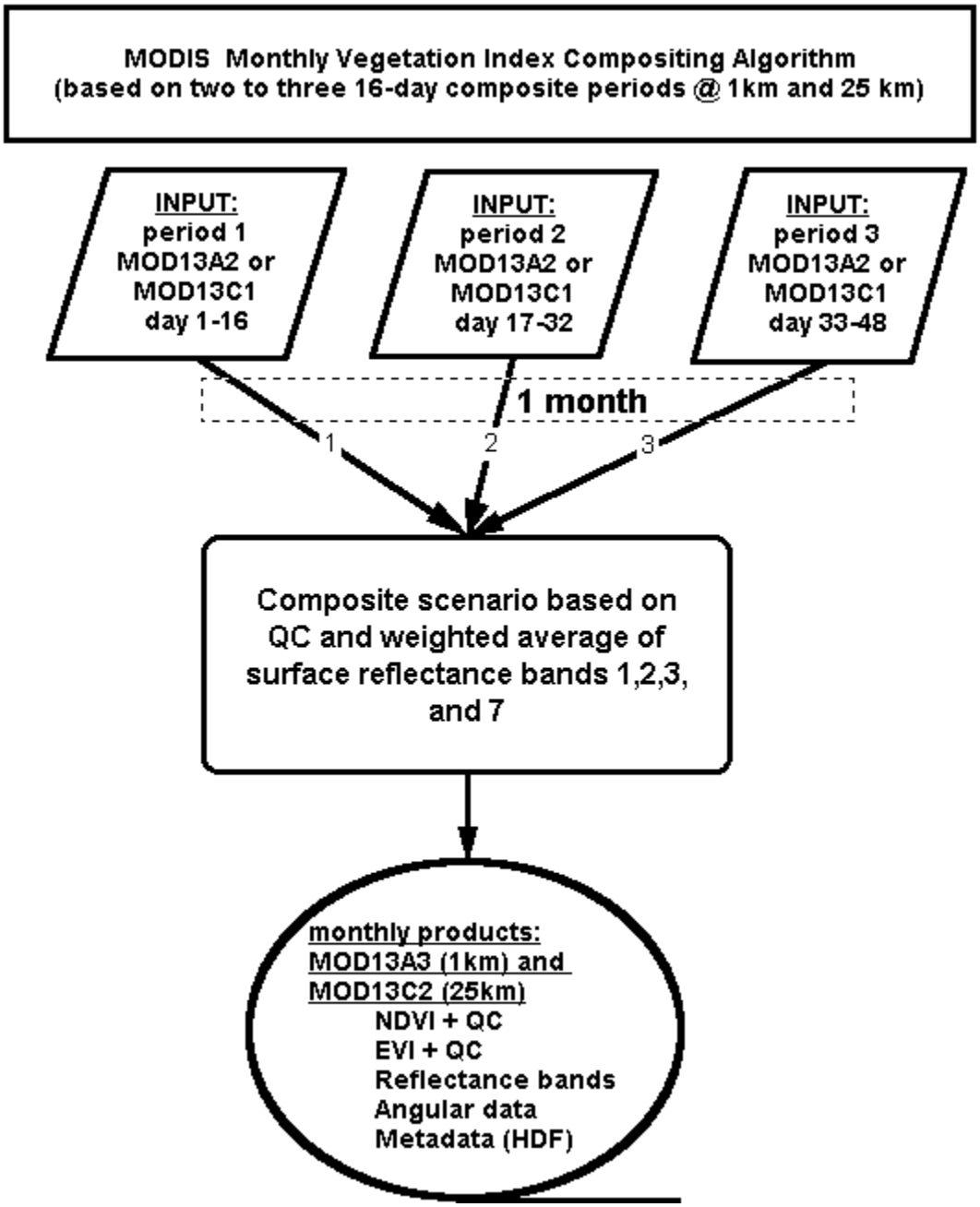

Figure 3.2.6: Diagram showing the sequence of MODIS processing steps for the compositing of monthly MODIS VI products at 1km and 25km spatial resolution.

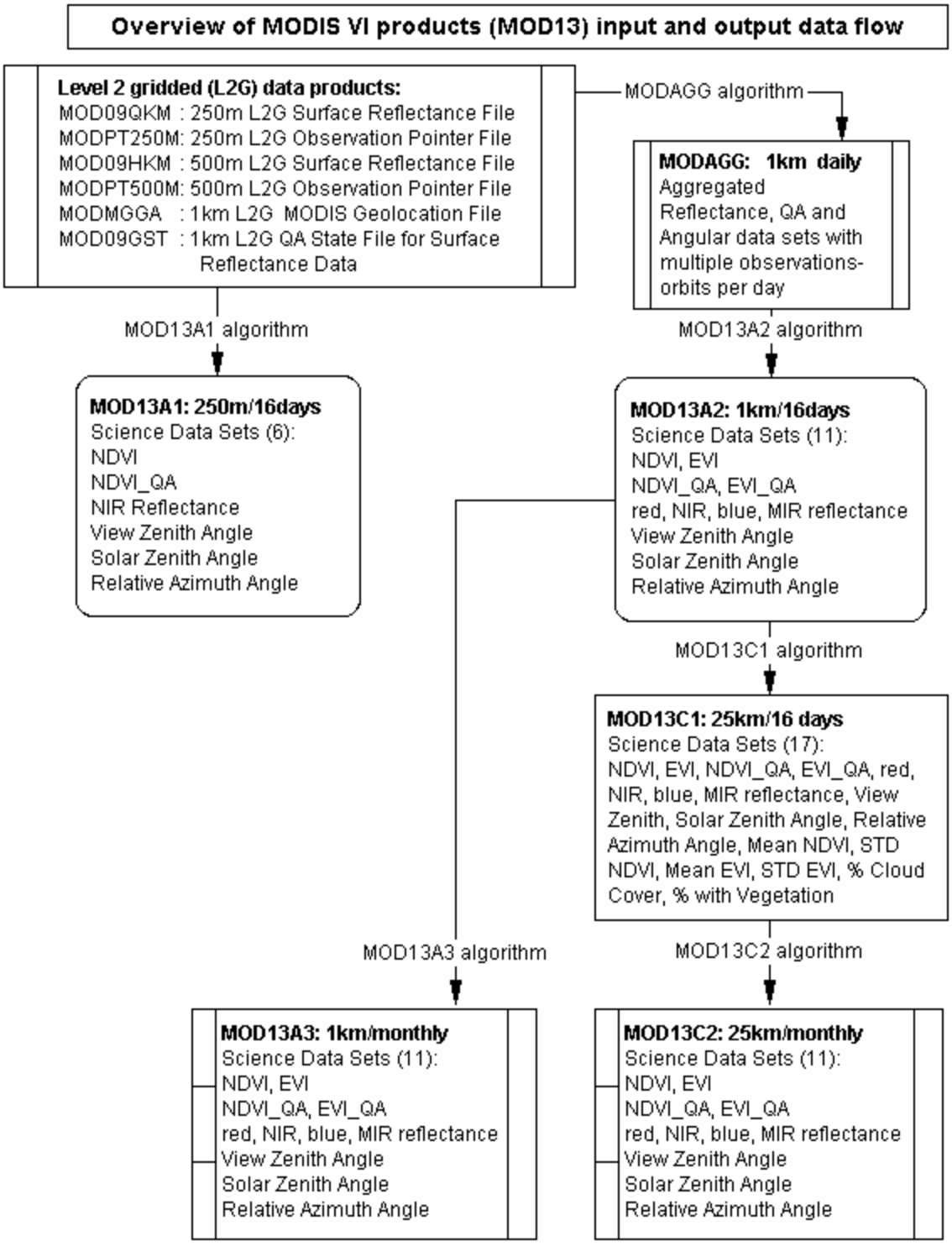

Figure 3.2.7: Schematic overview of all the input files needed to produce the MOD13 VI products and their associated science data sets.

3.2.7 Pre-launch MODIS VI prototypes

AVHRR Pathfinder data

One year (1989) of daily Pathfinder AVHRR data over land (James and Kalluri, 1994) was obtained from the GSFC-DAAC (Goddard Space Flight Center- Distributed Active Archive Center) to test and prototype the MODIS vegetation index compositing (van Leeuwen et al., 1999). The daily Pathfinder data is mapped to a global 8 km equal area grid using the Goode Interrupted Homolosine projection, resulting in global spatial dimensions of 5004 by 2168 pixels (columns and rows). The AVHRR data was in the Hierarchical Data Format (HDF) and consisted of twelve data fields: NDVI, CLAVR (cloud algorithm for AVHRR) cloud flags, Quality assurance flags, Scan angle, Solar zenith angle, Relative azimuth angle, Channel 1 reflectance, Channel 2 reflectance, Channel 3 brightness temperature, Channel 4 brightness temperature, Channel 5 brightness temperature, Date and hour of the observation. The reflectance data was already corrected for Rayleigh scattering and ozone absorption. Cloud flags were produced by NOAA's cloud algorithm for AVHRR (CLAVR; Stowe et al., 1991). The land/sea mask was an ancillary data layer used in the processing. More specific information on the Pathfinder AVHRR land data can be found in the User's manual (Agbu and James, 1994).

AVHRR temporal VI profiles

Applying the MODIS and MVC compositing algorithms to 1 year of daily AVHRR data resulted in twenty-three consecutive global composites of the NDVI. The mean global $NDVI_{MODIS}$ and $NDVI_{MVC}$ values were obtained for all pixels, composite periods and different MODIS compositing scenarios. Globally, the $NDVI_{MODIS}$ was between 5 to 8 % lower then the $NDVI_{MVC}$. Using the QA information, for each pixel where the BRDF model was applied, the MVC was computed as well and the relative difference computed for these pixels. Whenever the MODIS-BRDF was applied, the resulting NDVI values were between 20 to 30% lower than the $NDVI_{MVC}$ (van Leeuwen et al., 1999**).** Figure 3.2.8 shows seasonal profiles of the $NDVI_{MODIS}$ for each continent. The peak of the growing season is different for each continent. The relative differences [100 ($NDVI_{MVC}$ - $NDVI_{MODIS}$) / $NDVI_{MVC}$] were computed for each continent and ranged between 1 and 24 % for all 16-day composite periods during the 1989 AVHRR observations (Leeuwen et al., 1997b).

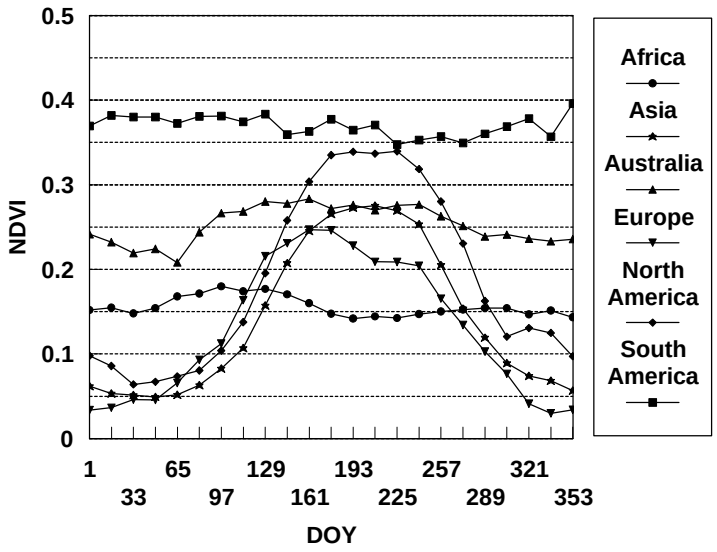

Figure 3.2.8: Continental NDVI profiles for the MODIS composite algorithm; AVHRR (8km).

Desert and deciduous broadleaf forest temporal VI profiles

The relative accuracy of the MODIS-BRDF algorithm was evaluated through temporal NDVI, red and NIR value profiles from pixels extracted from Desert and Deciduous Broadleaf Forest (Figure 3.2.9 and Figure 3.2.10). The composited reflectance data is utilized in VI computation and is also output with the VI, providing additional data fields for vegetation studies. Figure 9a shows an example of a seasonal $NDVI_{MODIS}$ and $NDVI_{MVC}$ profiles, with the $NDVI_{MODIS}$ being equal or slightly lower then the $NDVI_{MVC}$. $NDVI_{MODIS}$ profiles are slightly smoother than the $NDVI_{MVC}$ profiles (Figs. 3.2.9a and 3.2.10a,b). The temporal red and NIR reflectance profiles (Figure 3.2.9b) are following the same trend for both MVC and MODIS composite methods. The combination of MODIS BRDF and CV-MVC composite methods performed well.

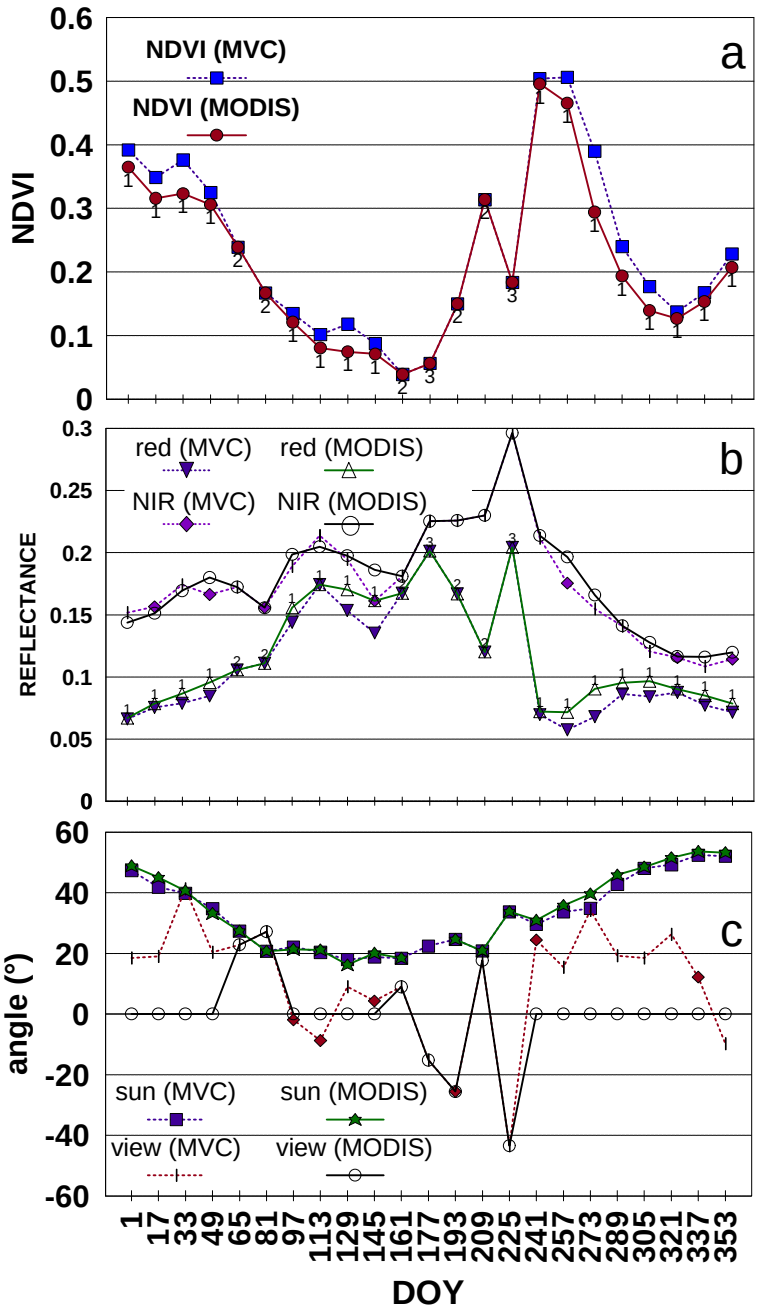

Figure 3.2.9: Example of temporal profiles of a) NDVI , b) red and NIR reflectance values, and c) sun and view zenith angles, for one pixel in a broadleaf deciduous (Lat. 22.92 °N, Long. 75.98°E) forest (vegetation classification based on Kuchler's (1995) world natural vegetation map) for the MODIS and the MVC composite approaches using AVHRR data. For each composite period the MODIS composite method is indicated with a number: 1- BRDF; 2 - CV-MVC; 3 - MVC.

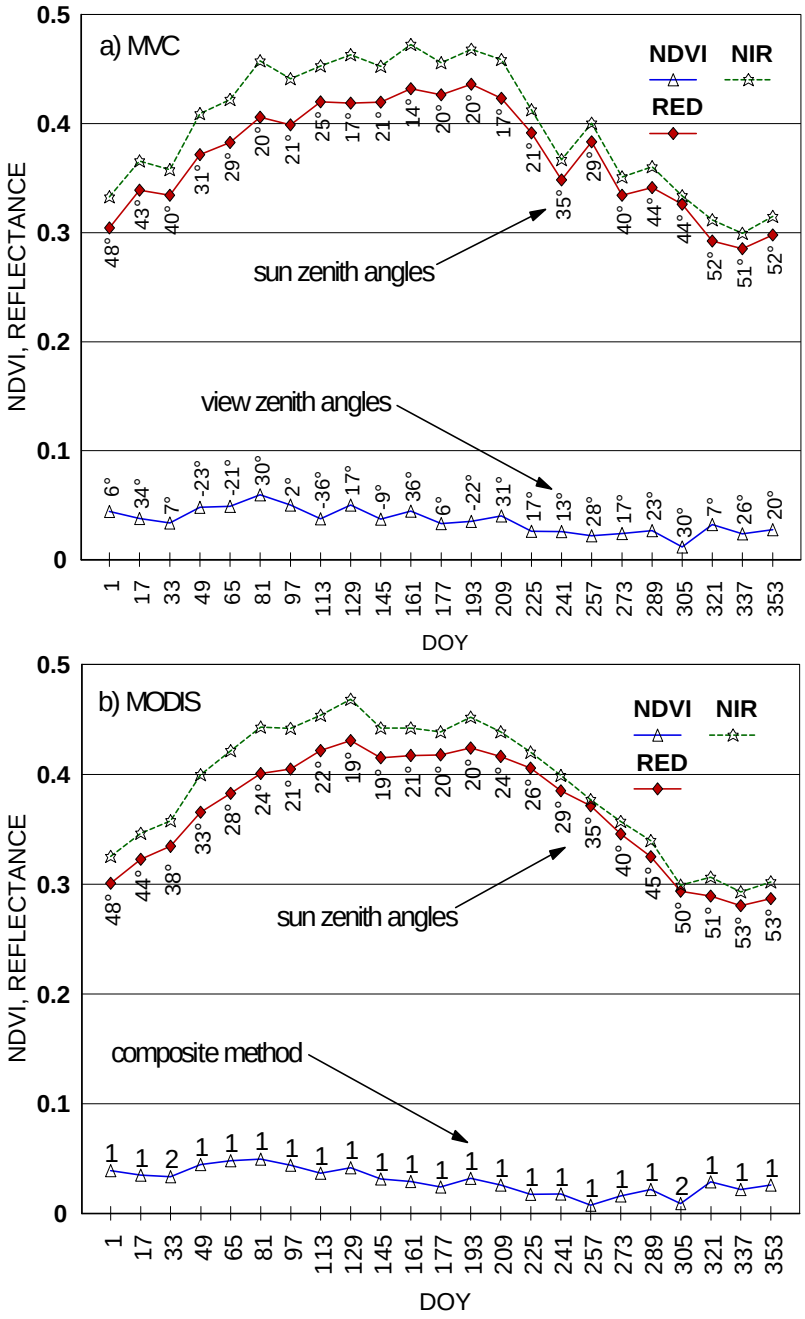

Figure 3.2.10: Example of temporal profiles of NDVI, red and NIR reflectance values for one desert vegetation pixel (Lat. 22.0°N, Long. 27.15°E) (vegetation classification based on Kuchler's (1995) world natural vegetation map) for the a) MVC and b) MODIS composite approaches using AVHRR data. For each composite period the MODIS composite method is indicated with a number: 1-BRDF; 2 - CV-MVC. The sun zenith angle and view zenith angle are also shown for each composite period. The negative and positive view angles are indicated for the respective backscatter and forward scatter view direction. The view zenith angle for the MODIS-BRDF corrected data is 0°.

Prototype of MODIS VI imagery

Figures 3.2.11 and 3.2.12 are prototype images of the global MODIS-NDVI and QA product for one 16-day composite period. The combination of MODIS BRDF and CV-MVC (constraint view angle maximum value composite) composite methods performed well. Obvious discontinuities or artifacts due to the combined use of two to three composite methods were not observed. The pseudo color image of the NDVI allows for fast visual examination of vegetation density and photosynthetically active regions of the world. The associated pseudo color quality assurance (QA) image permits for quality checks of the algorithm, cloud cover persistence and examination of region with missing data.

Temporal and spatial VI trend analysis will be a powerful tool to detect effects of climate change and monitor vegetation dynamics. Note that the BRDF correction is limited to the semi-arid/arid regions, where cloud cover is less persistent than over other regions of the world. It is likely that the cloud cover will be less for the AM overpass time of MODIS in comparison with the afternoon overpass time of AVHRR. Consequently, the BRDF correction will be more frequently applied relative to the AVHRR PM data.

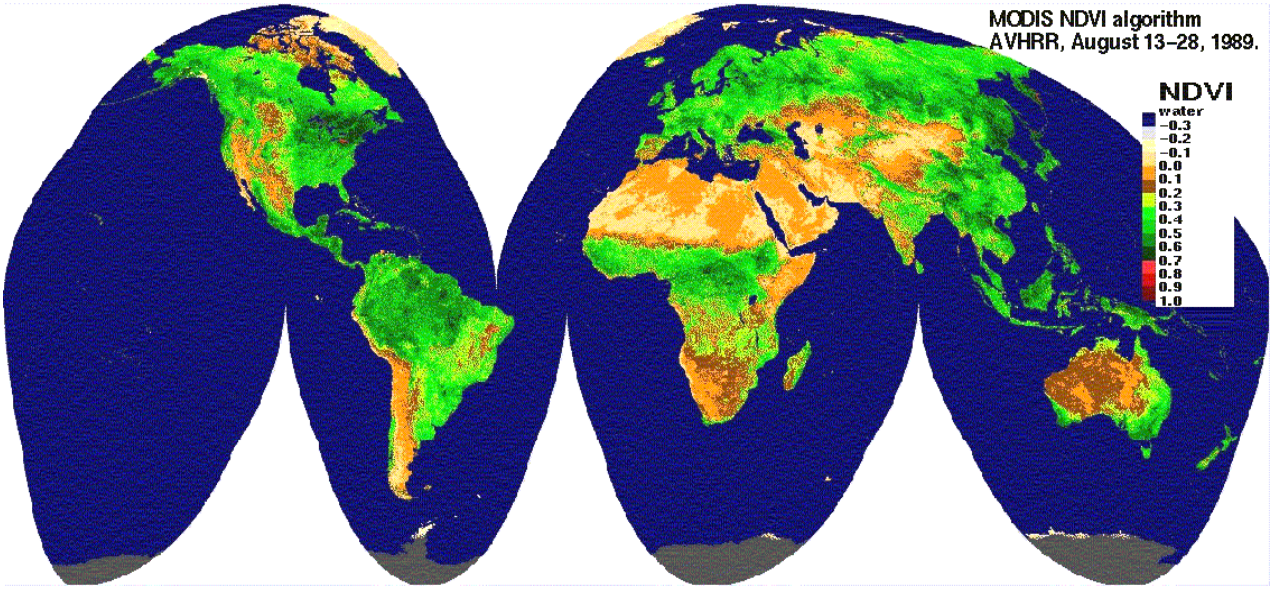

Figure 3.2.11: Global NDVI image (pseudo color) using the MODIS VI composite algorithm (BRDF/ CV-MVC/ MVC approach).

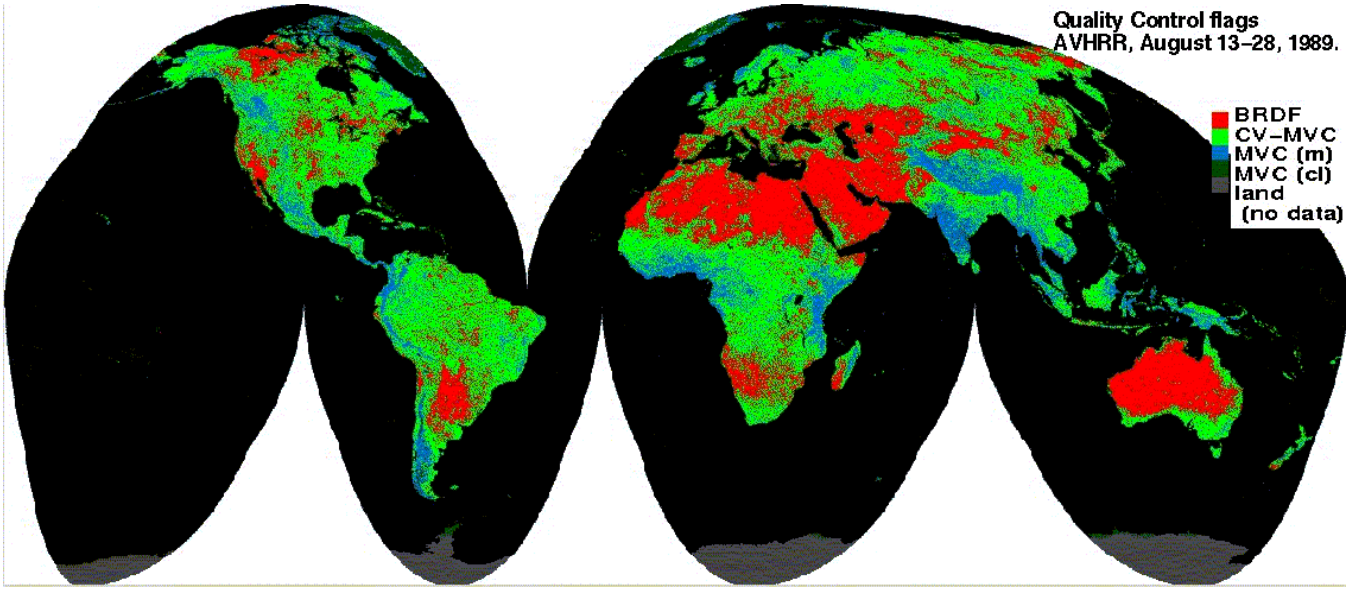

Figure 3.2.12: Color coded quality assurance flags for a Global NDVI composite using the MODIS approach (BRDF/CV-MVC/MVC); MVC (pr) the cloud mask indicated the pixels to be probably cloudy; MVC (cl)=cloudy pixels; land surfaces without data were indicated with a dark color gray.

AVHRR view angle distribution

The benefit of the MODIS compositing approach is noticeable by the smaller or equal view angles and the associated smaller pixel sizes. The view angle distribution of the MVC algorithm is more biased towards the forward scatter direction than the view angle distribution of the MODIS algorithm (Figure 3.2.13). The strong peak at nadir view angles is due to the BRDF standardization of the reflectance factors to nadir. The view angle distribution of the CV-MVC algorithm is also less biased towards the forward scatter (positive angles) in comparison with the MVC algorithm as shown in Figure 3.2.13

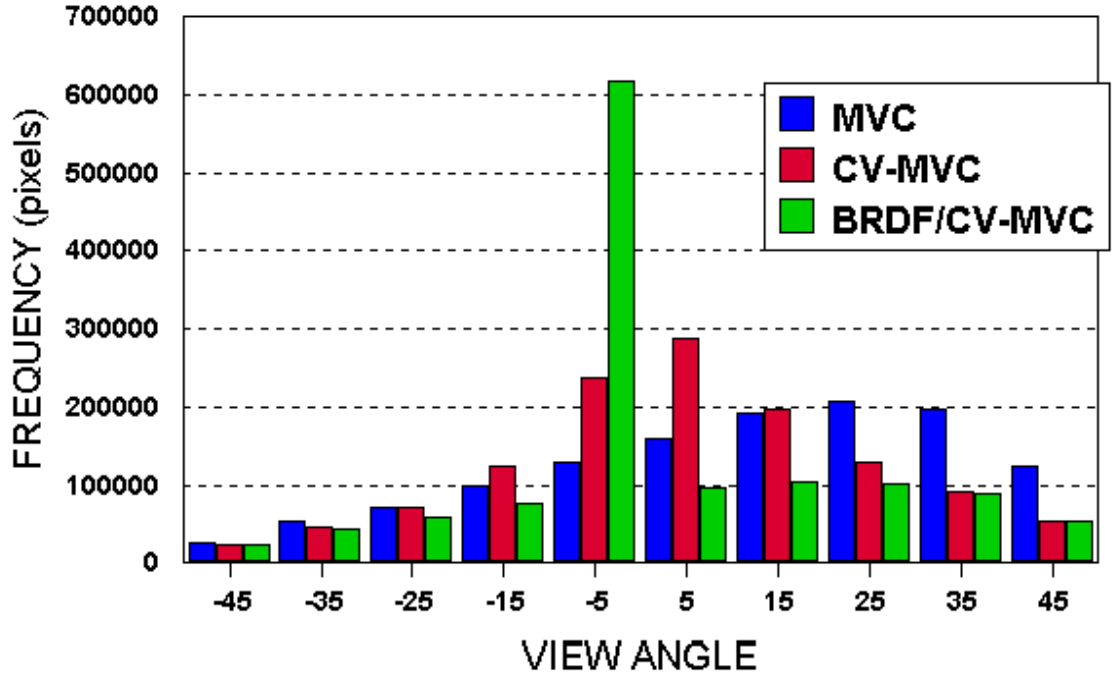

Figure 3.2.13: Global view angle distribution (including all continents) for a 16-day composite period (August 13-August 28, 1989) for the MODIS (BRDF/CV-MVC) and CV-MVC and MVC algorithms.

SeaWiFS prototype

One set of 16 days of continuous global SeaWiFS (Sea-viewing Wide Field-of-view Sensor) reflectance (surface reflectance data corrected for Rayleigh scattering, Ozone and water vapor) and sun-sensor geometry data (5000 columns x 2500 rows; 8 km spatial resolution; for 16 days during 1997; September 15 to October 1; Sept. 17 data were missing; Robinson projection) were used to test and prototype the MODIS vegetation index compositing algorithms. The SeaWiFS vegetation index data were composited in space and time to monitor vegetation changes in a spatial continuous fashion.

The SeaWiFS was tilted 20°, preventing nadir looks of the Earth's surface. A scanner tilt mechanism enables the instrument to be oriented in the along-track

direction to +20, 0 -20 degrees to avoid sun glint from the sea surface. The scanner was tilted 20° for all data and results presented.To apply the MODIS compositing algorithm, a cloud mask was developed for the SeaWiFS data using a reflectance threshold for the visible bands. A cloud flag was set for all pixels with a reflectance threshold: $\theta_3 > 0.25$. Note that the cloud mask is not distinguishing between clouds and snow. If all observations with a good data integrity bit were cloudy, a vegetation index (VI) was still produced based on the MVC. A land/water mask in the Robinson projection was used to compute the VI over land only. The integrity of the reflectance data was examined based on thresholds for all SeaWiFS reflectance data: $0<\rho_{SeaWiFS}<1$.

Although the MODIS compositing algorithms were successfully applied to the SeaWiFS data, the MVC algorithm, a MODIS back-up algorithm, might be more reliable for SeaWiFS since it automatically filters out cloud affected pixels. The MODIS composite algorithm will be most reliable if accurate cloud information is available for each observation so that cloud affected pixels will be rejected in the BRDF part of the MODIS algorithm.Table 2 provides a comparison of the spectral bandwidths for MODIS and SeaWiFS used for spectral vegetation indices over land (visible and near-infrared).

Table 2: MODIS and SeaWiFS spectral bandwidths

SeaWiFS Band #	$r_{SeaWiFS}$ ***(nm)***	***MODIS Band #***	r_{MODIS} ***(nm)***
1	402-422		
2	433-453		
3	480-500	3	459-479
4	500-520		
5	545-565	4	545-565
6	660-680	1	620-670
7	745-785		
8	845-885	2	841-876

The cloud mask generally worked well, although snow/ice regions were flagged as cloudy. Since SeaWiFS has no thermal bands, the determination of cloud affected observations will be challenging. If the data from these regions had good data integrity, a VI was still computed using the MODIS back-up algorithm, which will choose the highest VI as a representative of the composite period. Temporal reflectance comparisons (visible bands) over forested areas indicated the inclusion of some higher sub-pixel cloud reflectance values. Inter-comparison of reflectance observations during a composite period as well as the use of vegetation type information could help filter out the sub-pixel cloud affected observations. Limited cloud information can be obtained from the visible and NIR SeaWiFS reflectance observations, because bright soils, snow and cloud spectral signatures are very similar. Furthermore, contributions of sub-pixel clouds to the 8 km SeaWiFS pixel response are difficult to quantify without detailed mixture component analysis.

Figure 3.2.14 is a prototype of the MODIS NDVI and EVI and quality assurance flags using the SeaWiFS data as input for the MODIS-VI- compositing algorithm. The

NDVI values were standardized to 20° view zenith angle, the SeaWiFS tilt angle. Notice that the EVI is not computed for most of Greenland and Antarctica. About 54% of the valid EVI pixels over land were BRDF corrected. The mean MODIS-NDVI (2686 and 2723 for the MODIS-20° and MODIS-nadir composite scenarios) was about 22% lower than the MVC-NDVI (3302) results. The tilt of SeaWiFS and its unreliable cloudmask are distinct obstacles in using the SeaWiFS and MODIS (MODIS provides a sophisticated cloud mask) data interchangeably and for cross validation purposes. Under these circumstances, the MVC might be more reliable for compositing SeaWiFS vegetation indices since it automatically filters out most cloud affected pixels. The MODIS composite algorithm can not be reliably applied to SeaWiFS data without appropriate attention to the SeaWiFS tilt angle and cloud mask (van Leeuwen et al., 1998).

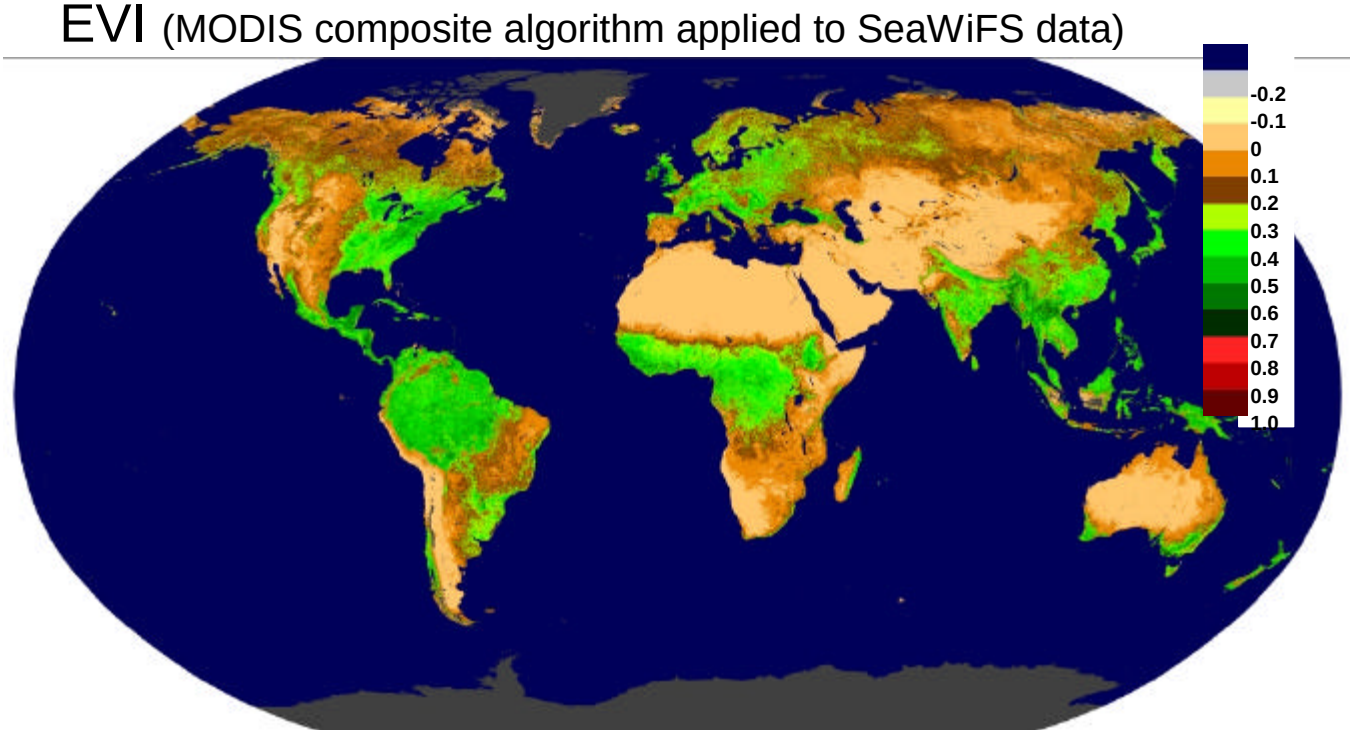

Figure 3.2.14a: See caption below.

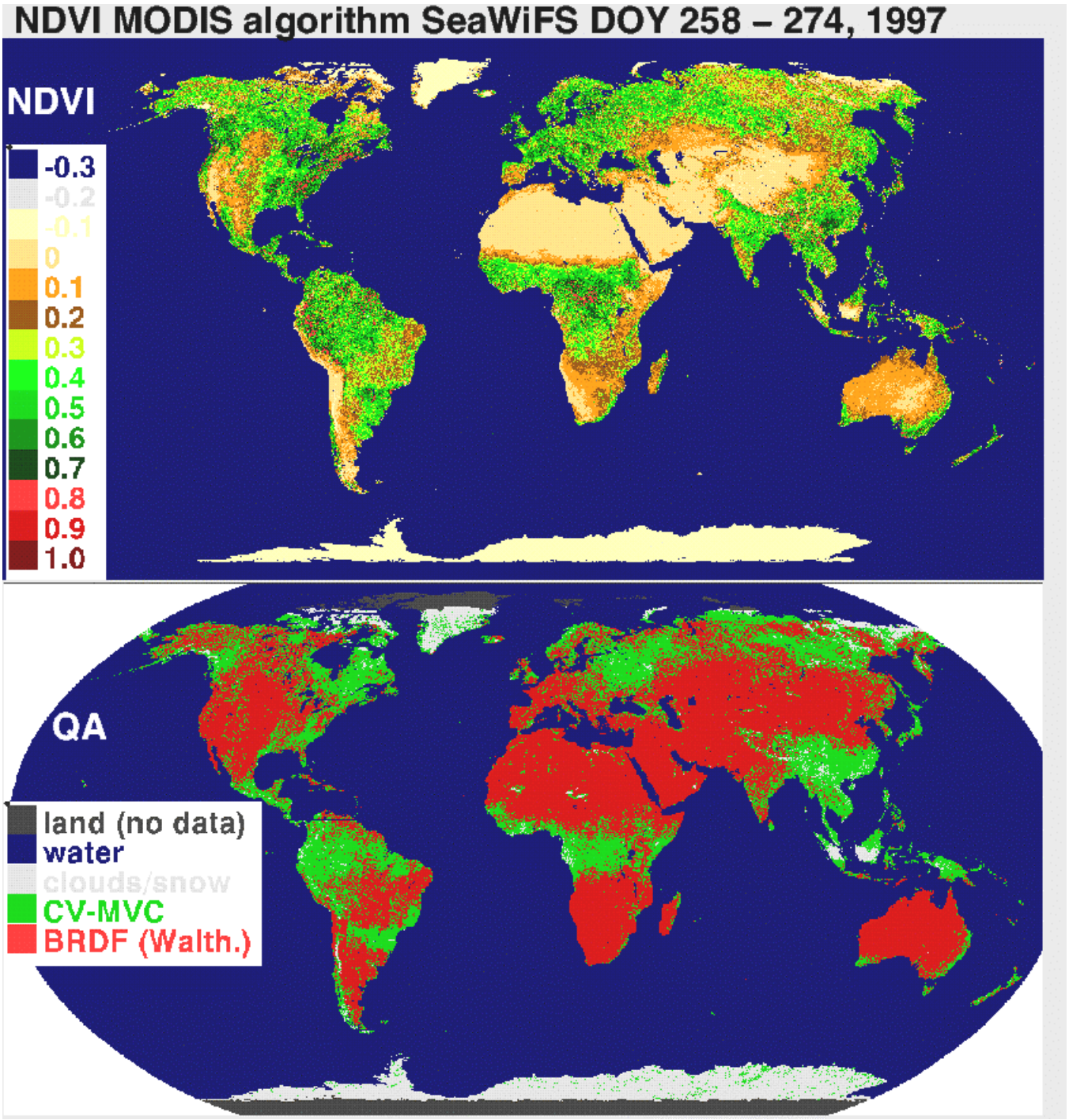

Figure 3.2.14: Global EVI (a) and NDVI (b) image (pseudo color) using the MODIS VI composite algorithm (BRDF/ CV-MVC/ MVC approach). (c) Color coded quality assurance flags for a Global NDVI composite (very similar for EVI) using the MODIS approach (BRDF/CV-MVC/MVC)

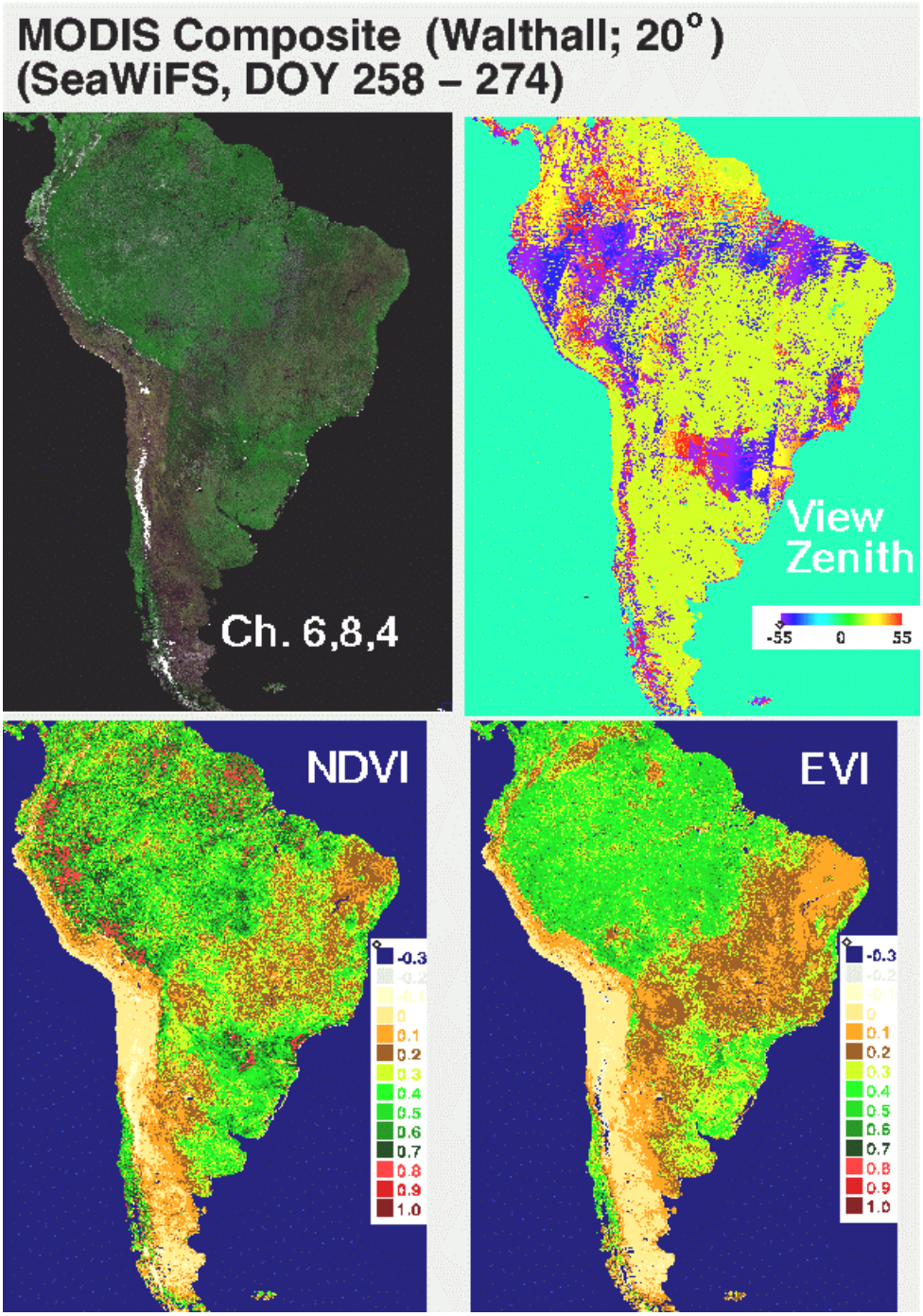

Figure 3.2.15: SEAWIFS color composite, NDVI, EVI and view angle distribution for South America.

Figure 3.2.15 shows a SEAWIFS color composite with some slight traces of smoke and clouds still visible. The NDVI and EVI have different dynamic ranges. The view angle distribution for South America shows that large areas where standardized by using a BRDF based compositing approach.

3.2.8 Alternative VI compositing approaches

The MODIS/MISR BRDF production scheme will generate BRDF parameters and albedo every sixteen days with a 1 km spatial resolution with a required minimum of ten cloud-free observations to be reliable (Strahler et al., 1996). The MODIS BRDF database is currently incompatible with the needs of the 250m gridded MODIS NDVI product due to the coarser spatial and temporal resolutions of the BRDF product. Since the MODIS VI compositing algorithm has the specific aim of deriving nadir equivalent reflectance values, and not the complete BRDF (needed for albedo), five observations are considered sufficient for nadir interpolation. The feasibility of applying the BRDF product (1 km) to finer resolutions (250 m) (sharpening mode of the BRDF product) was investigated by Leeuwen et al. (1997a) showing promising results for relatively homogeneous land cover types. The use of previous composite BRDF results or a historic BRDF data base is also being investigated for situations where it is impossible to derive nadir reflectance values due to a limited number of observations (Leeuwen et al, 1997a; Wanner et al., 1997; Lucht et al, 1999).

Standardization of VI to nadir view and a certain sun angle is being investigated for a monthly CMG VI product. Monthly compositing would ensure sufficient input data for BRDF determination using inversion of a simple BRDF model (Rahman's; Rahman et al., 1993). The VI would be globally normalized to a constant solar-view geometry (possibly determined by the angle most sensitive to canopy biomass) at 0.25° spatial resolution (25 km). At the lower temporal resolution, this product would be catered towards modelers and those doing inter-annual comparisons. Local/regional work demanding more frequent data would probably rely on the 16 day level 3 VI as planned.

A second approach to NDVI values for variations in solar zenith angles is by using empirical relationships between the NDVI and solar zenith angle for a range of biomes. These empirical relationships can be established through in situ nadir radiometric measurements for a range of sun amgles. Table 3 shows a range of the expected variation in sun angle for low and high latitudes.

Table 3: The maximum and minimum mean solar zenith angles for land and the different continents based on the AVHRR composited data. As expected, the approximate Day of Year (DOY) the minimum and maximum sun angles occur, are during spring and fall.

Continents	***Sun angle (°)***	
All (Global)	33°	53°
South America	46°	33°
North America	30°	67°
Europe	28°	66°
Australia	51°	32°
Asia	27°	62°
Africa	26°	46°
DOY	161	337

3.2.9 VI compositing conclusions

Because reflectance properties of the land surface are anisotropic in nature, vegetation indices, derived from bi-directional reflectance values, are strongly affected by the angular properties at which the target was viewed and illuminated. Retrieval of the bidirectional reflectance distribution function and angular standardization of these reflectance data are essential for the proper interpretation of vegetation index data and their derived parameters.

The improved capabilities of MODIS will offer the opportunity to cross-validate the historical and ongoing AVHRR-NDVI time series (since 1982) with the MODIS-NDVI time series. Especially the differences between the AVHRR and MODIS sensors in the spectral, radiometric, and spatial domain need to be translated to meet the needs of global change research. Biophysical parameters such as percent cover, biomass, fAPAR and LAI, have been derived from the NDVI measured at variable view and sun angles. Standardizing these angular effects will also allow for more accurate derivations of biome specific or global biophysical parameters from VIs. The EVI was successfully prototyped on a global scale with SeaWiFS data because it included a blue band. The EVI will extend sensitivity into dense vegetation types such as forests and agricultural areas while reducing the noise effects of canopy background and atmospheric aerosols (Justice et al., 1998).

There is some concern that the MODIS compositing approach, a combination of the BRDF and back-up MVC (maximum value composite) methods, will affect data purity and cause more discontinuities on a regional scale than a single criteria composite method (e.g. MVC). At this point, the MODIS approach has the advantage over the MVC approach through standardization of view angles and emphasis on the selection of nadir (finest spatial resolution) observations. However, the MODIS approach is more adversely affected by cloud and atmospheric effects than the MVC. The selection of the maximum NDVI tends to mask the natural vegetation variations in more densely vegetated areas due to saturation effects. A final evaluation of the MODIS composite approach will be based on the quality of the actual MODIS data, product evaluations and user community requirements.

Since many uncertainties remain as to how the actual MODIS instrument and the developed algorithms are going to perform, some flexibility is being built into the current MODIS VI compositing algorithm, that allows for unexpected (e.g. unreliable geo-registration, cloud mask and atmospheric correction) data input flows. The compositing algorithm thresholds and parameters can be relaxed or tightened depending on the quality of the data. For instance, immediately after launch, the BRDF module of the compositing algorithm can be switched off to accommodate less ideal data due to unsuccessful cloud-masking or inaccurate day to day geo-registration. The quality of the MODIS data processing algorithms and the MODIS specific spatial, temporal, spectral and radiometric quality of the data after the initial post launch processing will greatly determine if all the MODIS compositing goals can be achieved.

- The following conclusions can be drawn based on prototyping the MODIS vegetation index approach with AVHRR and SeaWiFSdata:
- A simple BRDF model and few observations (5) per pixel were needed to standardize the NDVI and EVI to nadir view angles and thus improve the interpretation of the anisotropic VIs.
- The Walthall BRDF model was successfully used in prototyping global MODIS-EOS/NDVI composite scenarios with AVHRR and SeaWiFS data.
- Results of a BRDF approach are more representative of vegetation changes over a 16-day period than the MVC approach, because it incorporates all 'good' observations and changes during a 16-day period.
- The present MODIS-BRDF composite scenario automatically extrapolates to finer (nadir) spatial resolutions.
- A reliable cloud-mask is crucial to the BRDF-component of the MODIS compositing algorithm to exclude observations of cloud affected pixels.
- A backup composite algorithm was needed for the pixels with a limited number of "good" observations since the BRDF model can not be reliably inverted if the Earth's surface is frequently covered with clouds.
- On a continental scale, the MVC based NDVI values were 1-30% higher than the NDVI values derived from the MODIS algorithm.

Since the vegetation indices are radiometric measures of the spatial and temporal variations of vegetation biophysical properties, validation activities will focus on the relationship of the radiometric and biophysical changes of the land surface and incorporate multi-angular measurements as well. Research and validation activities are in progress to demonstrate the utility of the MODIS vegetation indices to improve the understanding of the Earth system and its dynamics due to interactions between climate and land processes and human activity.

3.3 MODIS VI Quality Assurance (QA)

The quality of the vegetation index (VI) products will be assessed regularly to monitor the accuracy and integrity of the data products over long time frames that are of critical importance to studies of global change and climate. Run time and post-production QA evaluations will take place at the TBRS-SCF (Terrestrial Biophysics and Remote Sensing - Science Computing Facility) and the LDOPE (Land Data Operational Product Evaluation) Facility at GSFC (Goddard Space Flight Center). The LDOPE will focus mostly on day to day operational QA, while the SCF will focus more on in-depth QA analysis and product validation related to science questions. Although only a fraction of the total amount of data need to be put through the SCF and LDOPE, automation of the QA procedures will be optimized as much as possible to cope with the vast amounts of data. It is assessed that the input data stream to the TBRS-SCF will be 2.0 GB/day. This is an average data stream, but it is expected that peak volumes could approach 24 GB per day due to the fact that 16 days of input data are needed to do the in-depth QA analysis on the 250 m VI product and its input products.

3.3.1 QA definition and scope

Definition of Quality Assurance (QA): Flag data products in operational mode which do not conform to the expected accuracies of that product, and store operational production system information/data that is useful for post production quality assurance.

QA results will be derived for each pixel by (QA science data set) :

- examination of the input and output data (reflectance, VI, view-sun geometry and QA-flags) in spatial and temporal domain
- science decision making represented by the options inside the coded algorithms
- accuracy estimates derived from input and output data QA flags and system noise and algorithm specifications
- validation of the vegetation indices at validation sites (specific goals)

QA results will be derived for each tile by (metadata stored in the HDF file):

- summary of critical per pixel QA over the tile (e.g. MODLAND QA and summary statistics)
- monitoring the computational and production stability of the code.
- flagging of a state or condition related to the run time production.
- accumulating and summarizing the QA of all files used in the production of a tile
- generalized accuracy estimates derived from input and output data QA flags and system noise and algorithm specifications
- documentation of the code versions and processing history of the data products

Anticipated quality related problems for VI products are related to three categories:

Product (output) and Input science data sets and metadata:

- VI product data integrity (check against product spec) and validity (missing tiles, beyond logical/acceptable thresholds)
- Input data integrity and its validity (missing tiles, beyond logical/acceptable thresholds)

Vegetation Index Science Issues:

- Reflectance standardization using BRDF and CV_MVC (spatial and temporal)
- Code evaluation to fine tune some of the threshold values set inside the code to catch outliers

Software change issues:

- Software problem at SDST or SCF components,
- Processing environment

- Program performance

Several choices of action can be entertained based on the results of the performed QA analysis. The first two action items are related to metadata fields and have to be set for each tile that has been or is being investigated. It is also possible to set these flags based on an inferred qualification from the actually investigated tiles. Paths of action based on QA results:

1. Set science quality flag
2. Set science quality flag explanation
3. Operational work-around or fix
4. Discontinue or decrease production
5. Develop a plan to fix the problem

Thus, the QA (quality assurance) analysis can result in algorithm and metadata adjustments. The QA analysis allows us to accumulate science quality output analysis to make informed decision on code adjustments (data base). A plan of implementation needs to be developed to incorporate minor and major code changes. The set up of a web site with QA results and a reference with the science quality flag explanation might be necessary. It is important to keep in mind that QA = “pass” or approvals from SCF’s or LDOPE will propagate to upstream products. On the other hand: QA = “fail”, problems and code changes propagate to downstream products. It is envisioned that the QA and validation efforts will be strung together to make efficient use of limited resources (personnel and hardware) at the SCF. The QA and validation efforts will consist of:

1. In depth QA analysis of 1 land tile per composite period requiring access to all input files (chosen from the validation site list). These QA activities will be mostly interactive.
2. Continuous QA and trend analysis for 50 validation sites using subsets of up to 50 land tiles and the 16-day composited VI products. These QA activities will be mostly automated.
3. QA analysis of spatially continuous data on a global scale (4 times per year) using 16-day composites
4. Ad hoc QA analysis of land tiles based on LDOPE or MODLAND team findings

3.3.2 MODIS 13 product formats and QA related metadata and science data sets

Appendix B gives an overview of MODIS 13 VI products, data field descriptions and data types.The metadata fields that are associated with each VI product are defined in Appendix B. The per pixel QA flag explanation is described in Appendix C. The four MODLAND wide (MODIS Land team) flags, represented by the first 2 bits, are also described in Appendix C. Since the input to the NDVI is based on two bands, the least good QC flag from the reflectance product will be representative for the VI QC flag. The

EVI will have 3 input QC flags from the reflectance product (3 spectral bands), and thus the least good QC flag will be chosen to represent the VI QC. Appendix D gives the "Usefulness" scale interpretation key for MODIS Level 3 products. . More detailed information regarding QA fields can be found through several web sites (Huete et al., 1999; http://modland.nascom.nasa.gov/QA_WWW/v2specs/ mod13.html). Note that the MODIS 250 m/16-day NDVI product (Appendix B) will not include the red reflectance observations. This was to reduce the volume of the data that needs to be archived. The red reflectance data, however, can be retrieved using the relationship between NDVI and ρ_{NIR} :

$$r_{red} = \frac{(r_{NIR} - r_{NIR}\,\mathrm{NDVI})}{(1+\mathrm{NDVI})} \tag{14}$$

3.3.3 Definition and evaluation of VI product quality metrics

Measures of the input and output product quality were defined to check for unreasonable and unexpected values (physical boundaries and constraints) as described by the following list of metrics:

- -0.2 <=VI<=1.0; VI values below -0.2 and above 1 (scale 10000) will be discarded (These values are the current thresholds but might change in the future).
- 0<=reflectance input<=1.0; Reflectance values below zero or above 1 (scale 10000) will be discarded
- The fill-value will be -3000 for VIs and -1000 for reflectance values; Pixels with clouds and shadow and bad data integrity will be discarded.
- VI_MVC-0.3<=VI_BRDF<= VI_MVC+0.05; The BRDF derived VI values should not deviate further then indicated by these thresholds. These are set up to avoid outliers in the VI due to outliers fed to the BRDF model.
- Close correlation between MODIS spectral signatures with spectral libraries. Desert and dense vegetation spectral signatures change very little over the growing season.
- Temporal continuity and dynamics for different vegetation covers
- Non-linearity between VI's; If the two produced VI's are correlated non linearly, the information content of NDVI is likely to be different from the EVI
- Spatial continuity and dynamics (use land cover map); Patterns of landcover types, VI values and reflectance values should be correlated
- The view angle distribution should peak at nadir view angles; this is indicative for the selection of the finest spatial resolution (a VI composite objective) and least atmospheric pathway.
- Artefacts (VI response over e.g. antarctica or Sahara desert); VI values should be low and constant for these cases.

- Correlation with biophysical properties (LAI, fAPAR, % green cover, biomass, NPP); The VI values should follow seasonal patterns similar to biophysical properties

Based on the quality metrics as described above, the VI product specific multi-dimensional QA analysis will include:

- VI radiometric analysis (VI dynamic range and acceptable boundary analysis cross sensor comparison and translation)
- Algorithm performance (wrong tiles/ missing tiles/ missing data, view angle histogram (θv should peak around nadir); QA flag histograms, threshold settings, algorithm switch (Code should be able to switch to CV-MVC only in case BRDF does not perform due to unstable input), QA flag transfer from L1 to L2(input))
- Spectral analysis (reflectance signatures (band 7 response), range inspection, scatter plots, spectral library and cross sensor comparison
- Spatial analysis (speckle, artifacts, missing data, geometric pixel to pixel registration, tile mosaic, sun view geometry info of the input data)
- Atmospheric analysis (atmospheric correction QA, cloud mask at 250 m and 1km, land water/mask)
- Temporal analysis (time series analysis; sensor drift, standard deviation of predicted (model/cross sensor) vs. observed value.
- VI biophysical analysis (multiple VI's and biophysical parameters)

3.4 Practical Considerations

3.4.1 Numerical computation considerations

Practically all floating point computation will take place within the BRDF compositing algorithm. For the BRDF models under consideration, a least-squares solution for model parameters requires that a 3 variable system of linear equations is solved. In the current version, this is achieved through a partial-pivoting matrix inversion, performed by a standard LU decomposition/back-substitution procedure. In the case of the Walthall BRDF model, where the final kernel "c" is defined as the nadir reflectance value, the first two kernels do not necessarily need to be explicitly solved. The nadir approximation can then be directly determined through forward Gaussian elimination rather than a complete matrix inversion at a substantial savings in floating point operations.

3.4.2 Programming /Procedural considerations

The MODIS vegetation index Level 3 algorithms were developed in two phases:

- Scientific algorithm design
- Data I/O staging design

The scientific algorithm was developed, maintained, and tested at the University of Arizona SCF, focus was placed on the integrity and scientific performance. As depicted by figure 3.4.1, the science code performs its operation on a pixel basis. The original data I/O was developed by the MODIS land science team and currently maintained by the University of Arizona SCF personnel.

Overall, the five products (1km 16 day composite, 250m 16 day composite, 1km Monthly composite and both CMG products) will provide the user community with a consistent set of searchable products.

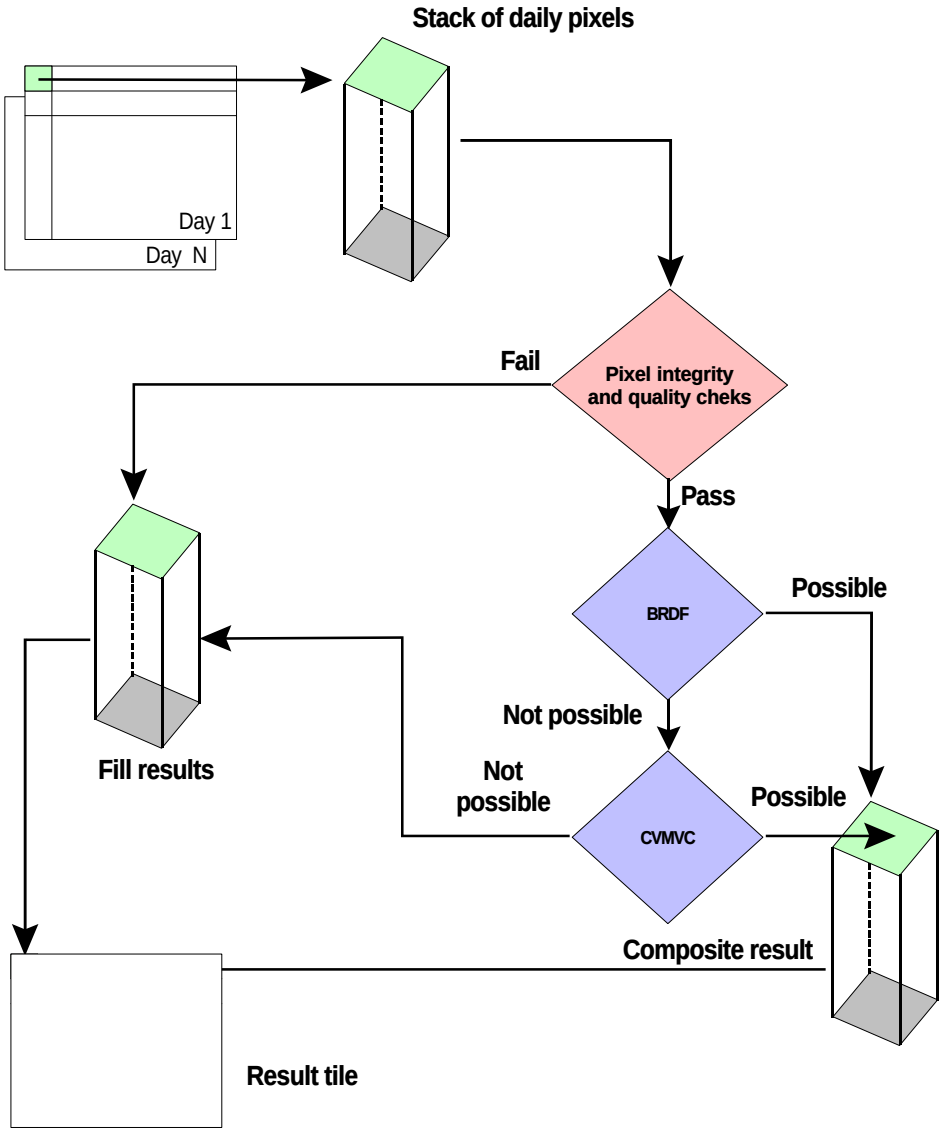

Figure 3.4.1: Vegetation index scientific algorithm operation flow.

Implementation software environment

All vegetation index algorithms were written in compliance with the MODIS algorithm development standards using ANSI C and are POSIX 1.x compliant. The five algorithms rely heavily on NASA's Software Data Production Toolkit library (SDPTK v.5.2.4) and the NASA HDF-EOS library (v.2.4) for data staging and metadata manipulation. On average each algorithm measures approximately 20,000 lines, with a total of 100,000 lines for the five MOD13 algorithms, which include mandatory prologues and maintenance comments.

Even though HDF was conceived around self describing data sets, we found it necessary to sometimes circumvent the HDF-EOS library in order to comply with performance requirements and overcome some problems relating to the SDPTK and HDF-EOS, especially when manipulating input or output product metadata. All development and testing was conducted on UNIX-SGI platforms running IRIX 6.x.

Software design

The at launch vegetation index algorithms were conceived around the central idea of expandability and maintainability. Given the complexity and the numerous aspects of the data being processed, the current ECS production code was separated into four major categories:

1. Science code: performs all necessary data integrity, compositing operations, and quality flag assignments.
2. Metadata manipulation: allows for all necessary staging and evaluation of the input and output data.
3. Data staging: performs overall data integrity, sorting and organizing the input data.
4. HDF manipulation: performs all operations required to manipulate the scientific data sets

Reliance on the Process Control File (PCF) to provide flow control parameter that directs the algorithm operation was recently added to allow for greater flexibility and enables our SCF to test and recommend different routes during post-launcg activities. For example threshold values, the number of points required by the BRDF, and the number of points required by CVMVC can all be set in the PCF file without recourse to new compilation or code changes. Figure 3.4.2 details the different phases of the algorithm, we note that the same scheme applies to all products with minor differences. During processing all errors are logged to the appropriate files for later analysis, this is accomplished by the Status Message File (SMF) tool set calls.

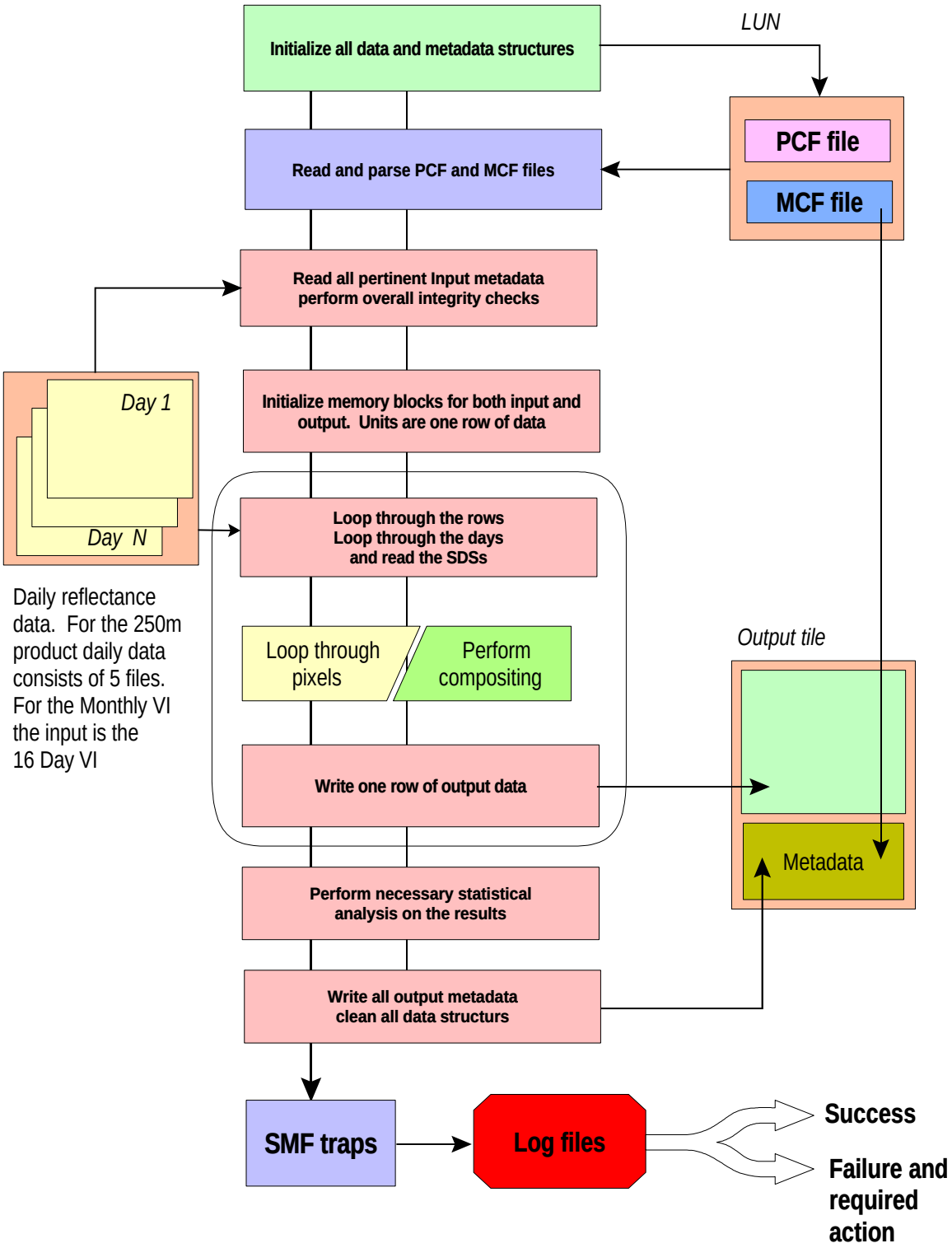

Figure 3.4.2: Vegetation Index algorithms major components

MOD13 land production, projection and tile ID

MODIS VI products (MOD13A1, MOD13A2, MOD13A3, MOD13C1, MOD13C2) will be produced based on the Integerized Sinusoidal Grid, a map projection derived from the sinusoidal map projection. To be able to composite the data over time, the MODLAND team has accepted a tiling and gridding system that will be the same for each L3 product. The globally gridded projection is split in 36 (horizontal) by 18 (vertical) tiles, each with a resolution of approximately 10° by 10°. Figure 3.4.3 shows an overview of the projection, tiles and tile ID's. The tile coordinate system starts at (0,0) (vertical tile number, horizontal tile number) in the upper left corner and proceeds downward (vertical) and rightward (horizontal). The tile in the bottom left corner is (17, 35). Dark blue tiles contain only water (no land). More information regarding the tile boundary coordinates (corner latitude and longitude) can be found at http://modland.nascom.nasa.gov/developers/bndrytb2.html. The total number of tiles is 648, of which about 290 tiles will be classified as land and thus a VI product produced. The MOD13 algorithms will not produce the products over oceans and deep inland water. Each tile will be 1200 by 1200 1km pixels or 4800 by 4800 250m pixels, each pixel maintaining its geolocation through time.

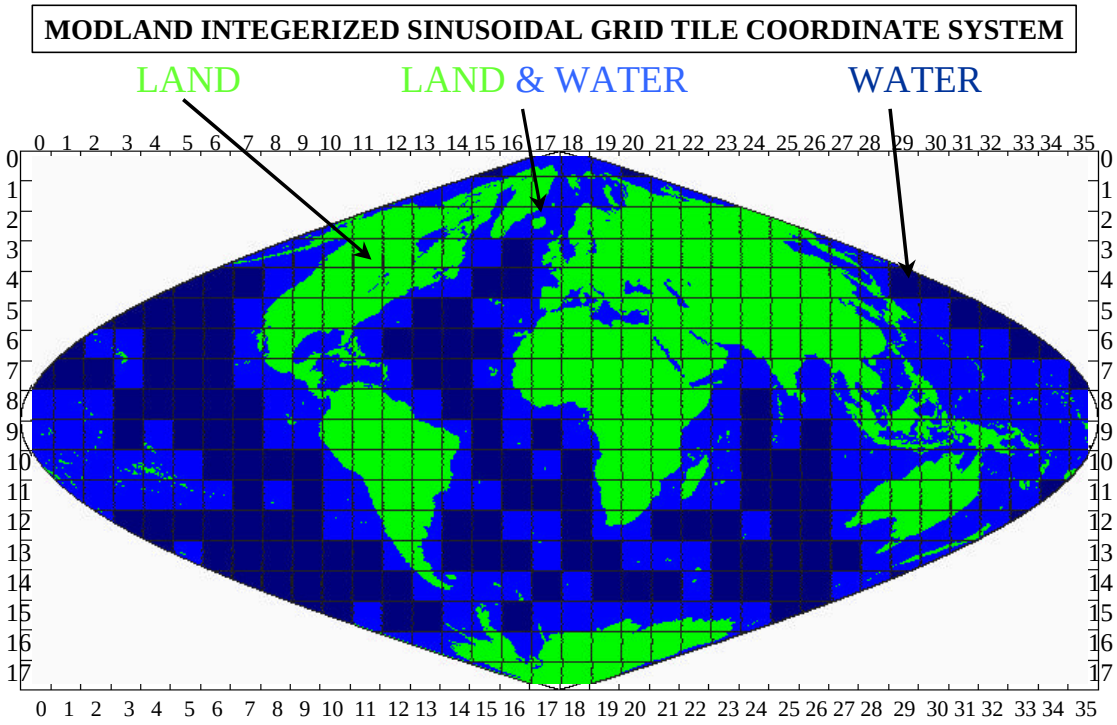

Figure 3.4.3: Display of the Integerized sinusoidal projection as it will be tiled and gridded for the MODIS level 3 products. The horizontal tile ID's (range0,35) and vertical tile ID's (range 0,17) are indicated in the border of the image. The tiles with land areas (green) and ocean (light blue) will be processed. Dark blue ocean tiles will not be processed. White tiles are not covering any land or ocean.

Data flows and dependencies

Both 250m and 1km 16 day products are expected to start execution each time 16 days worth of data become available for a given tile. Nonetheless, the algorithms will wait an extra 5 days in case the series data is not yet available. At the end of the 21st day the algorithm will proceed with the currently available data series. The monthly 1km algorithm will wait until all 16 day composite outputs become available (a maximum of 3 periods), it follows that the algorithm will wait an extra five days for the last 16 day composite period of the month. All dates are to start from January 1 of each year, and ran into the new year if necessary, however dates are again reset to January 1st.

Even though all algorithm perform thorough checking on the input data, the overall performance and data flow is highly dependent on upstream processes, notably L2G (Level 2 Grid) and MODPRAGG (Aggregated 1km surface reflectance) as depicted by Figure 3.2.7. Currently all algorithm define a set of error-action protocols that will facilitate troubleshooting execution problems and indicate the necessary actions culminating in notifying our SCF which in turn will provide prompt patches if necessary.

Performance and storage load estimates

The floating point efficiency of the compositing algorithm was tested using the Walthall BRDF model for 8 and 16 day composite periods. Addition, subtraction, multiplication, and division were equally ranked as one FPO (Floating Point Operation), and comparisons, typecasts, and assignments were not recorded.

Accumulating the coefficients of the Walthall least squares matrix required 24 FPOs per data point per channel at a minimum of 5 data points and a maximum of 8 or 16. Solving explicitly for Wathall's 3 kernels using matrix inversion required a fixed cost of approximately 116 FPOs per channel. The total cost of a Walthall BRDF derived pixel therefore lies between 700 and 1500 FPOs when matrix inversion is used. In calculating only the Walthall "c" (nadir) kernel by Gaussian elimination, the fixed cost of solving the linear system is reduced to an estimated 30 FPOs, reducing the overall costof a BRDF corrected pixel to between 450 and 1250 FPOs.

According to trials on global 8km AVHRR Pathfinder data, BRDF modeling comprised approximately 18% of pixels for 8 day composites and 40% of pixels for 16 day composites. The average number of data points contributing to the BRDF modeled pixels was found to be roughly 5 points for the 8 day composite and 8 points for the 16 day composite. This adjusts the average number of FPOs per pixel to about 90 FPOs for the 8 day composite and 270 FPOs for the 16 day composite as the standard case.

Given a complete tile of 4800 x 4800 land pixels, this gives an average requirement of 2.1 billion FPOs per channel per tile for 8 day composites and 6.2 billion FPOs per channel per tile for a 16 day composite. As a worst case scenario, where the entire composite tile is composed of BRDF derived pixels over the entire composite period, 15.3 billion FPOs are required to produce an 8 day composite tile and 28.6 billion FPOs for 16 days.

The MODPR13 input and output file sizes are presented in Table 4. The storage loads of Level 2 gridded and MODPRAGG input products are given per day as well as the total of these input files per composite periods. It should be noted that the CMG product input and output volumes are given for the complete globe, since they will be processed in a globally continuous fashion. The total global number of tiles is 648.

Table 4: Storage loads of MODIS 13 I/O products

Product names	***Input Sizes (MB)***	***Output Size (MB)***
Level 2 Gridded (L2G) data	~1,500/day	
MODPRAGG: 1km daily	~180/day	
MODPR13A1: 250m/16days	~24,000 (tile)	~276 (tile)
MODPR13A2: 1km/16days	~2,880 (tile)	~32 (tile)
MODPR13A3: 1km/Monthly	~96 (tile)	~32 (tile)
MODPR13C1: 25km/16days	~20,736 (global)	~45 (global)
MODPR13C2: 25km/Monthly	~135 (global)	~33 (global)

*The actual number of global land tiles is 289

3.5 Calibration and Validation

3.5.1 Introduction

Validation of the vegetation index requires both a radiometric as well as geophysical component. Validation of VI performance in discriminating spatial and temporal vegetation differences is accomplished through independent means which include surface biophysical measurements, theoretical canopy modeling, bioclimatic model outputs, and precursor airborne and satellite data sets. Post-launch validation with the MODIS sensor includes correlative measurements and emphasizes the long term performance and quality of the VI product. The validation of the VI products are highly dependent on coupling of the VI values with ground-based "real" variations in photosynthetic and/ or canopy structural activity.

The validation approach and measurements required are related to the science objectives and planned uses of the algorithm. In this section, we outline a validation strategy for the VI equations over a wide range of vegetation conditions. The reliability, sensitivity, limitations, assumptions, and spatial/temporal error fields associated with the algorithm will be determined, clearly stated, as will the conditions/ situations where the algorithm becomes weak or invalid.

Measurements and science objectives:

Spectral vegetation indices (VIs) are widely used in remote sensing as precise radiometric measures of the spatial and temporal patterns of vegetation photosynthetic activity, and the derivation of biophysical vegetation parameters such as leaf area index (LAI), fraction of absorbed photosynthetic active radiation (fPAR), net primary production (NPP), biomass, and percent green cover (see Justice et al., 1985; Sellers

et al., 1994; Townshend et al., 1991). The ubiquitous nature of a global-based VI mandates that it be robust and applicable over all biomes of the earth.

The primary science objectives of the VIs include:

- Spatial and temporal discrimination of vegetation differences (precision);
- Seasonal vegetation profiles of the growing season (phenological);
- Coupling and translation of VIs to biophysical parameters.

Thus, the vegetation indices have both radiometric and biophysical components. The VI units themselves are useful for change detection and analysis of inter- and intra-annual variability patterns in vegetation growth. The goal is to be able to detect vegetation 'changes' at such a resolution as to evaluate the impacts of both climatic and human processes on terrestrial systems/ processes. Derivation of biophysical parameters is a much more sophisticated use of the vegetation index and thus requires a more complex validation strategy. However, in both cases (radiometric and biophysical), it needs to be made clear, that the validation of the VI algorithm concerns the outputs, and not inputs, of the VI product. Having well calibrated and validated red and NIR reflectances does not constitute validation of the VI, as validation is concerned with the performance of the output results, which is the ability of VI values to depict spatial/temporal variations as well as phenology and biophysical parameters.

3.5.2 Validation criteria

Validation of the VI algorithm involves testing and confirmation that the VI is performing as designed in meeting its primary science objectives, or intended uses. Pre-launch validation efforts are aimed at testing the robustness of the algorithm with simulation (MODIS-like) data sets. Post-launch validation efforts incorporate actual instrument performance, product interdependence and long term performance and stability.

There are six general components to the VI validation plan:

1 Comparisons with output from canopy radiant transfer models:

These are utilized to provide a theoretical and physical basis to the VI equations to ensure that the performance and behavior of the VI agrees with that of radiant transfer theory. Radiant transfer modeling is used to vary sensor specifications, vegetation structure and amounts, canopy backgrounds, atmosphere conditions, and sun-target-view geometries. The vegetation indices are tested with simulated data sets generated from simplified 2-stream models, SAIL, and Myneni 3-d canopy models. The 3-d models of Myneni will be conducted over six major, structurally variant, land cover types.

2 Field-based correlative measurements:

Radiant transfer models can only give a preliminary and restrictive indication of algorithm performance. We are constrained to those surfaces which are readily modeled and in which the models themselves have been validated. A more realistic

sampling of the spatial, radiometric, and temporal characteristics of the land surface are obtained with experimental, field measurement campaigns. Field-based radiometry enable data collection under very controlled conditions (sun, view angles, soil, etc.) with negligible atmospheric concerns. Field-based correlative data sets will be used in both pre- and post-launch validation activities and will involve both radiometric and biophysical measurements over a distributed series of test sites. These generally involve point-based measurements which can be coupled with intensive biophysical measurements and destructive vegetation sampling.

3 Experimental aircraft data:

These are valuable in generating correlative data over larger 'footprints' or pixel sizes. These data sets are also generally accompanied with ground biophysical measurements as part of larger field campaigns. AVIRIS, ASAS, AirMISR, and MAS data collected over various land cover types are particularly beneficial in validation of the MODIS VIs in that they allow for approximate simulation of MODIS spectral bandwidths, viewing angles, and can be degraded to MODIS pixel sizes (250 & 500 m). Airborne data sets are being amassed over major biome types and processed into simulated MODIS VI data sets.

4 Existing satellite data sets:

These primarily include the Landsat Thematic Mapper (TM), the NOAA-AVHRR, and SeaWiFS. The Landsat TM possess the spectral bands useful in simulation nadir-based, VI imagery at 250 m and 500 m pixel sizes. The AVHRR and SeaWiFS data, with daily acquisitions, are useful in simulation and testing of the Level 3 compositing algorithm. Landsat TM, SeaWiFS, and AVHRR data sets are being collected and processed over the major biome types.

Sampling requirements and tradeoffs:

As no sensor can simulate the spatial, spectral, temporal, and radiometric resolutions of the MODIS sensor, we must use, in the pre-launch phase, a limited quantity of data derived from a suite of satellite sensors. The sampling requirements are constrained by both the availability of global (spatial and temporal) image data sets and by the amount of biophysical ground sampling that can be accomplished.

Spatial and temporal global coverage is best accomplished with a combination of Landsat TM, SeaWiFS, and AVHRR sampling over the major land cover types. We will use 50-60 'test sites', in accordance with the MODIS-EOS test site program, for a thorough documentation of VI spatial and temporal performance over major land cover types. TM imagery can potentially simulate the 16-day composited MODIS- VI product since TM is readily degraded into the 250m and 500m MODIS channels and is at near-nadir view. The daily, temporal data from the AVHRR and SeaWiFS are suited to evaluate the ability of the level 3 composited VI to construct 'growing season' and phenological curves throughout the year amidst the angular problems and distortions in such data. Furthermore, over the major land cover types, we plan to construct Landsat TM and AVHRR/SeaWiFS growing season profiles to validate the VI compositing

algorithm and determine their performance and accuracy in depicting 'changes' associated with seasonal phenomena.

Measures of success:

The accuracy and performance of the VI will be assessed for each of its intended uses/objectives. In field-measured experimental data sets, Landsat TM data, and canopy model output, changes in biophysical parameters (LAI, fPAR, biomass, green cover) should result in corresponding changes in the VI values for a wide range of vegetation canopies, densities, and structural conditions. The VI should be able to discriminate differences in vegetation within and between the major land cover types and allow for true intercomparisons of spatial and temporal vegetation variations on a global basis.

In the temporal domain, we are concerned with atmospheric residual contamination and angular view angle effects on the VI compositing algorithm which may give false indications of 'change' as well as modify the true nature of a temporal profile. In situ measures of BRDF over some of the test sites as well as ASAS overflights at numerous sites provide for 'true' bidirectional correction of the data and an assessment as to how well the compositing routine is minimizing angular noise. Similarly, seasonal measures of biophysical vegetation parameters, like LAI, provide a "true" seasonal profile of a vegetation growing season.

The 'continuity' role of the NDVI requires appropriate translation coefficients between the AVHRR-NDVI product and the MODIS-NDVI product. These will be obtained on a regular basis over the 'test' sites via co-registration of the AVHRR and MODIS data, post-launch. In the pre-launch period, AVIRIS data are convoluted to simulate both sensors over different land cover types.

The true measure of success of the VI product will be its performance in discriminating spatial/temporal vegetation patterns. This will mean coupling the VI values with ground biophysical measures that can be independently confirmed (measured) to vary or to have changed. The VI algorithms will be evaluated with field-measured biophysical variables, including LAI, fPAR, ground cover, and structure. We will periodically check on a set of translation coefficients to go from VI to biophysical parameters, over many of the land cover types.

In the case of the enhanced VI, there should also be minimal changes in VI values due to canopy background differences (dry/wet soil, snow, litter, soil color, etc.) and the capability of the EVI in removing atmospheric residual contamination (e.g., smoke plumes) will be determined with in situ data sets and sun photometer measures. Over limited periods, the sun photometer network will be used to manually correct for atmosphere and assess the performance of the atmospheric resistance component of the EVI equation. The accuracy of the 'operational' atmospheric correction algorithm, based on dark object subtraction, and its impact on the VI product, will also be evaluated.

Examples of tests to be conducted as measures of success for the NDVI and enhanced VI include:

- **Baseline test:** VI values will be extracted over a global set of hyperarid sites (no vegetation) for spatial and temporal (long term) invariance of the VI values. Some of these tests will be conducted jointly with MCST level 1b calibration sites over uniform areas devoid of vegetation.
- **Saturation test:** VI values will be extracted over a global set of densely forested, grassland, and agricultural sites to check and monitor the upper sensitivity range of the VIs, including 'saturation' problems.
- **Threshold test:** this involves a performance analysis of VI values in arid & semiarid regions to determine lower vegetation detection limits of the vegetation indices.
- **Correlative measurements:** biophysical measurements will be collected and monitored (long term) over the major land cover test sites to ensure linearity and sensitivity of the VI equations over a wide range (desert to forests) of vegetation conditions.
- **Seasonal profiles:** detailed correlative field data and meteorological data will be collected to assess the accuracy of the level 3 composited product in depicting growing season (phenologic) profiles for the major land cover types.
- **Transition zones:** gradients in climatic variation (precipitation, temperature, and topography) which are known to produce corresponding differences in vegetation are ideal and will be used to test VI sensitivities.
- **In-situ nadir-based reflectances:** these will be measured, in conjunction with sun photometer measures, to assess the accuracy of nadir-generated output from the level 3 compositing algorithm. This will include a sensitivity analysis of the atmospheric correction product on VI performance.

3.5.3 Pre-launch algorithm test/development activities

In the pre-launch period, a combination of sensors and data sets are used to simulate MODIS data for the anticipated range of terrestrial surfaces with atmospheric, topographic, and angular variations. Initial validation of the VI equations themselves is accomplished with canopy radiative transfer models such as the Myneni 6 biome canopy code, the SAIL model, and two-stream canopy model. Field experimental data sets are also widely used including radiometric measures (e.g., PARABOLA) and aircraft sensor data. Aircraft and helicopter field measured BRDF data sets are very valuable in simulating MODIS view, angular relationships. Atmospheric radiative transfer codes are also utilized to superimpose varying degrees of atmospheric contamination onto the experimental and canopy model data sets. In this manner, the sensitivity of the VI equations to the atmosphere as well as angular variations can be assessed. Finally, precursor satellite data from the Landsat TM and AVHRR are extremely important in VI validation on a global basis. Pre-launch activities are summarized in Table 5.

Table 5: Summary of pre-launch validation activities

Campaign/Data Set	***Dates***	***Sensors***	***Purpose***
Chile - GLCTS (Test Sites)	September, 1996	Cimel, Exotech, (Ground and Light Aircraft)	•VI-saturation test (rainforest) •VI-baseline test (hyper-arid) •VI-threshold test (arid/semiarid) •VI-biophysical (all)
LTER Sites, U.S.A. (Long-Term Ecological Research)	Ongoing, 1992 - (Annual and Seasonal)	TM, AVHRR, ASAS, MAS	•VI-seasonality, compositing •Field correlative measures - biophysical - phenologic
SCAR-B (Brasil)	August to September, 1995	MAS, AVIRIS, Exotech, Cimel	•VI-smoke analysis •VI-saturation (bandwidths) •VI-biophysical •Continuity analysis (AVHRR, MODIS) (Tropical forest/cerrado)
HAPEX-Sahel (Niger, Africa)	August to October, 1992	ASAS, TM, Exotech, Cimel	•VI-biophysical, angular compositing threshold (Semiarid)
OTTER Transect (Oregon)	1992	ASAS, TM	•VI-biophysical, angular, compositing saturation (Forests)
Monsoon '90	August to September, 1990 September, 1991 Seasonal, 1992	ASAS, AVIRIS, TM, Exotech, (Air, Ground), Spectron	•VI-angular, compositing threshold •VI-seasonality, biophysical (semiarid)
FIFE (Kansas, USA)	May to September, 1987 and July to August, 1989	ASAS, TM	•VI-biophysical, angular, compositing (grassland)
BOREAS (Canada)	August to September, 1995	ASAS, TM	•VI-biophysical, angular, smoke, compositing (boreal forest)
Global-TM/AVHRR GLCTS Pathfinder	1985 to Present	TM, AVHRR	•VI intercomparisons (global) •VI-compositing
MAC (Maricopa Agricultural Center, Arizona)	1986 to Present	TM, Exotech, Sun Photometer, BRDF	•VI-seasonal; biophysical, angular •Dry-wet backgrounds

Some of the field experiments already incorporated into the VI validation effort include:

- SCAR-B experiment in the primary and secondary (regrowth) tropical forests of the Amazon. We have AVIRIS and MAS imagery for the 1995 campaign under clear and very smoky (burning season) conditions. In addition, we collected ground radiometric and biophysical data such as canopy transmittance, ceptometer readings for LAI and fPAR, and sun photometer measurements. Historical and recent values of LAI are also available from various INPE scientists for many of the sites.

- BOREAS experiment in the boreal forests of Canada. This includes MAS (1994) and AVIRIS (1996) overflights over boreal forests in the growing and snow covered seasons. An intensive ground measurement campaign was conducted, including biophysical, and radiometric (Parabola-SE-590) measurements, including sun photometers.

- OTTER experiment in the coniferous forests of the Oregon coastal range as well as Cascade Mountains. We have ASAS and TM data as well as LAI transects and sun photometers.

- FIFE experiment in the tall-grass prairie, Konza Prairie, Kansas. There is ASAS, TM, and ground-based biophysical and radiometric measurements as well as sun photometers.

- HAPEX-Sahel experiment in the semiarid zones of Niger, West Africa. This also includes airborne (ASAS) and satellite data (TM) as well as ground measurements of vegetation and soil biophysical and radiometric properties, and sun photometers.

- Walnut Gulch MONSOON-90 experiment in the arid/semiarid watershed of southeastern Arizona. There is ASAS and AVIRIS data, a multitemporal series of seven Landsat TM scenes covering the 1992 growing season, and a large amount of ground biophysical and radiometric data, including sun photometers.

- Agricultural, uniform crop canopy areas near the Konza Prairie and Maricopa Agriculture Center (MAC), Arizona. These well- controlled, precision grown broadleaf and cereal crops represent homogeneous areas for VI validation. The advantage of these areas are their wide temporal and canopy structural range of vegetation conditions ('zero' vegetation prior to planting and densely vegetated conditions just prior to harvest). The broadleaf and cereal crops present a good set of architectural canopy differences.

Existing satellite data:

In 1992, approximately 20 Landsat 4 & 5, TM scenes were made available to the MODIS team over some of the GLCTS candidate test sites, including broadleaf deciduous and evergreen forests, grasslands, savanna, and deserts. These TM scenes have been processed to simulate MODIS nadir-looking imagery at 250 and 500 m pixel

resolutions. The data have been processed into reflectances with a new set of calibration (vicarious) coefficients, exo-atmosphere irradiances, and atmospheric correction algorithms. The atmospheric corrections include corrections based on in-situ measurements of optical depth; and automated dark object subtraction (DOS) procedures. The derived MODIS-like reflectances are then used as input into the VI algorithms. This data set has been useful in assessing the performance of the VI equations over a global range of vegetation conditions from sparse desert vegetation to very dense temperate and tropical forests.

A Landsat TM multitemporal data set of seven images during the 1992 growing season at the Walnut Gulch Experimental Watershed in southeastern Arizona has also been processed into MODIS simulated VI imagery. These Landsat scenes include the U.S. - Mexican border where differences in land-use yield contrasting differences in pixel responses on both sides of the border. The data set is thus quite useful in analyzing spatial vegetation patterns associated with land use differences and temporal phenological patterns associated with the monsoon and growing seasons. This is useful as a threshold test in both the spatial and temporal domains.

Daily 1 km AVHRR data sets over HAPEX-Sahel, Konza Prairie, H.J. Andrews, and Coweeta sites are being initially used for development and validation of the compositing algorithm. We plan on using daily AVHRR from other GLCTS sites as the data become available. The 8 km Pathfinder data is also useful in evaluating temporal seasonal VI profiles over major global land cover types.

3.5.4 Post-launch activities

In the post-launch period, the primary focus will be on the validation of the global data product. This includes an assessment as to how the products will be evaluated through the operational life of the sensor (or product). In the post-launch period, correlative measurement activities will continue over the test sites and the performance of the algorithm over time will be carefully evaluated from which quality controls will be presented.

Correlative measurement activities in support of VI product validation will occur over a global-based distributed network of community core test sites. Post-launch validation and the community core sites are described in the MODIS validation plan; http://modarch.gsfc.nasa.gov/MODIS/LAND/VAL/core_sites.html.

3.5.5 MQUALS

The ‘MODLAND Quick Airborne Looks’ (MQUALS) is an airborne radiometric system (instruments and protocol) for rapid and low cost land product validation over a range of terrestrial biome types. The package can be flown ‘below the atmosphere’ at altitudes of 150m to 300m AGL for accurate and independent characterization of surface reflectances. The package can be flown at higher altitudes (500 - 1000m AGL) for scaling or large area studies. The basic package consists of calibrated and traceable “transfer radiometers”, digital spectral cameras, an infrared thermometer and

a set of albedometers, all connected to a laptop computer for synchronized measurements. A key feature of MQUALS is the rapid processing, “turn-around” of the measured results to within 7 - 10 days. Through MQUALS, validation sites will be characterized and geolocated with GPS in a consistent manner with an identical and ‘traceable’ radiometric package. In conjunction with simultaneous field sampling, MQUALS will allow us to collect a self-contained set of biophysical and radiometric data from the same ground pixels, which can be correlated and compared with ASTER, Landsat ETM+, and MODIS/MISR pixel values.

Objectives

The main goal is to provide a 'ground truth' characterization of land cover surface types to aid in EOS product validation, support linkages between radiometric accuracies and scientific goals, and accurately tie satellite products to measurements on the ground. MQUALS has the following primary objectives in support of land product validation:

- a land surface optical characterization, including measurement of multispectral radiances, spectral vegetation indexes, and albedo over transects up to 10 - 20 kilometers,
- a consistent, well-calibrated and “traceable” instrument package, coupled to EOS vicarious calibration activities, for radiometric accuracy analysis,
- analysis of dependencies of MODIS data on sampling geometry, target scene, sun angle, and atmosphere,
- extension, correlation and scaling of ground-based vegetation biophysical (leaf area index, %cover, biomass) and radiometric (fraction of absorbed photosynthetically active radiation) measurements to MODIS pixel sizes (250 m, 500 m and 1 km),
- documentation of surface conditions and sampling of landscape variability with high resolution, spectral-digital camera imagery, providing qualitative and semi-quantitative checks of MODIS data.

In addition, MQUALS can provide quality assessments, uncertainty analyses, and generation of error bars with respect to product performance. MQUALS can also provide feedback on calibrated radiance (Level 1B) processing differences and their impacts on land products and provide for systematic assessments of long term stability for monitoring studies.

System design

The basic sensor package consists of a digital, multi-camera array, a nadir-looking Exotech radiometer with MODIS filters, two albedometers, an infrared thermometer (optional), and a laptop computer with Labview software for programmed and coordinated data acquisition. The sensor package can be mounted on a variety of small aircraft. The mounted setup is illustrated in Figure 3.5.1. The ground component of MQUALS consists of a Spectralon reference panel with a second Exotech mounted for continuous measurements of site irradiance.

Exotech radiometer (Model 100 BX) with 4 filter set

The Exotech radiometer is a stable, durable, and calibrated radiometer with four spectral MODIS bands (Table 6). The four channels are co-aligned to within ±0.5 degrees.

Table 6: Spectral characteristics of MQUALS components.

Filter/ Sensor	***MODIS sensor***	***Exotech Radiometer***	***Digital Camera***
Channel 1, red	620 - 670nm	623 - 670nm	635 - 667nm
Channel 2, NIR	841 - 876	838 - 876	835 - 870
Channel 3, blue	459 - 479	456 - 475	455 - 465
Channel 4, green	545 - 565	544 - 564	-----

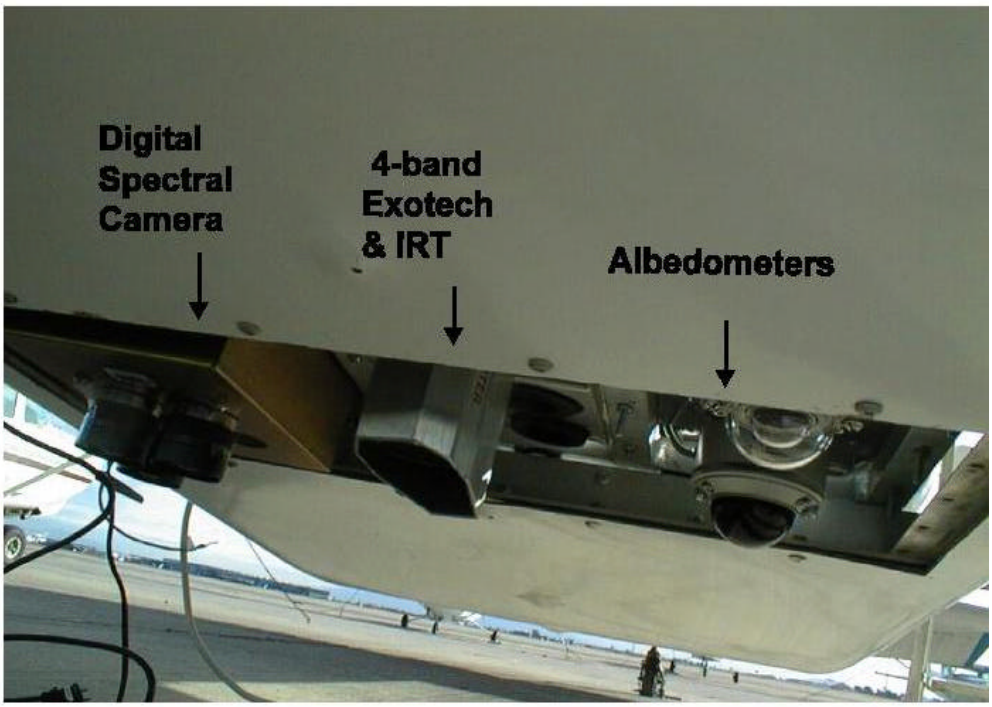

Figure 3.5.1: Mounted setup of the MQUALS radiometric package.

We will fly the aircraft on multiple transects (3 km to 20 km in length) over a selected site. The flight lines are designed on a case by case basis but will generally (1) traverse uniform areas of the dominant land cover type, and (2) span the land cover heterogeneity, including land cover subtypes and gradients to encompass the range of variability in site parameters. Typical flight transects would occur at an altitude (150 m AGL) corresponding to Exotech 'pixel' resolutions of 40 meters. Pixel size could be increased to 100 m or more by flying at higher altitudes. At a speed of 150 km/hr, the

aircraft can traverse a 10 km length transect in approximately 4 minutes, collecting approximately 240 Exotech samples at a nearly constant sun angle-target-sensor geometry (Figure 3.5.2).

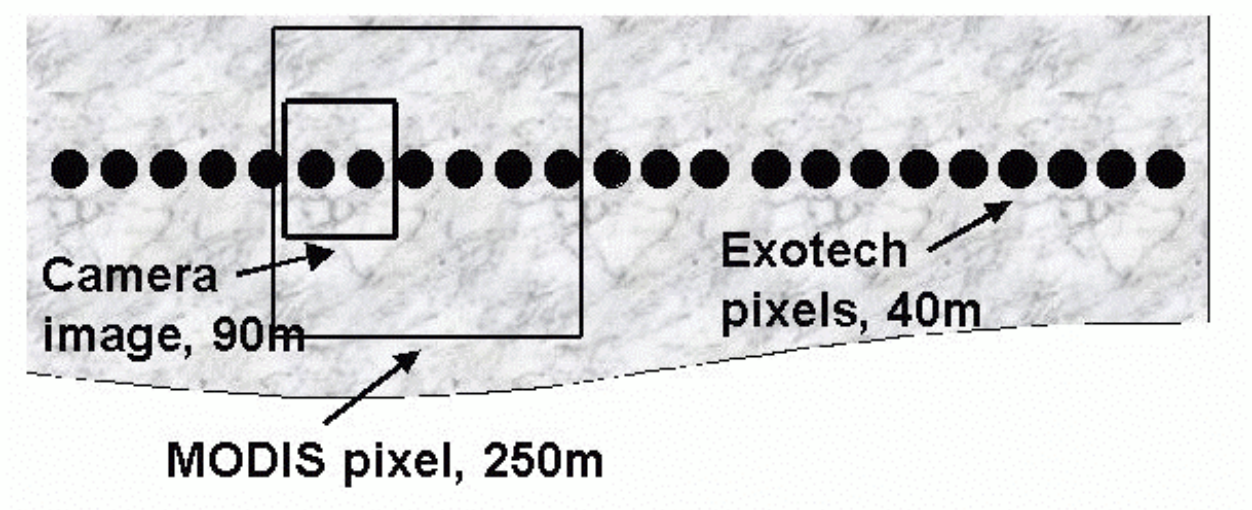

Figure 3.5.2: Diagram of Exotech and camera airborne data acquisitions in relation to a MODIS pixel for 150 m AGL and 15 ^{o} field-of-view Exotech.

Dycam ADC modular 4 camera system

This multi-camera array consists of three cameras, upgradeable to a fourth camera, with an optical mount and parallel port software. The spectral characteristics of the cameras are summarized in Table 6. The total field-of-view for the 1/4 inch detector array (640 x 480 pixels) in combination with a 6 mm focal length lens is 33 o (horizontal) by 25 o (vertical). The swath width and dimensions of the imagery are presented in Table 2. At 150 m AGL, a 90 m swath is imaged while at 1000 m AGL a 600 m swath is imaged. The camera system and software is also designed to be able to measure 'reference' panels for derivation of reflectance-based imagery and computation of vegetation indexes.

Spectralon diffuse reflectance target

Field and low-altitude airborne measurements of radiance reflected from a surface require an assessment of the irradiance in order to derive the reflectance factor (RF). One can approximate irradiance by sampling radiance reflected from a Spectralon panel that is calibrated to account for its inherent nonlambertian properties. A commercially produced, Spectralon diffuse reference panel (Labsphere) is utilized on the ground in combination with a second Exotech radiometer to measure irradiance conditions at the site continuously. They have an anodized aluminum frame covered with a specially formulated white reflectance coating (Spectraflect) with a reflectivity of 99% over an effective spectral range of 300 to 2400 nm and a thermal stability of 100^{o} C. An 18 inch by 18 inch panel constructed from four, 9 inch panels is used for MQUALS. These plates are weather-resistant and washable.

Kipp and zonen albedometers

MQUALS will use two airborne and one ground-based pyranometers/albedometers from Kipp and Zonen. The clear-dome albedometer provides shortwave broadband albedo in the range of 305 - 2800 nm and the red dome albedometer provides NIR broadband albedo in the range of 695 - 2800 nm. An upward looking, clear-dome pyranometer is mounted on top of the airplane for irradiance measurements. Another set of albedometers is mounted on the ground.

Laptop computer for data logging

A Gateway 233 MHz laptop computer is used as a data logger and instrument controller. Data logging frequency for all of the on-board instruments and start and stop times are programmed prior to the flight transects. The computer logs the data from all instruments simultaneously. Special purpose software (LabView) is used to synchronize these activities.

LabVIEW instrument control software with PC cards (Version 4.0)

This software is an icon-based graphical programming and data acquisition tool with front panel user interface for control and data visualization. Complex acquisition, analysis and presentation applications can be generated in real time using a graphical methodology. Different data acquisition systems such as the Exotech, digital camera and albedometers can be controlled using this software, and data acquired from these instruments can be checked visually for problems. PC cards, including those for signal conditioning, voltage modulation accessories, and data acquisition, are used to connect the computer with the instruments.

GPS system (from aircraft):

Geo-positioning of the air transects is accomplished using the GPS receiver on board the aircraft. Plans are being made to acquire a differential GPS and connect it directly to the laptop computer.

Calibration and traceability

The Exotech radiometers are stable and durable optical instruments that are easily calibrated in the laboratory and can be cross-calibrated with similar instrumentation used in the field as well as on other airborne platforms. These “transfer radiometers” can also be cross-calibrated with the radiometric equipment utilized by MODIS Calibration Support Team (MCST) activities, including simultaneous on-site measurements at vicarious calibration field sites. The MQUALS package is currently being calibrated by the Remote Sensing Group within the Optical Sciences (OSC) Department at the University of Arizona. There are three aspects to the calibration of the Exotech radiometers used as part of MQUALS. One aspect is to calibrate radiometers in flight using "vicarious calibration" techniques similar to those used for Landsat-5 Thematic Mapper. These methods rely heavily upon collecting ground-based data from a well-understood radiometer (an ASD FieldSpec FR in this case) with reference to a field reflectance standard (Spectralon in this case). The field reference is calibrated in the Optical Sciences laboratory prior to the field experiment to determine

its bi-directional reflectance with reference to a NIST-traceable standard of reflectance. Differences in the spectral response of the Exotech radiometer relative to MODIS are taken into account by measuring the Exotech spectral response using the Optical Sciences monochromator. An additional tool for the vicarious calibration of the Exotech radiometer, and the digital cameras as well, are a set of calibrated tarps (7 meters on a side) that are setup at the calibration sites to be viewed by the airborne camera. This enables characterization of the spectral response and linearity of the camera array system.

A similar technique to the vicarious calibration approach is to cross-calibrate the Exotech radiometer to the ground-based radiometer using the field reflectance standard to transfer the calibration from one instrument to the other. Since the ASD spectroradiometer is hyperspectral, effects due to band differences in the two radiometers are minimized. This method can either rely on an absolute calibration of the ASD spectroradiometer to obtain the absolute calibration of the Exotech, or one can simply do the cross-calibration in terms of reflectance. The latter has the advantage of "reducing" the uncertainty by not relying on the absolute calibration of one of the radiometers but a relative calibration of the reflectance standard. A similar calibration can be done in the lab, but the field-based approach has the advantage of using the same spectral source that the MQUALS data set uses.

The third aspect of the MQUALS calibration is to provide a “traceable” link to the MODIS Instrument (Figure 3.5.3). This is accomplished through the use of ultrastable laboratory radiometers that took part in a calibration round-robin to characterize the Santa Barbara Remote Sensing (SBRS) primary standard source (a large spherical integrating source) used in the pre-launch calibration of the MODIS instrument. These radiometers have also been used to calibrate the Optical Science's sources and reference panels. Thus, any instrument calibrated using Optical Science's laboratory will have traceability to the MODIS sensor.

Note that at this point, we do not know of the radiometric stability of the multispectral digital camera system, however we will make efforts to calibrate this instrument if possible. If not, this instrument will primarily be used for characterization of scene heterogeneity and qualitative variability of component optical properties.

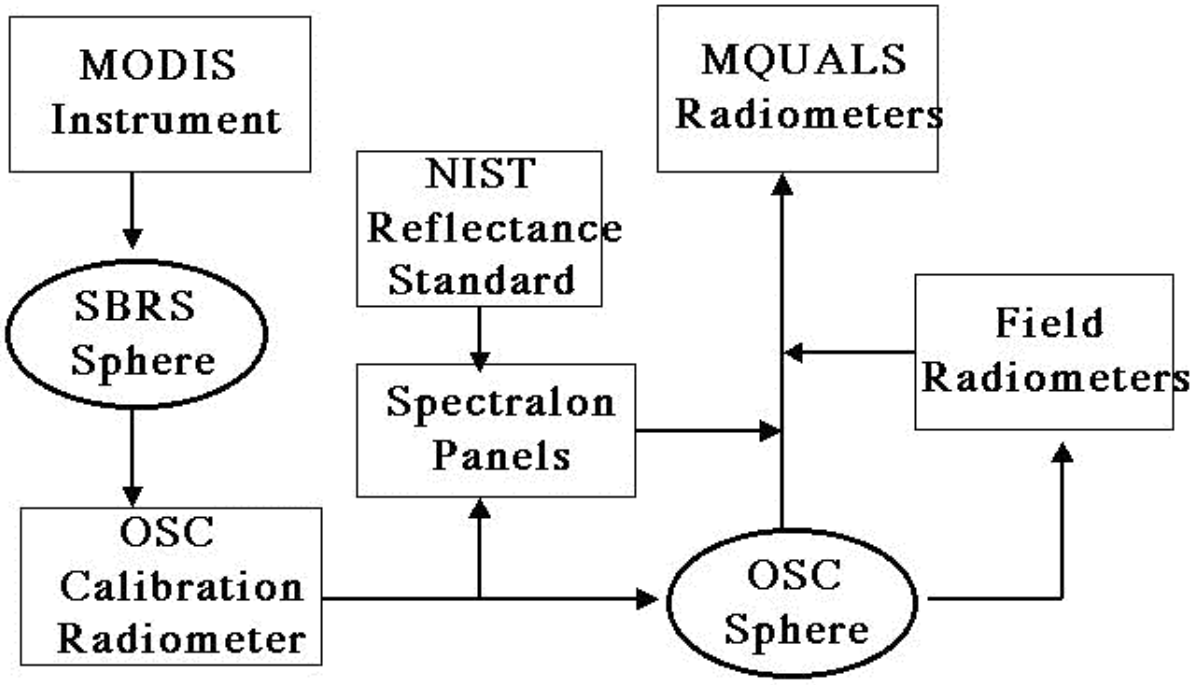

Figure 3.5.3: Diagram of the traceability of field validation measurements to the MODIS instrument.

MQUALS schedule for 1999

Testing of the MQUALS package is ongoing and has occurred mostly in the vicinity of the Semi-Arid Land-Surface-Atmosphere (SALSA) area in southeast Arizona (http://www.tucson.ars.ag.gov/salsa/salsahome.html), over a fairly uniform dry grassland. We also are testing and calibrating the system in a barren uniform area near the Tucson International Airport. The current schedule for 1999 MQUALS deployments is listed in the table below.

Table 7: 1999 MQUALS deployments

Site	***Dates***	***Land Cover***	***Other***
Railroad Playa, NV	Late April-early May	Barren, vicarious calibration	Landsat ETM+
La Jornada, NM	Late May & September	Semi-arid grass/ shrub	LTER site
*Bondville , IL	July - August	Cropland	BigFoot site
ARM-CART or Konza	July - August	Grassland/ agriculture	Possible MAS/AirMISR overflight
BOREAS NSA	August-September	Boreal Forest	BigFoot site

* tentative

The Railroad Playa calibration experiment is expected in late April – early May , following the April 15 launch of Landsat ETM+. In this experiment we aim to (1) cross calibrate the MQUALS package with the MODIS vicarious calibration team; (2) register MQUALS data with Landsat ETM+ for a homogeneous site with no vegetation; and (3) establish a zero baseline condition for vegetation indexes. The Jornada Experimental Range (La Jornada) near Las Cruces, New Mexico will be flown in late May (dry season) and September (wet season) time frames. This is a semi-arid validation Core Site with desert shrub, grassland, and mixed grass/ shrub subsites located in a protected area which is part of the NSF's Long Term Ecological Research (LTER) site network. The Bondville, IL and BOREAS NSA (Canada) overflights will occur in conjunction with BigFoot vegetation validation work in the July-September time frame. The objective of the BigFoot program is to provide ground validation of MODIS land cover, LAI, and FPAR, with special consideration of multiple scaling issues (http://www.fsl.orst.edu/larse/bigfoot/plan.html). The MQUALS data will provide insight for scaling from field data to 250 m spatial resolution. Finally we would like to underfly the ER-2, with MAS/ AirMISR, over some of the ARM-CART or Konza grassland sites.

Product validation issues

We propose to characterize the optical properties of the validation sites and at various times of the season. These validation, 'ground truth' sites will be both optically and biophysically characterized, and atmospheric effects will be simultaneously measured with sunphotometers. Precise measurements will include both the heterogeneity and uniformity of the sites and measurements will be conducted at high resolution as well as scales equivalent to that of the MODIS pixel (250 m to 1km). We will initially focus on the surface reflectance, vegetation indexes, albedo, LAI, FPAR and landcover products from MODIS. MQUALS could also be useful for the snow and land surface temperature products.

The level 3 and 4, composited products result in cloud-free maps at 16-day intervals. These products possess a wide range of view and sun angles and 'residual' atmospheric and cloud effects. Ground truth measurements are necessary to assess how well the composited, as well as daily, MODIS products represent actual surface conditions. For example, with an independent determination of nadir-based, 'true' surface reflectance, we can analyze where the uncertainties in the MODIS products lie and identify systematic errors. Errors associated with MODIS sensor calibration, instrument noise, atmosphere correction, BRDF correction, and the cloud mask algorithm will propogate into the final product. However, MQUALS measurements will similarly be affected by calibration, bidirectional reflectance, spectral sensitivity, and diffuse/direct irradiance effects. Thus, independent measures acquired for product validation will always differ somewhat from MODIS. Surface heterogeneity also presents difficulties in the measurement of biophysical parameters over MODIS pixel sizes. The error and lack of reproducibility in field measurements may exceed those from the satellite.

We are currently drafting field validation methods and protocol documentation as a guide in the standardization of EOS field collected validation data. MQUALS flights, for

example, will generally be made at multiple times of the day in order to bracket a range of sun angles and allow for extrapolation of the radiometric data to specific solar zenith angles for standardization purposes. A single MODIS scene or composited product may contain solar zenith angles that vary by 20°, along with sensor view angles that vary ±55°. End-to-end validation examples involving MQUALS prior to the launch of the Terra Earth Observing satellite will be the subject of a forthcoming article. The URL address for MQUALS is http://gaia.fcr.arizona.edu/newmqual.html.

3.6 Exception Handling

Exceptions will be handled under three possible scenarios:

i. Tile is unavailable, incomplete, or corrupted.

ii. Tile is flagged as not usable through information contained in the metadata fields. This includes problems with tiles at high latitudes associated with low illumination conditions. These are sometimes referred to as the terminator effect (Holben, 1986).

iii. Tile is determined not usable after unsuccessfully attempting to process it. Conditions include unfavorable atmospheric correction procedures, heavy cloud cover, missing data, unfavorable image geometry, and unusable reflectance values.

Under all three scenarios, daily products cannot be produced. No files are written and the output metadata is flagged appropriately. Composite products are capable of filtering the input files and only use the tiles with acceptable quality, provided there is at least one usable day available. Otherwise, no output products are written and the metadata fields are flagged accordingly.

3.7 Error Analysis and Uncertainty Estimates

Improved predictions of global change will depend greatly on the quality and stability of satellite-derived time series products depicting Earth surface states and processes. As a key EOS facility instrument, the MODIS will provide a validated, high quality, 15-year data set. Error anlaysis and uncertainty estimation are vital in order to evaluate the quality of products and algorithm performances, and to provide “reliability” estimates (confidence level) of the products as an input to the “downstream” products.

The VI error/uncertainty analyses are aimed at:

- developing a theoretical basis and set of error/uncertainty propagation equations which allow for modeling of the propagation and accumulation of errors/uncertainties from all the “upstream” data processing steps into the VI products,
- estimating both radiometric and biophysical uncertainties of the VI products, and
- evaluating and characterizing the VI algorithm performances.

The resulting secondary products will include error maps over a globe and error budgets over the well-characterized core validation sites. Error budgets will identify the major sources of errors for the VI products and thus allow for an overall performance evaluation of the algorithms. These secondary products will be integrated into the QC/QA plan. The results of the analyses and uncertainty estimates will be summarized in a living document that will be available to the user communities through the web.

The following sections describe the planned strategies for error analyses and uncertainty estimations as well as the current uncertainty estimates for several sources of errors.

3.7.1 Analysis approaches

The estimation of the MODIS VI uncertainties are being conducted on a step-by-step basis (e.g., Miura et al., 1999). These steps will follow the VI product generation system (PGS) which consists of four main steps as described in Section 2.2.10 (Figure 3.7.1). Potential sources of uncertainties that may significantly impact the VI accuracies have been identified for each level of the upstream processing steps (Figure 3.7.1). Additional sources of errors/uncertainties will be included as they are identified.

We currently utilize the "law of propagation of uncertainty" as a basis for modeling the propagation and accumulation of uncertainties from each of potential sources into the VI products (NCSL, 1997; Taylor and Kuyatt, 1994). We start with a functional relationship f that describes an estimate of a quantity of interest y, determined from estimates of N other quantities x_1, x_2, … , x_N :

$$y = f(x_1, x_2, \ldots, x_N) . \tag{15}$$

The law of propagation of uncertainty estimates the standard uncertainty of the measurement result y, denoted by $u(y)$, from the standard uncertainties of the input estimates x_i, denoted by $u(x_i)$, based on the partial derivatives of the functional relationship between y and x_i :

$$u^2(y) = \sum_{i=1}^{N}\sum_{j=1}^{N}\frac{\partial f}{\partial x_i}\frac{\partial f}{\partial x_j}u(x_i, x_j) = \sum_{i=1}^{N}\left(\frac{\partial f}{\partial x_i}\right)^2 u^2(x_i) + 2\sum_{i=1}^{N-1}\sum_{j=i+1}^{N}\frac{\partial f}{\partial x_i}\frac{\partial f}{\partial x_j}u(x_i, x_j) . \tag{16}$$

The uncertainty propagation equation (16) is based on a 1st-order Taylor series approximation of equation 15. A set of uncertainty propagation equations designed for reflectance calibration uncertainties into atmospherically-corrected VIs are shown in Appendix F (Miura et al., 1999).

Uncertainty estimations are being and will be coupled strongly with both pre- and post-launch validation activities. As part of the pre-launch validation activities, we continue to develop uncertainty propagation equations and estimate uncertainties for each potential source of error as well as to evaluate algorithm performances. Simulated, field experimental, and the existing airborne/satellite-borne remote sensing data (i.e., AVIRIS, ASAS, TM, SPOT, AVHRR, and SeaWiFS) are being used.

Assessments of the algorithm performances and accuracies have been conducted with data sets simulated from canopy radiative transfer models (Huete and Liu, 1994), acquired during intensive field campaigns including the BOREAS (Leeuwen et al., 1996) and SCAR-B (Miura et al., 1998) experiments.

During the post-launch validation activities, the error analysis activities will specifically focus on the evaluation of the overall product accuracies. We plan to integrate uncertainty propagation equations for a complete estimation of total-accumulated uncertainties on a pixel-by-pixel basis and to utilize these uncertainty estimates for the validation of the VI products. In each intensive field campaign, the uncertainty propagation equations will be applied and error budgets identifying the major sources of errors will be produced. These uncertainty estimates for each intensive field campaign will be summarized in a living document available to the user communities through the web.

The other main focus of the error analyses during the intensive field campaigns will be on the analysis of VI-biophysical relationships followed by the biophysical uncertainty estimations. This will be conducted over each validation site as well as on a global scale, which will result in the estimations of both biome-specific and global biophysical uncertainties of the VI products.

Error budgets will continue to be produced and updated over the core validation sites and be coupled with the long term stability monitoring as part of the QC/QA plan (see Section 3.5.2). The baseline test for the long term stability checking of the VI products will be also utilized to examine the validity of the uncertainty propagation equations and estimated uncertainties.

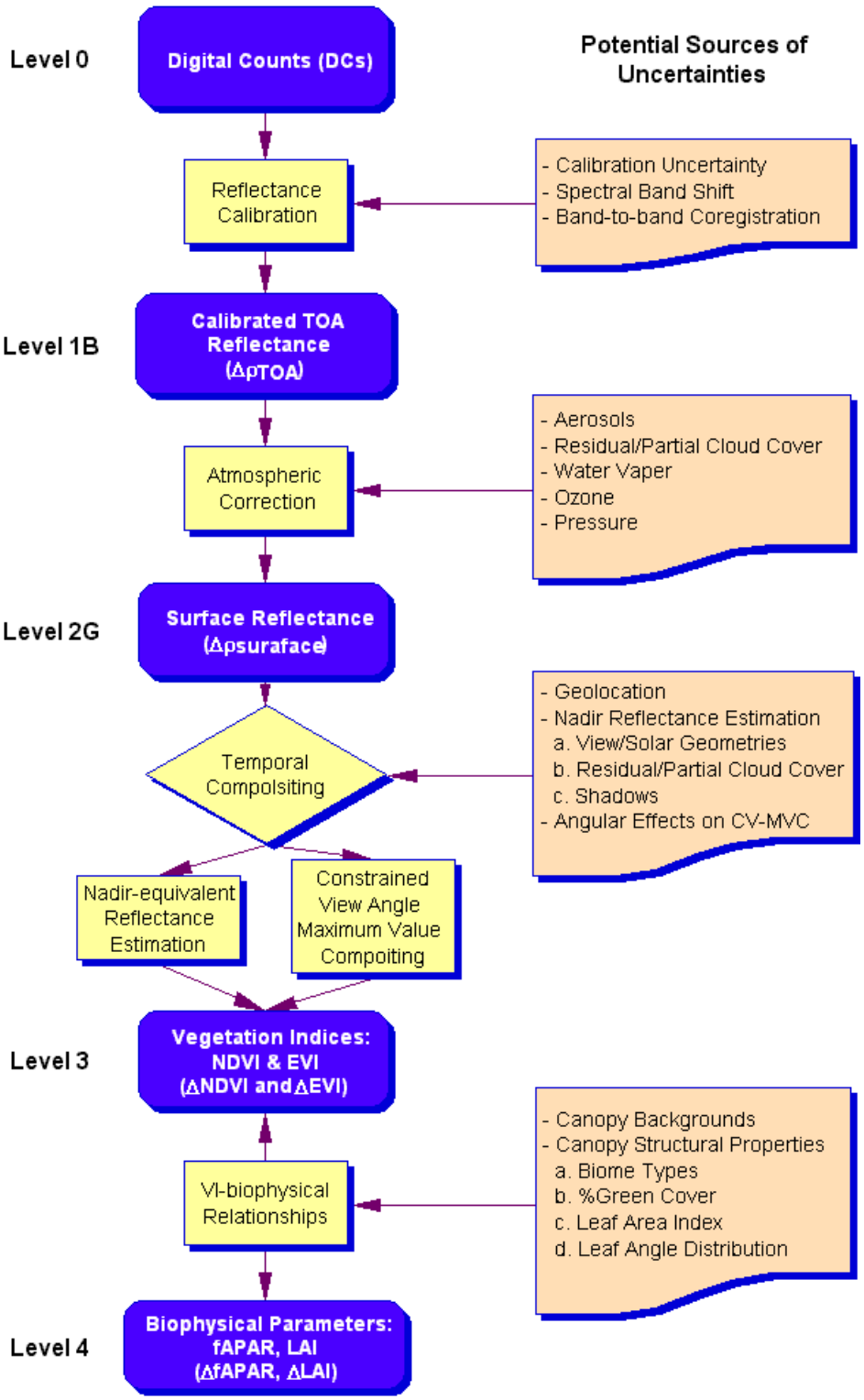

Figure 3.7.1: "End-to-end" analysis approaches of the VI error/uncertainties. Potential sources of errors and uncertainties considered in each upstream processing step are also listed.

3.7.2 Uncertainty estimates

Among many potential sources of error and uncertainties, we have so far evaluated the VI product accuracies due to 1) reflectance calibration uncertainty, 2) spectral band shift, and 3) band-to-band coregistration error. The following summarizes the results of these analyses.

Reflectance calibration uncertainty

The radiometric calibration of the AVHRR sensors has been one of the most intensively studied problems. Numerous studies have shown that the calibration of the AVHRR instrument has changed substantially following launch and drifted subsequently over time, which in turn creates interannual variability in NDVI assessments unrelated to global vegetation dynamics (Frouin and Gautier, 1987; Holben et al., 1990; Che and Price, 1992; Kaufman and Holben, 1993; Rao 1993; Teillet et al., 1990). As a key EOS instrument, the MODIS has placed a strong emphasis on its calibration algorithm. Its three on-board calibrators for the calibration of the solar reflective regions will accomplish a higher precision in calibration results and will be periodically validated through vicarious calibration techniques for detection and correction of drift in calibration gains over time (Barbieri et al., 1997).

Miura et al. (1999) and Huete and Liu (1994) evaluated the impact of reflectance calibration uncertainties on the accuracies of the VI product using the experimental data set (Huete et al., 1985) with the 6S radiative transfer code (Vermote et al., 1997a) for atmosphere simulations. Miura et al. (1999) developed an approach to model propagation of uncertainties from calibrated top-of-atmosphere (TOA) reflectances to atmospherically-corrected VIs (Appendix F).

The resultant VI uncertainties u_{cal}(VI) varied with both surface reflectances and atmospheric conditions (Miura et al., 1999). The largest uncertainties of the NDVI and ARVI were observed for dark targets with little or no vegetation (Figure 3.7.2a,c). The SAVI uncertainties were nearly constant throughout a range of target brightness and vegetation abundance (Figure 3.7.2b). The EVI uncertainties linearly increased with increasing EVI values (Figure 3.7.2d). Atmosphere turbidities increased calibration uncertainties in all the VIs through its effect on TOA reflectances. The VI uncertainties were also found to decrease when the calibration errors were positively correlated between bands.

The mean VI uncertainties were estimated to be +/- 0.01 VI units for the NDVI and SAVI, and +/- 0.02 VI units for the ARVI and EVI under normal atmosphere conditions (>= 20 km visibility) and a 2% reflectance calibration uncertainty (Miura et al., 1999). The higher uncertainties in the ARVI and EVI resulted from the inclusion of the blue band, adding to the overall calibration uncertainty budget.

Their sensitivity analyses showed that the VI uncertainties increased linearly with increases in reflectance calibration uncertainties for all the VIs examined in their study, from which the required calibration uncertainties to attain a desired VI accuracy were obtained (Table 8).

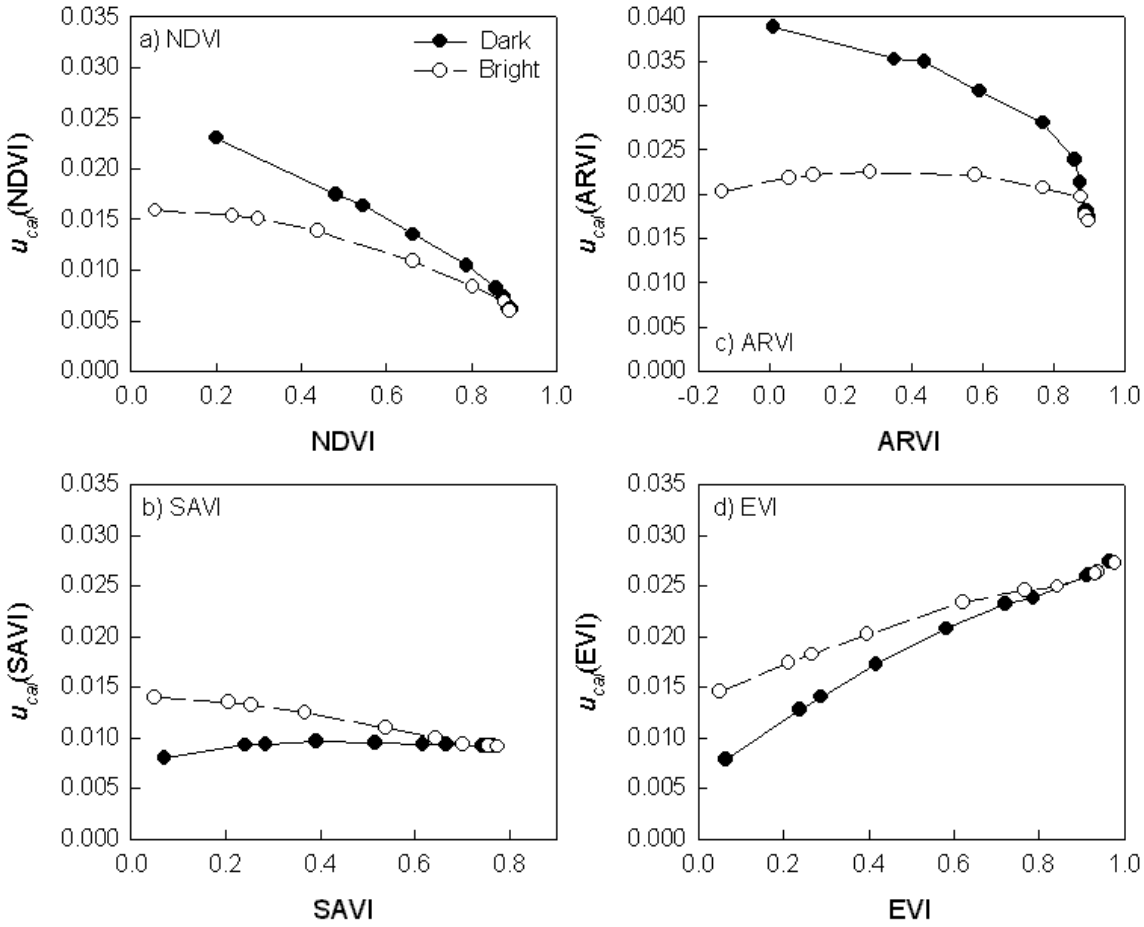

Figure 3.7.2: Uncertainties of the a) NDVI, b) SAVI, c) ARVI, and d) EVI due to a 2% reflectance calibration uncertainty, u_{cal}(VI), propagated through a turbid atmosphere (continental aerosols with a 10 km visibility). The band calibration errors were treated as uncorrelated. The figure includes u_{cal}(VI) for dark (Cloverspring) and bright (Superstition) backgrounds.

Table 8: Predicted Reflectance Calibration Uncertainties (%) Requirements for Desired Levels of VI Uncertainty

	Required Reflectance Calibration Uncertainties (%)			
u_{cal}(VI) Desired	*NDVI*	*SAVI*	*ARVI*	*EVI*
0.01	1.9%	2.1%	1.0%	1.2%
0.02	3.8%	4.2%	1.9%	2.4%
0.05	9.4%	10.5%	4.8%	5.9%
0.10	18.9%	21.1%	9.6%	11.9%

Spectral band shift and band-to-band coregistration error

In addition to the calibration uncertainty, the MODIS L1B product will include the spectral band shift information in the solar reflective bands and the coregistration accuracy of other bands relative to the reference band per granule basis (Barbieri et al., 1997).

Huete and Liu (1994) assessed expected errors of the VIs due to a 2 nm center wavelength shift and a 20% band-to-band coregistration error. A SAIL model simulation (Verhoef, 1984) was performed using a single-layer one-component canopy model with a uniform leaf angle distribution. The reflectance and transmittance properties of cedar tree leaves were used with canopy LAI values from 0.0 to 3.0 for a solar zenith angle of 40^{O} and nadir view.

All of the VIs examined in the study (the NDVI, SAVI, ARVI, and EVI) have an error of +/- 0.01 VI unit due to a 2 nm center wavelength shift. For the band-to-band coregistration error, the NDVI and EVI have an error of +/- 0.01 VI unit while the SAVI and ARVI have an error of +/- 0.03. The results are summarized in Table 9.

Table 9: Expected VI Error due to the Spectral Band Shift and Band-to-band Coregistration Error (in VI unit)

	NDVI	*SAVI*	*ARVI*	*EVI*
Band Shift	0.01	0.01	0.01	0.01
Coregistration	0.01	0.03	0.03	0.01

4 Constraints, Limitations, and Assumptions

Only day time, cloud free data should be processed to produce the VI. We assume that the data is cloud-free and that sub-pixel clouds will be filtered with a compositing cycle. We are assuming fairly good geolocation and registration of multi-temporal data (within MODIS specifications) and we will need a careful assessment of geometric performance post-launch. We are assuming that a first order topographic correction will be made post-launch in the derivation of surface reflectances. We envisage that 16 days of data will be stored and kept on-line in order to look for anomalies.

REFERENCES

Ackerman, S., Strabala, K., Menzel, P., Frey, R., Moeller, C., Gumley, L., Baum, B., Schaaf, C., Riggs, G., and Welch, R. (1996), Discriminating Clear-sky from Cloud with MODIS Algorithm Theoretical Basis Document V3, http://eospso.gsfc.nasa.gov/atbd/modistables.html.

Agbu, P. A. and James, M. E. (1994), The NOAA/NASA Pathfinder AVHRR Land Data Set User's Manual. Goddard Distributed Active Archive Center, NASA, Goddard Space Flight Center, Greenbelt, MD.

Archard, F., Malingreau, J. P., Phulpin, T., Saint, G., Saugier, B., Seguin, B., and Vidal Madjar, D. (1994), A mission for global monitoring of the continental biosphere. VEGETATION International Users Committee Secretariat, Joint Research Centre, Institute for Remote Sensing Applications, I-21020 ISPRA (Va) Italy. http://www-vegetation.cst.cnes.fr:8050/.

Asrar, G., Fuchs, M., Kanemasu, E. T., and Hatfield, J. L. (1984), Estimating absorbed photosynthetic radiation and leaf area index from spectral reflectance in wheat, *Agron. J.*, 76:300-306.

Asrar, G., Myneni, R. B., and Choudhury, B. J. (1992), Spatial heterogeneity in vegetation canopies and remote sensing of absorbed photosynthetically active radiation: a modeling study, *Remote Sens. Environ.*, 41:85-101.

Barbieri, R., Montgomery, H., Qiu, S., Barnes, B., Knowles, D., Jr., Che, N., and Goldberg, I. L. (1997), The MODIS Level 1B Algorithm Theoretical Basis Document Version 2.0 (ATBMOD-01), NASA Goddard Space Flight Center, Greenbelt, Maryland 20771, USA, 68p.

Baret, F. and Guyot, G. (1991), Potentials and limits of vegetation indices for LAI and APAR assessment, *Remote Sens. Environ.*, 35:161-173.

Baret, F., Guyot, G., and Major, D. (1989), TSAVI: a vegetation index which minimizes soil brightness effects on LAI and APAR estimation, *in 12th Canadian Symp. on Remote Sensing and IGARSS'90*, Vancouver Canada, 10-14 July 1989.

Barker, J. L., Brown, K. S., and Harnden, J. M. K. (1993), MODIS: Calibration & Characterization Algorithm Theoretical Basis Document (Cal ATBD), Version 0, 1 July, 1993.

Bartlett, D. S., Hardisky, M. A., Johnson, R. W., Gross, M. F., Klemas, V., and Hartman, J. M. (1988), Continental scale variability in vegetation reflectance and its relationship to canopy morphology, *Int. J. Remote Sens.*, 9:1223-1241.

Bausch, W. (1993), Soil background effects on reflectance-based crop coefficients for corn, *Remote Sens. Environ*, 46:1-10.

Begue, A. (1993), Leaf area index, intercepted photosynthetically active radiation, and spectral vegetation indices: a sensitivity analysis for regular-clumped canopies, *Remote Sens. Environ.*, 46:45-59.

Buschmann, C., and Nagel, E. (1993), In vivo spectroscopy and internal optics of leaves as basis for remote sensing of vegetation, *Int. J. Remote Sens*., 14:711-722.

Che, N. and Price, J. C. (1992), Survey of radiometric calibration results and methods for visible and near infrared channels of NOAA-7, -9, and -11 AVHRRs, *Remote Sens. Environ.*, 41:19-27.

Choudhury, B. J. (1987), Relationships between vegetation indices, radiation absorption, and net photosynthesis evaluated by a sensitivity analysis, *Remote Sens. Environ*., 22:209-233.

Cihlar, J., Manak, D., and D'Iorio, M. (1994a), Evaluation of Compositing Algorithms for AVHRR Data over Land, *IEEE Trans. Geosc. Remote Sens.*, 32:427-437.

Cihlar, J., Manak, D., and Voisin, N. (1994b), AVHRR bidirectional reflectance effects and compositing, *Remote Sens. Environ.*, 48:77-88.

Cihlar, J. C., Ly, H., Li, Z., Chen, J., Pokrant, H., and Huang, F. (1997), Multi temporal, multichannel AVHRR data sets for land biosphere studies—Artifacts and corrections, *Remote Sens. Environ.*, 60:35-57.

Clevers, J. G. P. W. (1989), The application of a weighted infrared-red vegetation index for estimating leaf area index by correcting soil moisture, *Remote Sens. Environ.*, 29:25-37.

Clevers, J. G. P. W. and Verhoef, W. (1993), LAI estimation by means of the WDVI: a sensitivity analysis with a combined PROSPECT-SAIL model, *Remote Sens. Rev.*, 7:43-64.

Colwell, J. E. (1974), Vegetation canopy reflectance, *Remote Sens. Environ.*, 3:175-183.

Cooper, K., Smith, J. A., and Pitts, D. (1982), Reflectance of a vegetation canopy using the adding method, *Appl. Opt.*, 21: 4112-19.

Curran, P. J. (1980), Relative reflectance data from preprocessed multispectral photography, *Int. J. Remote Sens.*, 1:77-83.

Curran, P. J. (1982), Multispectral remote sensing for estimating biomass and productivity, *in Plants and the Daylight Spectrum, edited by H. Smith,* London Academic Press.

Daughtry, C. S. T., Gallo, K. P., Goward, S. N., Prince, S. D., and Kustas, W. P. (1992), Spectral estimates of absorbed radiation and phytomass production in corn and soybean canopies, *Remote Sens. Environ*, 39:141-152.

Deering, D. W. and Leone (1986), A sphere-scanning radiometer for rapid directional measurements of sky and ground radiance, *Remote Sens. Environ.*, 19:1-24.

Deering, D. W. (1978), Rangeland reflectance characteristics measured by aircraft and spacecraft sensors. Ph.D. Dissertation, Texas A & M University, College Station, TX, 338 pp.

Demetriades-Shah, T. H., Steven, M. D., and Clark, J. A. (1990), High resolution derivative spectra in remote sensing, *Remote Sens. Environ*., 33:55-64.

Eidenshink, J. C. and Faundeen, J. L. (1994), The 1km AVHRR global land data set: first stages in implementation, *Int. J. Remote Sensing*, 15(17):3443-3462.

Elvidge, C. D. and Chen, Z. (1995), Comparison of broad-band and narrow-band red and near-infrared vegetation indices, *Remote Sens. Environ.*, 54:38-48.

Flittner, D. E. and Slater, P. N. (1991), Stability of narrow-band filter radiometers solar-reflective range, *Photogramm. Eng. Remote Sens.*, 57:165-171.

Franklin, J. F., Bledsoe, C. S., and Callahan, J. T. (1990), Contributions of the long-term ecological research program, *BioScience*, 40:509-523.

Fraser, R. S. and Kaufman, Y. J. (1985), The relative importance of aerosol scattering and absorption in remote sensing, *IEEE Trans. Geosci. Remote Sens.*, 23: 625-633.

Frouin, R. and Gautier, C. (1987), Calibration of NOAA-7 AVHRR, GOES-5, and GOES-6 VISSR/VAS solar channels, *Remote Sens. Enviorn.*, 22:73-101.

Fung, Y., Tucker, C. J. and Prentice, K. C. (1987), Application of Advanced Very High Resolution Radiometer vegetation index to study atmosphere-biosphere exchange of CO_2, *J. Geoph. Res.*, 92, 2999-3015.

Gallo, K. P., Daughtry, C. S. T., and Bauer, M. E. (1985), Spectral estimation of absorbed photosynthetically active radiation in corn canopies, *Remote Sens. Environ.,* 17:221-232.

Gitelson, A. A., Kaufman, Y. J., and Merzlyak (1997), An atmospherically resistant "green" vegetation index (ARGI) for EOS-MODIS, *Remote Sens. Environ.*, 58:289-298.

Goel, N. S. (1988), Models of vegetation canopy reflectance and their use in estimation of biophysical parameters from reflectance data, *Remote Sens. Rev.,* 4: 1-222.

Goward, D. G., Turner, S., Dye, D. G., and Liang, J. (1994), University of Maryland improved Global Vegetation Index, *Int. J. Remote Sensing*, 15(17):3365-3395.

Goward, S. N., Markham, B. L., Dye, D. G., Dulaney, W., and Yang, J. (1991), Normalized difference vegetation index measurements from the Advanced Very High Resolution Radiometer, *Remote Sens. Environ.*, 35:257-277.

Goward, S. N. and Huemmrich, K. F. (1992), Vegetation canopy PAR absorptance and the normalized difference vegetation index: an assessment using the SAIL model, *Remote Sens. Environ.*, 39:119-140.

Goward, S. N., Markham, B., Dye, D. G., Dulaney, W., and Yang, J. (1991), Normalized difference vegetation index measurements from the Advanced Very High Resolution Radiometer, *Remote Sens. Environ.*, 35:257-277.

Goward, S. N., Tucker, C. J., and Dye, D. G. (1985), North American vegetation patterns observed with the NOAA-7 advanced very high resolution radiometer, *Vegetatio*, 64:3-14.

Graetz, D. (1990), Romote sensing of terrestrial ecosystem structure: an ecologist's pragmatic view, In *Remote Sensing of Biosphere Functioning*; Ch. 2.,pp 5-30. Springer Verlag, N.Y., 312pp.

Gutman, G. (1991), Vegetation indices from AVHRR: an update and future prospects, *Remote Sens. Environ.*, 35:121-136.

Hall, F. G., Huemmrich, K. F., and Goward, S. N. (1990), Use of narrow-band spectra to estimate the fraction of absorbed photosynthetically active radiation, *Remote Sens. Environ.*, 32:47-54.

Heilmen, J. L. and Kress, M. R. (1987), Effects of vegetation on spectral irradiance at the soil surfaces, *Agron. J.*, 79:765-768.

Holben, B. N., Kaufman, Y. J., and Kendall, J. D. (1990), NOAA-11 AVHRR visible and near-IR inflight calibration, *Int. J. Remote Sens.*, 11(8):1511-1519.

Holben, B. N. (1986), Characterization of maximum value composites from temporal AVHRR data, *Int. J. Remote Sensing*, 7:1417-1434.

Hooker, S. B., Esaias, W. E., Feldman, G. C., Gregg, W. W., and McClain, C. R. (1992), An Overview of SeaWiFS and Ocean Color. NASA Tech. Memo. 104566, Vol. 1, S.B. Hooker and E.R. Firestone, Eds., NASA Goddard Space Flight Center, Greenbelt, Maryland, 24 pp.

Huete, A. R. (1988), A soil adjusted vegetation index (SAVI), *Remote Sens. Environ.*, 25:295-309.

Huete, A. R. and Liu, H. Q. (1994), An error and sensitivity analysis of the atmospheric- and soil-correcting variants of the NDVI for the MODIS-EOS, *IEEE Tans. Geosci. Remote Sens.*, 32(4):897-905.

Huete, A., Justice, C. and Liu, H. (1994), Development of vegetation and soil indices for MODIS-EOS, *Remote Sens. Environ.*, 49:224-234.

Huete, A. R. and Tucker, C. J. (1991), Investigation of soil influences in AVHRR red and near-infrared vegetation index imagery, *Int. J. Remote Sensing*, 12:1223-1242.

Huete, A. R. and Warrick, A. W. (1990), Assessment of vegetation and soil water regimes in partial canopies with optical remotely sensed data, *Remote Sens. Environ.*, 32:155-167.

Huete, A. R., Hua, G., Qi, J., Chehbouni, A., and van Leeuwen, W.J.D.G. (1992), Normalization of multidirectional red and NIR reflectances with the SAVI, *Remote Sens. Environ.*, 40:1-20.

Huete, A. R., Jackson, R. D., and Post, D. F. (1985), Spectral response of a plant canopy with different soil backgrounds, *Remote Sens. Environ.*, 17:37-53.

Huete, A. R., Liu, H. Q., Batchily, K., and van Leeuwen, W. (1997), A comparison of vegetation indices over a global set of TM images for EOS-MODIS, *Remote Sens. Environ.*, 59:440-451.

Hutchinson, C. F. (1991), Use of satellite data for Famine Early Warning in sub-Saharian Africa, *Int. J. Remote Sensing*, 12(6):1405-1421.

IGBP (1992), The International Geosphere-Biosphere Programme: A Study of Global Change, Improved Global Data for Land Applications, IGBP Report No. 20, Stockholm, Sweden: IGBP Secretariat.

Irons, J. R., Ranson, K. J., Williams, D. L., Irish, R. R., and Huegel, F. G. (1991), An off-nadir imaging spectroradiometer for terrestrial ecosystem studies, *IEEE Trans. Geosci. and Remote Sens.*, 29:66-74.

Jackson, R. D. and Huete, A. R. (1991), Interpreting vegetation indices, *Prev. Vet. Med.,* 11:185-200.

Jackson, R. D. and Pinter, Jr., P. J. (1986), Spectral response of architecturally different wheat canopies, *Remote Sens. Environ.*, 20:43-56.

Jacquemoud, S. and Baret, F. (1990), PROSPECT: A model of leaf optical properties spectra, *Remote Sense. Environ.*, 3: 43-47.

James, M. D. and Kalluri, S. N. V. (1994), The Pathfinder AVHRR land data set: An improved coarse resolution data set for terrestrial monitoring, Int. J. Remote Sensing, 15(17):3347-3363.

Jordan, C. F. (1969), Derivation of leaf area index from quality of light on the forest floor, *Ecology*, 50:663-666.

Justice, C., Hall, D., Salomonson, V., Privette, J., Riggs, G., Strahler, A., Lucht, W., Myneni, R.,Knjazihhin, Y., Running, S., Nemani, R., Vermote, E., Townshend, J., Defries, R., Roy, D., Wan, Z.,Huete, A., van Leeuwen, W., Wolfe, R., Giglio, L., Muller, J-P., Lewis, P., and Barnsley, M. (1998), The Moderate Resolution Imaging Spectroradiometer (MODIS): Land remote sensing for global change research, *IEEE Trans. Geosci. and Remote Sens.*, 36(4):1228-1249.

Justice, C. O., Townshend, J. R. G., Holben, B. N., and Tucker, C. J. (1985), Analysis of the phenology of global vegetation using meteorological satellite data, *Int. J. Remote Sensing*, 6:1271-1318.

Kaufman, Y. J. (1989), The atmospheric effect on remote sensing and its corrections, in *Theory and Applications of Optical Remote Sensing* (G. Asrar, Ed.), John Wiley & Sons Inc., New York, pp. 336-428.

Kaufman, Y. J. and Holben, B. N. (1993), Calibration of the AVHRR visible and near-IR bands by atmospheric scattering, ocean glint and desert reflection, *Int. J. Remote Sensing*, 14(1):21-52.

Kaufman, Y. J. and Tanre, D. (1992), Atmospherically resistant vegetation index (ARVI) for EOS-MODIS, *IEEE Trans. Geosci. Remote Sensing*, 30:261-270.

Kaufman, Y. J. and Tanre, D. (1996), Strategy for direct and indirect methods for correcting the aerosol effect on remote sensing: from AVHRR to EOS-MODIS, *Remote Sens. Environ.*, 55:65-79.

Kimes, D. S., Holben, B. N., Tucker, C. J., and Newcomb, W. W. (1984), Optimal directional view angles for remote-sensing missions, *Int. J. Remote Sensing*, 5(6):887-908.

Kimes, D. S., Newcomb, W. W., Tucker, C. J., Zonneveld, I. S., Van Wijngaarden, W., De Leeuw, J., and Epema, G. F. (1985), Directional reflectance factor distribution for cover types of Northern Africa, *Remote Sens. Environ.*, 18:1-19.

King, M. D., Kaufman, Y. J., Menzel, W. P., and Tanre, D. (1992), Remote sensing of cloud, aerosol, and water vapor properties from the Moderate Resolution Imaging Spectrometer (MODIS), *IEEE Trans. Geosci. Remote Sensing*, 30:2-27.

Kneizys, F. X., Shettle, E. P., Abreu, L. W., Chetwynd, J. H., Anderson, G. P., Gallery, W. O., Selby, J. E. A., and Clough, S. A. (1988), Users Guide to LOWTRAN 7, Report AFGL-TR-88-0177, AFRCL, Bedford, Mass., August, 137 pp.

Kuchler, A. W. (1995), Natural vegetation map, *In: Rand McNally Goode's World Atlas; 19th edition. Eds. Espenshade E.B. Hudson, J.C., Morrison, J.L.*, p 18-19.

Leeuwen van, W. J. D., Huete, A. R., and Laing, T. W. (1999), MODIS vegetation index compositing approach: A prototype with AVHRR data, Remote Sens. Environ. (accepted).

Leeuwen van, W. J. D., Huete, A. R., Jia, S., and Walthall, C. L. (1996), Comparison of vegetation index compositing scenarios: BRDF versus maximum VI approaches, IEEE-IGARSS '96, Lincoln, Nebraska, 3:1423-1425.

Leeuwen van, W. J. D., Huete, A. R., Duncan, J., and Franklin, J. (1994), Radiative transfer in shrub savanna sites in Niger -- preliminary results from HAPEX-II-Sahel: 3. Optical dynamics and vegetation index sensitivity to biomass and plant cover, *Agricultural and Forest Meteorology*, 69:267-288.

Leeuwen van, W. J. D., Huete, A. R., Didan, K., and Laing, T. (1997a), Modeling bi-directional reflectance factors for different land cover types and surface components to standardize vegetation indices, *In Proceedings of the 7th Int. Symposium on Physical Measurements and Signatures in Remote Sensing*, Courcheval, France; 7-11April 1997. pp 373-380.

Leeuwen van, W. J. D., Huete, A. R., and Laing, T. (1998), Evaluation of the MODIS vegetation index compositing algorithm using SeaWiFS data, IEEE- IGARSS'98, Seattle.

Leeuwen van, W. J. D., Laing, T. W., and Huete, A. R. (1997b), Quality assurance of global vegetation index compositing algorithms using AVHRR Data, *IEEE-IGARSS'97*, Singapore, pp 341-343.

Liu, H. Q., and Huete, A. R. (1995), A feedback based modification of the NDVI to minimize canopy background and atmospheric noise, *IEEE Trans. Geosci. Remote Sensing*, 33:457-465.

Lucht, W. (1998), Expected retrieval accuracies of bidirectional reflectance and albedo from EOS-MODIS and MISR angular sampling, *J. Geoph. Res.*, 103(D8):8763-8778.

Major, D. J., Baret, F., and Guyot, G. (1990), A ratio vegetation index adjusted for soil brightness, *Int. J. Remote Sensing*, 11:727-740.

Meyer, D., Verstraete, M., and Pinty, B. (1995), The effect of surface anisotropy and viewing geometry on the estimation of NDVI from AVHRR, *Remote Sens. Rev.*, 12:3-27.

Middleton, E. M. (1991), Solar zenith angle effects on vegetation indices in tallgrass prairie, *Remote Sens. Environ.*, 38:45-62.

Miura, T., Huete, A. R., van Leeuwen, W. J. D., and Didan, K. (1998), Vegetation detection through smoke-filled AVIRIS images: An assessment using MODIS band passes, *J. Geophys. Res.*, 103(D24):32,001-32,011.

Miura, T., Huete, A. R., and Yoshioka, H. (1999), Evaluation of sensor calibration uncertainties on vegetation indices for MODIS (*submitted to IEEE Tans. Geosci. Remote Sens.*).

Moody, A. and Strahler, A. H. (1994), Characteristics of composited AVHRR data and problems in their classification, *Int. J. Remote Sensing*, 15(17):3473-3491.

Morisette, J. T., Privette, J. L., Justice, C. O., and Running, S. W. (1998), MODIS Land Validation Plan; MODIS Land Discipline Team, http://modarch.gsfc.nasa.gov/MODIS/LAND/VAL/land_val_plan.pdf

Myneni, R. B. and Asrar, G. (1993), Atmospheric effects and spectral vegetation indices, *Remote Sens. Environ*, 390-402.

Myneni, R. B., Hall, F. G., Sellers, P. J., and Marshak, A. L. (1995), The interpretation of spectral vegetation indices, *IEEE Trans. Geosci. Remote Sensing*, 33(2):481-486.

Myneni, R. B, Keeling, C. D., Tucker, C. J., Asrar, G., and Nemani, R. R. (1997), Increased plant growth in the northern high latitudes from 1981 to 1991, *Nature* 386:698-702.

Nakajima, T. Y., Nakajima, T., Nakajima, M., Fukushima, H., Kuji, M., Uchiyama, A., and Kishino, M. (1998), Optimization of the Advanced Observing Satellite Global Imager channels by use of radiative transfer calculations, *Applied Optics*, 37(15):3149-3163.

NCSL (1997), *American National Standard for Expressing Uncertainty – U.S. Guide to the Expression of Uncertainty in Measurement*, ANSI/NCSL Z540-2-1997, National Conference of Standards Laboratories (NCSL), Boulder, CO, 101p.

Perry, C. R., Jr. and Lautenschlager, L. F. (1984), Functional equivalence of spectral vegetation indices, *Remote Sens. Environ.*, 14:169-182.

Pinter, P. J., Jr. (1993), Solar angle independence in the relationship between absorbed PAR and remotely sensed data for alfalfa, *Remote Sens. Environ*, 46:19-25.

Pinty, B. and Verstaete, M. M. (1992), GEMI: A non-linear index to monitor global vegetation from satellites, *Vegetatio*, 101:15-20.

Price, J. C. (1987), Calibration of satellite radiometers and the comparison of vegetation indices, *Remote Sens. Environ.*, 21:419-422.

Price, J. C. (1992), Estimating vegetation amounts from visible and near infrared reflectance measurements, *Remote Sens. Environ.*, 41:29-34.

Prince, S. D. and Justice, C. O. (1991), (Editorial) Special issue on coarse resolution remote sensing of the Sahelian environment, *Int. J. Remote Sensing*, 12(6):1137-1146.

Prince, S. D. (1991), A model of regional primary production for use with coarse resolution satellite data, *Int. J. Remote Sensing*, 12(6):1313-1330.

Prince, S. D., Justice, C. O., and Moore, B. (1994), Remote Sensing of NPP, IGBP DIS Working Paper #10, IGBP-DIS, Paris.

Prince, S. D., Kerr, Y. H., Goutorbe, J. P., Lebel, T., Tinga, A., Bessemoulin, P., Brouwer, J., Dolman, A. J., Engman, E. T., Gash, J. H. C., Hoepffner, M., Kabat, P., Monteny, B., Said, F., Sellers, P., and Wallace, J. (1995), Geographical, biological and remote sensing aspects of the Hydrologic Atmospheric Pilot Experiment in the Sahel (HAPEX-Sahel), *Remote Sens. Environ.*, 51:215-234.

Privette, J. L., Eck, T. F., and Deering, D. W. (1997), Estimating spectral albedo and nadir reflectance through inversion of simple BRDF models with AVHRR/MODIS-like data, *J. Geophys. Res.*, 102(D24):29,529-29,542.

Privette, J. L., Myneni, R. B., Emery, W. J., and Hall, F. G. (1996), Optimal sampling conditions for estimating grassland parameters via reflectance model inversions, *IEEE Trans. Geosci. Remote Sens.*, 34(1):272-284.

Qi, J. and Kerr, Y. (1997), On current compositing algorithms, *Remote Sens. Rev.*, 15:235-256.

Qi, J., Chehbouni, A., Huete, A. R., Kerr, Y. H., and Sorooshian, S. (1994), A modified soil adjusted vegetation index, *Remote Sens. Environ,* 48:119-126.

Qi, J., Huete, A. R., Hood, J., and Kerr, Y. (1994), Compositing multi-temporal remote sensing data sets, PECORA 11, Symposium on land information systems, Sioux Falls August 1993, p.206-213.

Qi, J., Huete, A. R., Moran, M. S., Chehbouni, A., and Jackson, R. D. (1993a), Interpretation of vegetation indices derived from multi-temporal SPOT images, *Remote Sens. Environ.*, 44:89-101.

Rahman, H., Pinty, B., and Verstraete, M. M. (1993), Coupled surface-atmosphere reflectance (CSAR) model 2. Semiemperical surface model usable with NOAA AVHRR, *J. Geophys. Res.*, 89(D11):20,791-20,801.

Raich, J. W. and Schlesinger, W. H. (1992), The global carbon dioxide flux in soil respiration and its relationship to vegetation and climate, *Tellus*, 44B:81-99.

Rao, C. R. N., Ed. (1993), Degradation of the visible and near-infrared channels of the Advanced Very High Resolution Radiometer on the NOAA-9 spacecraft: assessment and recommendations for corrections, NOAA Technical Report

NESDIS 70, Dept. of Commerce, NOAA, National Environmental Satellite, Data, And Information Service, 25p.

Richardson, A. J. and Wiegand, C. L. (1977), Distinguishing vegetation from soil background information, *Photogramm. Eng. Remote Sens.*, 43:1541-1552.

Roujean, J. L., Leroy, M., Podaire, A., and Deschamps, P. Y. (1992), Evidence of surface reflectance bidirectional effects from a NOAA/AVHRR multi-temporal data set, *Int. J. Remote Sensing*, 13(4), 685-698.

Roy, D. P. (1997), Investigation of the maximum normalized difference vegetation index (NDVI) and the maximum surface temperature (T_s) AVHRR compositing procedures for the extraction of NDVI and Ts over forest, *Int. J. Remote Sens.*, 18(11):2383-2401.

Running, S. W. (1990), Estimating terrestrial primary productivity by combining remote sensing and ecosystem simulation, *In Ecological Studies Vol "Remote Sensing of Biosphere Functioning", H. Mooney and R. Hobbs., eds.*, Springer-Verlag, pp.65-86.

Running, S. W. and Nemani, R. R. (1988), Relating seasonal patterns of the AVHRR vegetation index to simulated photosynthesis and transpiration of forest in different climates, *Remote Sens. Environ.*, 24:347-367.

Running, S. W., Justice, C. O., Salomonson, V., Hall, D., Barker, J., Kaufman, Y. J., Strahler, A. H., Huete, A. R., Muller, J. P., Vanderbilt, V., Wan, Z. M., Teillet, P., and Carneggie, D. (1994), Terrestrial remote sensing science and algorithms planned for EOS/MODIS, *Int. J. Remote Sensing*, 17:3587-3620.

Running, S. W., Nemani, R. R., Peterson, D. L., Band, L. E., Potts, D. F., Pierce, L. L., and Spanner, M. A. (1989), Mapping regional forest evapotranspiration and photosynthesis by coupling satellite data with ecosystem simulation, *Ecology*, 70:1090-1101.

Runyon, J., Waring, R. H., Goward, S. N., and Welles, J. M. (1994), Environmental limits on net primary production and light-use efficiency across the Oregon transect, *Ecological Applications*, 4:226-237.

Salomonson, V. V., Barnes, W. L., Maymon, P. W., Montgomery, H. E., and Ostrow, H. (1989), MODIS: advanced facility instrument for studies of the earth as a system, *IEEE Trans. Geosci. Remote Sens.*, 27:145-153.

Sellers, P. J. (1985), Canopy reflectance, photosynthesis and transpiration, *Int. J. Remote Sensing*, 6:1335-1372.

Sellers, P. J., Tucker, C. J., Collatz, G. J., Los, S., Justice, C. O., Dazlich, D. A., and Randall, D. A. (1994), A global 1° * 1° NDVI data set for climate studies. Part 2 - The adjustment of the NDVI and generation of global fields of terrestrial biophysical parameters, *Int. J. Remote Sensing*, 15:3519-3545.

Singh, S. M. (1988), Simulation of solar zenith angle effect on global vegetation index (GVI) data, *Int. J. Remote Sensing*, 9:237-248.

Slater, P. N. (1984), The importance and attainment of absolute radiometric calibration, *Proc. SPIE Critical Rev. Remote Sens.*, 475:34-40.

Slater, P. N. (1985), Radiometric considerations in remote sensing, *Proc. IEEE*, 73(6):997-1011.

Slater, P. N. and Jackson, R. D. (1982), Atmospheric effect on radiation reflected from soil and vegetation as measured by orbiting sensors using various scanning directions, *Appl. Opt.*, 21:3923-3931.

Stowe, L. L., McClain, E.P., Carey, R., Pellegrino, P., Gutman, G.G., Davis, P., Long, C., and Hart, S. (1991), Global distribution of cloud cover derived from NOAA/AVHRR operational satellite data, *Advances in Space Research*, 3:51-54.

Strahler, A, et al. (1996), MODIS BRDF/Albedo Product: ATBD version 4, http://eospso.gsfc.nasa.gov/atbd/modistables.html.

Tans, P. P., Fung, I. Y., and Takahashi, T. (1990), Observational constraints on the global atmosphere CO_2 budget, *Science*, 247:1431-1438.

Teillet, P. M., Slater, P. N., Ding, Y., Santer, R. P., Jackson, R. D., and Moran, M. S. (1990), Three methods for the absolute calibration of the NOAA AVHRR sensors in flight, *Remote Sens. Environ.*, 31:105-120.

Teillet, P. M. and Fedosejevs, G. (1995), On the dark target approach to atmospheric correction of remotely sensed data, *Canadian J. Remote Sens.* (in press).

Teillet, P. M., Staenz, K., and Willams, D. J. (1997), Effects of spectral, spatial, and radiometric characteristics on remote sensing vegetation indices of forested regions, *Remote Sens. Environ.*, 61:139-149.

Townshend, J. R. G. (1994), Global data sets for land applications from the AVHRR: an introduction, *Int. J. Remote Sensing*, 15:3319-3332.

Townshend, J. R. G., Justice, C. O., Gurney, C., and McManus, J. (1992), The impact of misregistration on the detection of changes in land cover, *IEEE Trans. Geosci. Remote Sens.*, 30(5):1054-1060.

Townshend, J. R. G., Justice, C. O., Li, W., Gurney, C., and McManus, J. (1991), Global land cover classification by remote sensing: present capabilities and future capabilities, *Remote Sens. Environ.*, 35:243-255.

Townshend, J. R. G., Justice, C. O., Skole, D., Malingreau, J. P., Cihlar, J., Teillet, P., Sadowski, F., and Ruttenberg, S. (1994), The 1 km resolution global data set: needs of the International Geosphere Biosphere Programme, *Int. J. Remote Sensing*, 15:3417-3441.

Tucker, C. J. and Sellers, P. J. (1986), Satellite remote sensing of primary productivity, *Int. J. Remote Sensing*, 7:1395-1416.

Tucker, C. J., Holben, B. N., Elgin, J. H., and McMurtrey (1981), Remote sensing of total dry matter accumulation in winter wheat, *Remote Sens. Environ.*, 11:171.

Tucker, C. J. (1979), Red and photographic infrared linear combinations for monitoring vegetation, *Remote Sens. Environ.*, 8:127-150.

Taylor, B. N. and Kuyatt, C. E. (1994), *Guidelines for Evaluating and Expressing the Uncertainty of NIST Measurement Results*, NIST Technical Note 1297, 1994 Ed., Gaithersburg, MD, 24p.

Verhoef, W. (1984), Light scattering by leaf layers with application to canopy reflectance modeling: the SAIL Model, *Remote Sens. Environ.*, 16:125-141.

Vermote, E., Tanré, D., Deuzé, J. L., Herman, M., and Mocrette, J. J. (1997a), Second Simulation of the Satellite Signal in the Solar Spectrum (6S): an overview, *IEEE Trans. Geosc. Remote Sens.*, 35(3):675-686.

Vermote, E., El Saleous, N., Justice, C. O., Kaufman, Y. J., Privette, J. L., Remer, L., Roger, J. C., and Tanré, D. (1997b), Atmospheric correction of visible to middle-infrared EOS-MODIS data over land surfaces: background, operational algorithm and validation, *J. Geoph. Res.*, 102(D14):17131-17141.

Vierling, L. A., Deering, D. W., and Eck, T. F. (1997), Differences in Arctic tundra vegetation type and phenology as seen using bidirectional radiometry in the early growing season, *Remote Sens. Environ.*, 60:71-82.

Viovy, N., Arino, O., and Belward, A. S. (1992), The best index slope extraction (BISE): a method for reducing noise in NDVI time series, *Int. J. Remote Sensing*, 13:1585-1590.

Vogelmann, T. C., Rock, B. N., and Moss, D. M. (1993), Red edge spectral measurements from sugar maple leaves, *Int. J. Remote Sens.*, 14:1563-1575.

Walter-Shea, E. A., Privette, J. L., Cornell, D., Mesarch, M. A., and Hays, C. J. (1997), Relations between spectral vegetation indices and leaf area and absorbed radiation in alfalfa, *Remote Sens. Environ.*, 61:162-177.

Walthall, C. L., Norman, J. M., Welles, J. M., Campbell, G., and Blad, B. L. (1985), Simple equation to approximate the bi-directional reflectance from vegetative canopies and bare soil surfaces, *Applied Optics*, 24(3):383-387.

Wanner W., Strahler, A. H., Hu, B., Lewis, P., Muller, J.-P., Li, X., Barker Schaaf, C. L., and Barnsley, M. J. (1997), Global retrieval of bidirectional reflectance and albedo over land from EOS MODIS and MISR data: Theory and algorithm, *J. Geoph. Res.*, 102(D14):17,143-17,161.

Wickland, D. E. (1989), Future directions for remote sensing in terrestrial ecological research, *In Theory and Applications of Optical Remote Sensing (G. Asrar, ed.)*, Wiley Series in Remote Sensing, Wiley, New York, pp. 691-724.

Wiegand, C. L., Richardson, A. J., Escobar, D. E., and Gebermann, A. H. (1991), Vegetation indices in crop assessments, *Remote Sens. Environ.*, 35:105-119.

Wolfe, R. E., Roy, D. P.,and Vermote, E. (1998), MODIS land data storage, gridding, and compositing methodology: Level 2 grid, *IEEE Trans. Geosci. and Remote Sensing*, 36(4):1324-1338.

Wu, A., Li, Z., and Cihlar (1995), Effects of land cover type and greenness on advanced very high resolution radiometer bidirectional reflectances: Analysis and removal, *J. Geophys. Res.*, 100(D5):9179-9192.

Yoder, B. J. and Waring, R. H. (1994), The normalized difference vegetation index of small Douglas-fir canopies with varying chlorophyll concentrations, *Remote Sens. Environ.*, 49:81-91.

Yoshioka, H., Huete, A. R., and Miura, T. (1999), Derivation of vegetation isoline equations in red-NIR reflectance space, *IEEE Trans. Geosci. Remote Sens.* (accepted).

Yoshioka, H. (1999), Applications of transport theory in optical remote sensing of land surfaces, dissertation, University of Arizona, Arizona, USA. (to be submitted)

APPENDIX A: Derivation of Vegetation Isoline Equations in Red-NIR Reflectance Space

Yoshioka et al. (1999) consider the simplest case of a homogeneous canopy layer with an underlying Lambertian surface soil background. This problem is analogous to the radiative transfer in a homogeneous atmosphere layer with the earth surface as the bottom boundary. There is a simple analytical RT model (Kaufman, 1989; raser and Kaufman, 1985; Kaufman and Tanre, 1996) widely used to represent the top-of-atmosphere radiances by considering the contribution of photons which are scattered multiple times by the bottom surface. Among many canopy RT models, the representation of the reflectance by the Cooper-Smith-Pitts model (Cooper et al., 1982) can be reduced to the same form by assuming a single canopy layer and a soil layer underneath the canopy. The reflectance, $\rho_\lambda(\theta,\varphi,\theta_0)$, of this system is written in reflectance units as (hemispherical-directional reflectance factor),

$$\rho_\lambda(\theta,\varphi,\theta_0) = \rho_{v\lambda}(\theta,\varphi,\theta_0) + \frac{T_{\downarrow v\lambda}(\theta_0)R_{s\lambda}T_{\uparrow v\lambda}(\theta)}{1-R_{v\lambda}R_{s\lambda}}, \quad \text{(A1)}$$

where $\rho_{v\lambda}(\theta,\varphi,\theta_0)$ is the vegetation canopy directional reflectance with a perfect absorber as background (or free surface), $T_{\downarrow v\lambda}(\theta_0)$ is the total downward transmittance (bi-hemispherical transmittance), equivalent to the normalized downward total flux with free surface at the bottom, $T_{\uparrow v\lambda}(\theta)$ is the upward transmittance into the direction of θ (hemispherical-directional transmittance factor), $R_{s\lambda}$ is the bi-hemispherical reflectance of the background which is assumed as a Lambertian surface throughout this study, and $R_{v\lambda}$ is the bi-hemispherical reflectance of the vegetation canopy for the background-reflected photons entering the bottom of the canopy layer and scattered back downward (Figure 3.1.4). Two problems with different source conditions are depicted in Figure 3.1.4 and need to be solved in the single canopy layer with no-soil (free boundary condition). One is the sun illumination problem or source at the top-of-canopy, and the other is the isotropic source located at the bottom surface of the canopy. $\rho_{v\lambda}(\theta,\varphi,\theta_0)$ and $T_{\downarrow v\lambda}(\theta_0)$ can be determined by the first problem, while $R_{v\lambda}$ and $T_{\uparrow v\lambda}(\theta)$ can be determined by simulating the second problem. These variables play an important role in determination of vegetation isolines, and thus need to be obtained. Although these two problems allow us to precisely estimate these variables, we approximate the second problem with an alternative approach.

We define the average transmittance as the logarithmic average of the downward and upward transmittance of the canopy layer,

$$T_{v\lambda}(\theta,\theta_0) = \sqrt{T_{\downarrow v\lambda}(\theta_0)T_{\uparrow v\lambda}(\theta)}\,. \quad \text{(A2)}$$

For brevity we will omit the functional arguments in $\rho_\lambda(\theta,\varphi,\theta_0)$, $\rho_{v\lambda}(\theta,\varphi,\theta_0)$ and $T_{v\lambda}(\theta,\theta_0)$ as ρ_λ, $\rho_{v\lambda}$ and $T_{v\lambda}$. Using the above equation, we rewrite Eq. (A1) as

$$\rho_\lambda = \rho_{v\lambda} + \frac{T_{v\lambda}^2 R_{s\lambda}}{1 - R_{v\lambda} R_{s\lambda}}. \quad \text{(A3)}$$

The first term of the right hand side (RHS) in Eq. (A3) is the reflectance contribution of only the vegetation canopy, i.e., the photons represented in this term never see the background. This value can be obtained by simply simulating the single-layer problem with a free surface boundary condition (or black surface). The second RHS term represents the contribution of multiple scattering (interaction) between the soil surface and the canopy layer. The numerator represents first-order soil-vegetation interactions while the denominator is a result of higher order interaction terms. Our next step is to separate the first order interaction term from the higher term by expansion of Eq.(A3) with a Taylor series,

$$\begin{aligned} \rho_\lambda &= \rho_{v\lambda} + T_{v\lambda}^2 R_{s\lambda} + \frac{T_{v\lambda}^2 R_{s\lambda}^2 R_{v\lambda}}{1 - R_{v\lambda} R_{s\lambda}}, \\ &= \rho_{v\lambda} + T_{v\lambda}^2 R_{s\lambda} + O_\lambda^2 \end{aligned} \quad \text{(A4)}$$

where

$$O_l^2 = \frac{T_{vl}^2 R_{vl} R_{sl}^2}{1 - R_{vl} R_{sl}}. \quad \text{(A5)}$$

In order to proceed, we rewrite Eq. (A4) for the red and NIR bands using the notation of R and N instead of λ,

$$\rho_N = \rho_{vN} + T_{vN}^2 R_{sN} + O_N^2, \text{ and} \quad \text{(A6)}$$

$$\rho_R = \rho_{vR} + T_{vR}^2 R_{sR} + O_R^2. \quad \text{(A7)}$$

We can couple these equations with the soil line equation, which is the relationship between the red and NIR reflectances for bare soil,

$$R_{sN} = a R_{sR} + b, \quad \text{(A8)}$$

where *a* and *b* are the soil constants. We can eliminate the soil reflectances, R_{sN} and R_{sR}, from Eqs. (A6)-(A8) to derive the vegetation isoline equation which is the relationship between the red and NIR reflectances. Using the following new definitions, the vegetation isoline equation becomes

$$\rho_N = a\gamma\rho_R + D + O^2, \quad \text{(A9)}$$

where the definitions of the variables used in the above are already introduced in 3.1.3.

We describe four steps to derive a vegetation isoline through use of a numerical radiative transfer model. We note that the numerical simulation model is only used to determine the transmittance and reflectance properties of the canopy layer separately from the soil layer. The essence of this technique is to obtain the vegetation isoline parameters, λ and D, which are defined by Eqs. (4a) and (4b). To determine these

two parameters we need the following parameters, T_{vR}, T_{vN}, ρ_{vN}, ρ_{vR}. R_{vR}, and R_{vN} are also needed to assess truncation of the higher order terms. We conduct two simulations for each band per canopy LAI with two canopy background reflectances (as boundary conditions). The first simulation is with the free surface or perfect absorber (the black soil). For the second simulation, any background can be used. Although the choice of the background for the second simulation is quite arbitrary, as we will see, darker backgrounds result in less error with the proposing technique. Since T_{vR}, T_{vN}, ρ_{vN}, ρ_{vR}, R_{vR}, and R_{vN} are purely functions of the canopy optical properties, we can determine these values regardless of the actual soil optical properties. The schematic procedure is summarized in Figure A1.

For this study we arbitrarily chose reflectances of 0.4 and 0.2 for red and NIR soil hemispherical reflectances. This pair which is on the line of $R_{sN} = 0.5R_{sR}$ is very far from the soil lines used in this study, whose slope and intercept are chosen to 1.2 and 0.04 respectively (Baret and Guyot, 1991). However, we chose these values to demonstrate that the vegetation isoline can be derived without knowledge of 'actual' soil reflectance. The details of four-step procedure for vegetation isoline derivation are summarized below, and the flow chart of the procedure is shown in Figure A1.

Step 1 Parameter set up:

The first step is to choose a set of canopy parameters to run a numerical simulation code. The parameters include LAI and any other optical properties of the canopy such as leaf angle distribution (LAD) and leaf transmittance and reflectance. Also included are sun and view angle conditions.

Step 2 Canopy RT simulation with the perfect absorber as the background:

The second step is the simulation of the canopy reflectance with the perfect absorber as the boundary condition. This simulation corresponds to setting $R_{s\lambda} = 0.0$ in Eq. (A3) so that the result of this simulation is equal to $\rho_{v\lambda}$.

Step 3 Canopy RT simulation with an arbitrary background:

The third step is the canopy simulation with an arbitrary background. Although the choice of the soil reflectance values is arbitrary, the values must be small enough to make the following approximation of average transmittance valid. Eq. (A3) is solved about T_{vl}^2 as,

$$T_{v\lambda}^2 = (\rho_\lambda - \rho_{v\lambda})(1 - R_{v\lambda}R_{s\lambda}) / R_{s\lambda}, \qquad \text{(A10)}$$

where ρ_λ is the result of the simulation executed in this step and $\rho_{v\lambda}$ is the canopy reflectance obtained by the previous black soil step. We still do not know the canopy bi-hemispherical reflectance at the bottom surface of the canopy (for the photons entering the canopy layer from the bottom surface and reflected toward the soil), but we can approximate this value by $\rho_{v\lambda}$. This approximation may be drastic, however, it

becomes insignificant if we choose a small value for $R_{s\lambda}$. Before we show this, we rewrite the above equation with the approximation:

$$T_{v\lambda}^2 \approx (\rho_\lambda - \rho_{v\lambda})(1 - \rho_{v\lambda} R_{s\lambda}) / R_{s\lambda} . \quad \text{(A11)}$$

The only difference of the above two equations is that the factor of $(1 - R_{v\lambda} R_{s\lambda})$ is approximated by $(1 - \rho_{v\lambda} R_{s\lambda})$. This approximation would be insignificant regardless of the approximation of $R_{v\lambda}$ by $\rho_{v\lambda}$ if both $R_{v\lambda} R_{s\lambda}$ and $1 - \rho_{v\lambda} R_{s\lambda}$ are smaller than 0.1 (comparing to 1.0). In order to keep these values smaller than 0.1, we must choose a small value for $R_{s\lambda}$ which is the input of the simulation done in this step. By choosing 0.4 for the red band, the value of $R_{v\lambda} R_{s\lambda}$ for this band will be smaller than 0.04 since both $R_{v\lambda}$ and $\rho_{v\lambda}$ of red band are normally lower than 0.1. On the other hand, for the NIR band both $R_{v\lambda}$ and $\rho_{v\lambda}$ are expected to be as high as 0.5. By choosing 0.2 for $R_{s\lambda}$ we can keep the value of $R_{v\lambda} R_{s\lambda}$ to be smaller than 0.1. Thus the error in the estimation of T_{vl}^2 associated with the approximation of $R_{v\lambda}$ by $\rho_{v\lambda}$ is approximately one order smaller than the original error. For example, if we assume that $\rho_{v\lambda}$ of 0.5 is used for $R_{v\lambda}$ whose true value is 0.3, then the approximation is affected by 0.04, which is much smaller than (1.0-0.3×0.2)=0.94 on the estimation of T_{vl}^2.

Although it is better to choose smaller values of $R_{s\lambda}$ for each band in this simulation to make the above approximation relatively insignificant, the choice of too small a value also causes error on the T_{vl}^2 estimation. The reason is that the numerical canopy model used for this step (and the previous step) has its own accuracy limitations. Since we have a subtraction term, $(\rho_\lambda - \rho_{v\lambda})$, the numerical error of the model in these two values may be enhanced if we choose a very small value for $R_{s\lambda}$. The difference of ρ_λ and $\rho_{v\lambda}$ will be negligible if we chose too small a value of $R_{s\lambda}$.

Step 4 Determination of the vegetation isoline parameters:

We finally determine the vegetation isoline parameters, γ and D, by using ρ_{vN}, ρ_{vR}, T_{vN} and T_{vR} obtained from steps 2 and 3. γ is computed by using Eq. (4a) which is totally independent of the soil line parameters. D, D_N and D_R are then computed from Eqs. (4b), (4c) and (4d). Although D and D_N are functions of the soil line parameters, other terms and factors (ρ_{vN}, ρ_{vR}, T_{vN}, and γ) are completely independent of the soil parameters *a* and *b*. Therefore, we can execute the previous three steps without knowledge of actual soil properties. Thus, we do not need to repeat steps 1-3 for the different soil parameters if the canopy and LAI are the same. We just need to repeat step 4 to compute the vegetation isoline for a different set of soil line parameters.

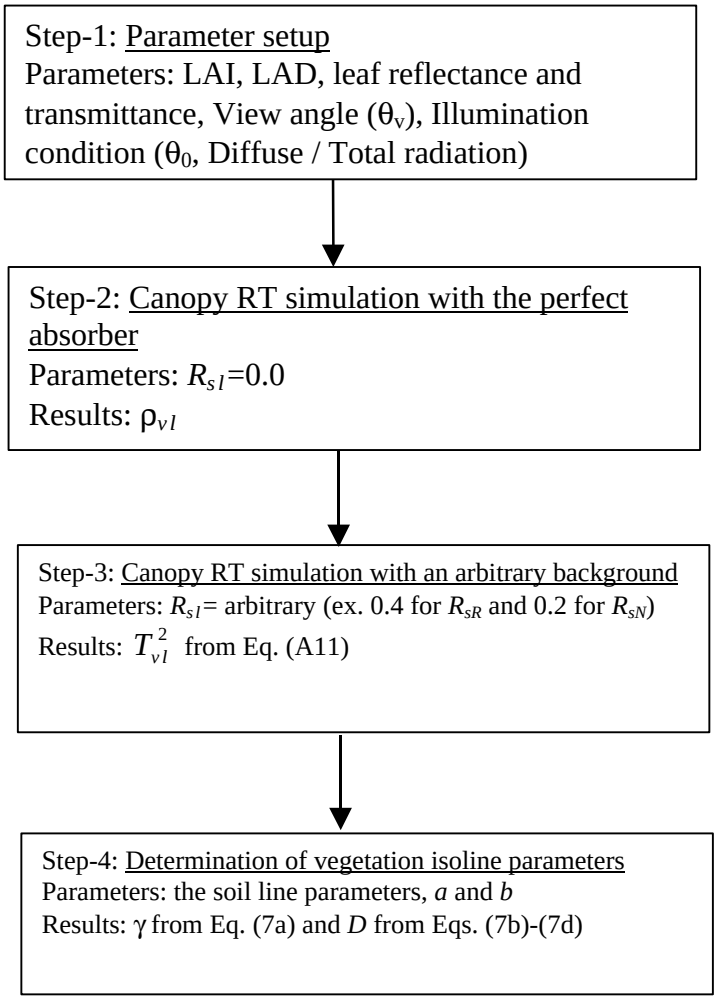

Figure A1: Procedure to obtain vegetation isoline parameters

APPENDIX B: Overview of MODIS 13 VI Products, Data Field Descriptions and Data Types

PRODUCT MOD13A1: 16 day 250 m NDVI

Data field	Name	Data type	Scale	Valid range	Fill value
DataField_1	250m 16 days NDVI	INT16	10000	-2000 to 10000	-3000
DataField_2	250m 16 days NDVI Quality	UINT16	N/A	0 to 65534	65535
DataField_3	250m 16 days NIR reflectance	INT16	10000	0 to 10000	-1000
DataField_4	250m 16 days average view zenith angle	INT16	100	-9000 to 9000	-10000
DataField_5	250m 16 days average sun zenith angle	INT16	100	-9000 to 9000	-10000
DataField_6	250m 16 days average relative azimuth angle	INT16	10	-3600 to 3600	-4000

PRODUCT MOD13A2: 16 day 1 km NDVI and EVI

Data field	Name	Data type	Scale	Valid range	Fill value
DataField_1	1 km 16 days NDVI	INT16	10000	-2000 to 10000	-3000
DataField_2	1 km 16 days EVI	INT16	10000	-2000 to 10000	-3000
DataField_3	1 km 16 days NDVI Quality	UINT16	N/A	0 to 65534	65535
DataField_4	1 km 16 days EVI Quality	UINT16	N/A	0 to 65534	65535
DataField_5	1 km 16 days red reflectance	INT16	10000	0 to 10000	-1000
DataField_6	1 km 16 days NIR reflectance	INT16	10000	0 to 10000	-1000
DataField_7	1 km 16 days blue reflectance	INT16	10000	0 to 10000	-1000
DataField_8	1 km 16 days MIR reflectance	INT16	10000	0 to 10000	-1000
DataField_9	1 km 16 days average view zenith angle	INT16	100	-9000 to 9000	-10000
DataField_10	1 km 16 days average sun zenith angle	INT16	100	-9000 to 9000	-10000
DataField_11	1 km 16 days average relative azimuth angle	INT16	10	-3600 to 3600	-4000

PRODUCT MOD13A3: monthly 1km NDVI and EVI

Data field	Name	Data type	Scale	Valid range	Fill value
DataField_1	1 km monthly NDVI	INT16	10000	-2000 to 10000	-3000
DataField_2	1 km monthly EVI	INT16	10000	-2000 to 10000	-3000
DataField_3	1 km monthly NDVI Quality	UINT16	N/A	0 to 65534	65535
DataField_4	1 km monthly EVI Quality	UINT16	N/A	0 to 65534	65535
DataField_5	1 km monthly red reflectance	INT16	10000	0 to 10000	-1000
DataField_6	1 km monthly NIR reflectance	INT16	10000	0 to 10000	-1000
DataField_7	1 km monthly blue reflectance	INT16	10000	0 to 10000	-1000
DataField_8	1 km monthly MIR reflectance	INT16	10000	0 to 10000	-1000
DataField_9	1 km monthly average view zenith angle	INT16	100	-9000 to 9000	-10000
DataField_10	1 km monthly average sun zenith angle	INT16	100	-9000 to 9000	-10000
DataField_11	1 km monthly average relative azimuth angle	INT16	10	-3600 to 3600	-4000

PRODUCT MOD13C1: CMG (25 km) 16 day NDVI and EVI product

Data field	Name	Data type	Scale	Valid range	Fill value
DataField_1	25km 16 days NDVI	INT16	10000	-2000 to 10000	-3000
DataField_2	25km 16 days EVI	INT16	10000	-2000 to 10000	-3000
DataField_3	25km 16 days NDVI Quality	UINT8	N/A	0 to 255	N/A
DataField_4	25km 16 days EVI Quality	UINT8	N/A	0 to 255	N/A
DataField_5	25km 16 days red reflectance	INT16	10000	0 to 10000	-1000
DataField_6	25km 16 days NIR reflectance	INT16	10000	0 to 10000	-1000
DataField_7	25km 16 days blue reflectance	INT16	10000	0 to 10000	-1000
DataField_8	25km 16 days MIR reflectance	INT16	10000	0 to 10000	-1000
DataField_9	25km 16 days average view zenith angle	INT16	100	-9000 to 9000	-10000
DataField_10	25km 16 days average sun zenith angle	INT16	100	-9000 to 9000	-10000
DataField_11	25km 16 days average relative azimuth angle	INT16	10	-3600 to 3600	-4000
DataField_12	25km 16 days mean NDVI	INT16	10000	-2000 to 10000	-3000
DataField_13	25km 16 days standard deviation NDVI	INT16	10000	-2000 to 10000	-3000
DataField_14	25km 16 days mean EVI	INT16	10000	-2000 to 10000	-3000
DataField_15	25km 16 days standard deviation EVI	INT16	10000	-2000 to 10000	-3000
DataField_16	25km 16 days percent cloud cover	UINT8	1	0 to 100	255
DataField_17	25km 16 days percent with vegetation	UINT8	1	0 to 100	255

PRODUCT MOD13C2: CMG monthly NDVI and EVI product

Data field	Name	Data type	Scale	Valid range	Fill value
DataField_1	25km CMG NDVI	INT16	10000	-2000 to 10000	-3000
DataField_2	25km CMG EVI	INT16	10000	-2000 to 10000	-3000
DataField_3	25km CMG NDVI Quality	UINT8	N/A	0 to 255	N/A
DataField_4	25km CMG EVI Quality	UINT8	N/A	0 to 255	N/A
DataField_5	25km CMG red reflectance	INT16	10000	0 to 10000	-1000
DataField_6	25km CMG NIR reflectance	INT16	10000	0 to 10000	-1000
DataField_7	25km CMG blue reflectance	INT16	10000	0 to 10000	-1000
DataField_8	25km CMG MIR reflectance	INT16	10000	0 to 10000	-1000
DataField_9	25km CMG average view zenith angle	INT16	100	-9000 to 9000	-10000
DataField_10	25km CMG average sun zenith angle	INT16	100	-9000 to 9000	-10000
DataField_11	25km CMG average relative azimuth angle	INT16	10	-3600 to 3600	-4000

APPENDIX C: Listing of the Metadata Fields Used for QA Evaluations of the 5 VI Products

I. Inventory Metadata fields for all VI products (searchable)	
QAPERCENTINTERPOLATEDDATA	
QAPERCENTMISSINGDATA	
QAPERCENTOUTOFBOUNDSDATA	
QAPERCENTCLOUDCOVER	
QAPERCENTGOODQUALITY	
QAPERCENTOTHERQUALITY	
QAPERCENTNOTPRODUCEDCLOUD	
QAPERCENTNOTPRODUCEDOTHER	
II. Product specific metadata (searchable)	
Product	**Specific Metadata variable name** (Best Quality)
MOD13A1	NDVI250M16DAYQCLASSPERCENTAGE
MOD13A2	NDVI1KM16DAYQCLASSPERCENTAGE
MOD13A2	EVI1KM16DAYQCLASSPERCENTAGE
MOD13A3	NDVI1KMMONTHQCLASSPERCENTAGE
MOD13A3	EVI1KMMONTHQCLASSPERCENTAGE
MOD13C1	NDVICMG16DAYQCLASSPERCENTAGE
MOD13C1	EVICMG16DAYQCLASSPERCENTAGE
MOD13C2	NDVICMGMONTHQCLASSPERCENTAGE
MOD13C2	EVICMGMONTHQCLASSPERCENTAGE
III. Archived Metadata (not searchable)	
Product	**Metadata variable name (Array of QA usefulness histogram)**
MOD13A1	QAPERCENTPOORQ250M16DAYNDVI
MOD13A2	QAPERCENTPOORQ1KM16DAYNDVI
MOD13A2	QAPERCENTPOORQ1KM16DAYEVI
MOD13A3	QAPERCENTPOORQ1KMMONTHNDVI
MOD13A3	QAPERCENTPOORQ1KMMONTHEVI
MOD13C1	QAPERCENTPOORQCMG16DAYNDVI
MOD13C1	QAPERCENTPOORQCMG16DAYEVI
MOD13C2	QAPERCENTPOORQCMGMONTHNDVI
MOD13C2	QAPERCENTPOORQCMGMONTHEVI

APPENDIX D: QA Flag Key and Description

Spatial and temporal resolution →		250m 16 days	1km/16days		1km/monthly.		CMG/16days		CMG/monthly.	
Parameter	**# bits**	**NDVI**	**NDVI**	**EVI**	**NDVI**	**EVI**	**NDVI**	**EVI**	**NDVI**	**EVI**
Quality	2	0-1	0-1	0-1	0-1	0-1	0-1	0-1	0-1	0-1
Usefulness	4	2-5	2-5	2-5	2-5	2-5	2-5	2-5	2-5	2-5
Aerosol	2	6-7	6-7	6-7	6-7	6-7	6-7	6-7	6-7	6-7
Adj. corr.	1	8	8	8	8	8				
Atm. corr.	1	9	9	9	9	9				
Mixed Clouds	1	10	10	10	10	10				
Land/Water	2	11-12	11-12	11-12	11-12	11-12				
Snow/Ice	1	13	13	13	13	13				
Shadow	1	14	14	14	--	--				
Mixed Comp.	1	--	--	--	14	14				
Comp. Method	1	15	15	15	15	15				

Key to bit positions:

Bit	**Parameter**	**Description**
0-1	VI quality (MODLAND)	01 VI produced, but check QA 00 VI produced, good quality; 10 pixel not produced due to cloud effects 11 pixel not produced due to other reasons than clouds
2-5	VI usefulness	0= highest quality,…., 7=intermediate quality, …,13=lowest quality, 14= quality too low to be useful, 15= not useful for any other reason (clouds)
6-7	Aerosol quantity	:00 climatology, 01 low, 10 average , 11 high
8	Atmosphere Adjacency correction:	0 no adjacency correction; 1 adjacency effect corrected
9	Atm. corr.	0 (no) 1 (yes) atmosphere BRDF correction performed
10	Mixed Clouds	0 no; 1 yes mixed clouds
11-12	Land/Water	00 Ocean/water; 01 Coast; 10 Wetland; 11 Land
	Where these four land /water categories were assigned one or more of the following descriptions:	
	Ocean/water:	***0. Shallow Ocean*** *(Ocean <5k from coast OR <50m deep; i.e., a buffer zone around all coastal areas and islands, plus shallow areas up to 50m deep that are further than 5 km from the land). Includes the appropriate parts of the Black Sea, Red Sea, Mediterranean Sea, Hudson Bay, and other ocean-connected seas.*
	Land	***1. Land*** *(not anything else).*
	Coast:	***2. Ocean Coastlines and Lake Shorelines*** *(an actual boundary line).*
	Coast:	***3. Shallow Inland Water*** *(Inland water<5km from shoreline or <50 m deep;i.e.. a buffer zone around all lake shores and inland islands, plus shallow areas up to 50m deep that are further than 5km from the land). Includes the appropriate parts of the Caspian Sea, Aral Sea, Great Lakes, 2-line rivers, etc.*
	Wetland:	***4. Ephemeral (intermittent) Water*** *(from Digital Chart of the World).*
	Ocean/Water:	***5. Deep Inland Water*** *(Inland water >5 km from shoreline AND >50m deep; i.e., Lake waters beyond 5 km from their shore or islands, and greater than 50m deep). Includes the appropriate parts of the Caspian Sea, Aral Sea, Great Lakes, etc.*
	Ocean/Water:	***6. Moderate and continental ocean***

	Ocean/Water:	***7. Deep Ocean*** *(Ocean >5km from coast AND >50m deep); i.e., Oceans beyond 5km from coastal areas and islands, and greater than 50m deep). Includes the appropriate parts of the Black Sea, Red Sea, Mediterranean Sea, Hudson Bay, and other ocean-connected seas.*
13	Snow/Ice	0 no; 1 yes possible snow/ice
14	Shadow	0 no; 1 yes possible shadow
14	Mixed Composite (1km monthly only):	0 no; 1 yes mixed composite methods used in monthly composite
15	Comp. Method	0 BRDF model based nadir equivalent VI 1 CVMVC (constraint view angle maximum value VI)

APPENDIX E: Usefulness Scale Interpretation Key for MODIS 13 Products

Marks (rating scheme) to be summed for each 250 m and 1 km pixel:
(Take the worst case scenario from day to day; Post launch revisions are expected)

Parameter	**Rating (mark)**
Aerosol quantity based on 1 km data:	
climatology	Mark 2
low	mark 0
average	mark 0
high	mark 3
no adjacency correction.	mark 1 (Not applicable for 1km product)
no atm. BRDF correction.	mark 2
Mixed clouds	mark 3
Possible shadow	mark 2
VIEW angle >40°	mark 1
SUNANGLE >60°	mark 1

VI usefulness scale for CMG 16 day composite:

Usefulness	**Description**
0	highest quality
1	
2-6	undefined
7	intermediate quality
8	
9	
10	low quality (76-99% clouds and high aerosols)
11	
12	lowest quality (76-99% clouds and high aerosols, view and sun angle)
13	uncertain about quality (if not determined; default)
14	quality too low to be useful
15	not useful for any other reason (clouds etc)

Marks (rating) to be summed for each CMG pixel to compute the usefulness index:

Parameter:	***Rating (marks)***
Aerosol quantity based on 1 km data (take worst case scenario):	
climatology	mark 1
low	mark 0
average	mark 0
high	mark 6
percentage clouds inside CMG pixel	
1-25	mark 1
26-50	mark 1
51-75	mark 2
76-99	mark 4
VIEW angle >40°	mark 1
SUNANGLE >60°	mark 1

APPENDIX F: Propagation of Reflectance Calibration Uncertainties Into Atmospherically-Corrected Vegetation Indices

This section describes a set of uncertainty propagation equations designed for modeling the propagation of reflectance calibration uncertainties into VIs through atmospheric correction (Miura et al., 1999). TOA reflectances can be derived by dividing the MODIS level 1B reflectance products by the cosine of the view zenith angle:

$$\rho^{TOA} = \frac{\rho^{TOA}\cos\theta_{EV}}{\cos\theta_{EV}}, \tag{F1}$$

where ρ^{TOA} is the TOA reflectance factor and θ_{EV} is the solar zenith angle at Earth scene.

The propagation equation of uncertainty from the level 1B product to TOA reflectances is derived by taking a partial derivative of the above equation with respect to $\rho^{TOA}\cos\theta_{EV}$:

$$u_{cal}^2(\rho^{TOA}) = \frac{1}{\cos^2\theta_{EV}} u_{cal}^2(\rho^{TOA}\cos\theta_{EV}) = \left(\frac{u_{cal}(\rho^{TOA}\cos\theta_{EV})}{\rho^{TOA}\cos\theta_{EV}}\right)^2 (\rho^{TOA})^2, \tag{F2}$$

where the uncertainty in view zenith angle is assumed to be negligible. The right hand side of (F2) indicates that the fractional standard uncertainty of TOA reflectances due to calibration is the same as that of $\rho^{TOA}\cos\theta_{EV}$.

TOA reflectances can be expressed in terms of surface reflectance and atmospheric parameters. For a Lambertian, homogeneous surface target case, the following can be used (Vermote et al., 1997):

$$\rho^{TOA}(\theta_s,\theta_v,\phi) = T_g(\theta_s,\theta_v)\left[\rho_{R+A}^{a}(\theta_s,\theta_v,\phi) + T_{R+A}(\theta_s,\theta_v)\frac{\rho_s}{1-S_{R+A}\cdot\rho_s}\right], \tag{F3}$$

where

θ_s = Solar zenith angle

θ_v = View zenith angle

ϕ = Difference between solar and view azimuth angles

ρ_s = Surface reflectance of a ground target

$T_g(\theta_s,\theta_v)$ = Gaseous transmittance (absorption)

$\rho_{R+A}^{a}(\theta_s,\theta_v,\phi)$ = Intrinsic atmospheric reflectance (normalized path radiance) due to Rayleigh and aerosol scattering

$T_{R+A}(\theta_s, \theta_v)$ = Two-way atmospheric transmittance due to Rayleigh and aerosol scattering

S_{R+A} = Spherical albedo due to Rayleigh and aerosol scattering.

Thus, atmospherically-corrected surface reflectance ρ^{ac} is derived by solving (F3) for ρ_s:

$$\rho^{ac} = \frac{\rho^{ac*}}{1 + \rho^{ac*} S_{R+A}}, \tag{F4}$$

where

$$\rho^{ac*} = \frac{\frac{\rho^{TOA}}{T_g} - \rho^{a}_{R+A}}{T_{R+A}} . \tag{F4a}$$

The standard uncertainty in ρ^{TOA} will propagate to ρ^{ac} and the uncertainty propagation equation is derived by taking a partial derivative of (F4) with respect to ρ^{TOA}:

$$u^2_{cal}(\rho^{ac}) = \left(\frac{\partial \rho^{ac}}{\partial \rho^{TOA}} \right)^2 u^2_{cal}(\rho^{TOA}) , \tag{F5}$$

where

$$\frac{\partial \rho^{ac}}{\partial \rho^{TOA}} = 1 \Bigg/ \left[\left(1 + \frac{\frac{\rho^{TOA}}{T_g} - \rho^{a}_{R+A}}{T_{R+A}} S_{R+A} \right) T_g T_{R+A} \right] . \tag{F5a}$$

The partial derivative or sensitivity coefficient (F5a) includes both ρ^{TOA} and atmospheric parameters used for atmospheric correction, indicating that the standard uncertainty in ρ^{ac} changes with both atmospheric conditions and surface reflectances. It should be noted that the uncertainty propagation equation here (F5) propagates reflectance calibration uncertainty and assumes the uncertainty in atmospheric corrections to be negligible.

VIs can then be calculated from the surface reflectances. For the NDVI:

$$NDVI = \frac{\rho_{NIR} - \rho_{red}}{\rho_{NIR} + \rho_{red}} , \tag{F6}$$

the uncertainty propagation equation is derived by taking partial derivatives of (F6) with respect to the red and NIR reflectances:

$$u^2_{cal}(NDVI) = \left(\frac{\partial NDVI}{\partial \rho_{NIR}} \right)^2 u^2_{cal}(\rho_{NIR}) + \left(\frac{\partial NDVI}{\partial \rho_{red}} \right)^2 u^2_{cal}(\rho_{red}) + 2 \frac{\partial NDVI}{\partial \rho_{NIR}} \frac{\partial NDVI}{\partial \rho_{red}} u_{cal}(\rho_{NIR}, \rho_{red}) , \tag{F7}$$

where

$$\frac{\partial NDVI}{\partial \rho_{NIR}} = \frac{2\rho_{red}}{(\rho_{NIR} + \rho_{red})^2} \ , \tag{F7a}$$

$$\frac{\partial NDVI}{\partial \rho_{red}} = \frac{-2\rho_{NIR}}{(\rho_{NIR} + \rho_{red})^2} \ , \tag{F7b}$$

$$\frac{\partial NDVI}{\partial \rho_{NIR}} \frac{\partial NDVI}{\partial \rho_{red}} = \frac{-4\rho_{NIR}\rho_{red}}{(\rho_{NIR} + \rho_{red})^4} \ . \tag{F7c}$$

As reported by Goward et al. (1991), all the partial derivatives [sensitivity coefficients, (F7a), (F7b), and (F7c)] are a function of both the red and NIR reflectances. Thus, the magnitude of the NDVI uncertainty varies with the magnitude of reflectance values. The sensitivity coefficient for the covariance term (F7c) has a negative sign, indicating that the total NDVI uncertainty decreases if the calibration uncertainties between the red and NIR bands are positively correlated and increases if they are negatively correlated.

The uncertainty propagation equations for the other indices, including the SAVI, ARVI, and EVI are derived in the same manner as well. For the SAVI:

$$SAVI = (1+L)\frac{\rho_{NIR} - \rho_{red}}{\rho_{NIR} + \rho_{red} + L} \ , \tag{F8}$$

and

$$u_{cal}^2(SAVI) = \left(\frac{\partial SAVI}{\partial \rho_{NIR}}\right)^2 u_{cal}^2(\rho_{NIR}) + \left(\frac{\partial SAVI}{\partial \rho_{red}}\right)^2 u_{cal}^2(\rho_{red}) + 2\frac{\partial SAVI}{\partial \rho_{NIR}}\frac{\partial SAVI}{\partial \rho_{red}} u_{cal}(\rho_{NIR}, \rho_{red}) \ , \tag{F9}$$

where

$$\frac{\partial SAVI}{\partial \rho_{NIR}} = (1+L)\frac{2\rho_{red} + L}{(\rho_{NIR} + \rho_{red} + L)^2} \ , \tag{F9a}$$

$$\frac{\partial SAVI}{\partial \rho_{red}} = (1+L)\frac{-(2\rho_{NIR} + L)}{(\rho_{NIR} + \rho_{red} + L)^2} \ . \tag{F9b}$$

For the ARVI:

$$ARVI = \frac{\rho_{NIR} - \rho_{rb}}{\rho_{NIR} + \rho_{rb}} \ , \tag{F10}$$

where

$$\rho_{rb} = \rho_{red} - \gamma(\rho_{blue} - \rho_{red}) \ , \tag{F10a}$$

and

$$u_{cal}^2(ARVI)=\left(\frac{\partial ARVI}{\partial \rho_{NIR}}\right)^2 u_{cal}^2(\rho_{NIR})+\left(\frac{\partial ARVI}{\partial \rho_{red}}\right)^2 u_{cal}^2(\rho_{red})+\left(\frac{\partial ARVI}{\partial \rho_{blue}}\right)^2 u_{cal}^2(\rho_{blue})$$
$$+2\frac{\partial ARVI}{\partial \rho_{NIR}}\frac{\partial ARVI}{\partial \rho_{red}}u_{cal}(\rho_{NIR},\rho_{red})+2\frac{\partial ARVI}{\partial \rho_{NIR}}\frac{\partial ARVI}{\partial \rho_{blue}}u_{cal}(\rho_{NIR},\rho_{blue})+2\frac{\partial ARVI}{\partial \rho_{red}}\frac{\partial ARVI}{\partial \rho_{blue}}u_{cal}(\rho_{red},\rho_{blue}) \quad ,(F11)$$

where

$$\frac{\partial ARVI}{\partial \rho_{NIR}}=\frac{2\rho_{rb}}{(\rho_{NIR}+\rho_{rb})^2}, \quad (F11a)$$

$$\frac{\partial ARVI}{\partial \rho_{red}}=\frac{-2(1+\gamma)\rho_{NIR}}{(\rho_{NIR}+\rho_{rb})^2}, \quad (F11b)$$

$$\frac{\partial ARVI}{\partial \rho_{blue}}=\frac{2\gamma\rho_{NIR}}{(\rho_{NIR}+\rho_{rb})^2}. \quad (F11c)$$

For the EVI:

$$EVI=G\frac{\rho_{NIR}-\rho_{red}}{\rho_{NIR}+C_1\rho_{red}-C_2\rho_{blue}+L}, \quad (F12)$$

and

$$u_{cal}^2(EVI)=\left(\frac{\partial EVI}{\partial \rho_{NIR}}\right)^2 u_{cal}^2(\rho_{NIR})+\left(\frac{\partial EVI}{\partial \rho_{red}}\right)^2 u_{cal}^2(\rho_{red})+\left(\frac{\partial EVI}{\partial \rho_{blue}}\right)^2 u_{cal}^2(\rho_{blue})$$
$$+2\frac{\partial EVI}{\partial \rho_{NIR}}\frac{\partial EVI}{\partial \rho_{red}}u_{cal}(\rho_{NIR},\rho_{red})+2\frac{\partial EVI}{\partial \rho_{NIR}}\frac{\partial EVI}{\partial \rho_{blue}}u_{cal}(\rho_{NIR},\rho_{blue})+2\frac{\partial EVI}{\partial \rho_{red}}\frac{\partial EVI}{\partial \rho_{blue}}u_{cal}(\rho_{red},\rho_{blue}) \quad , \quad (F13)$$

where

$$\frac{\partial EVI}{\partial \rho_{NIR}}=G\frac{(1+C_1)\rho_{red}-C_2\rho_{blue}+L}{(\rho_{NIR}+C_1\rho_{red}-C_2\rho_{blue}+L)^2}, \quad (F13a)$$

$$\frac{\partial EVI}{\partial \rho_{red}}=G\frac{-\{(1+C_1)\rho_{NIR}-C_2\rho_{blue}+L\}}{(\rho_{NIR}+C_1\rho_{red}-C_2\rho_{blue}+L)^2}, \quad (F13b)$$

$$\frac{\partial EVI}{\partial \rho_{blue}}=G\frac{C_2(\rho_{NIR}-\rho_{red})}{(\rho_{NIR}+C_1\rho_{red}-C_2\rho_{blue}+L)^2}. \quad (F13c)$$